Dynamics and Control of Fast Automated Guided Vehicles for High Load Applications

by

Mahyar Naraghi

A Thesis Presented to the University of Ottawa
in partial fulfilment of the requirements for the degree of

Doctor of Philosophy

in

Mechanical Engineering

Ottawa-Carleton Institute for Mechanical and Aeronautical Engineering
University of Ottawa
Ottawa, Ontario, Canada K1N 6N5
May 1996

ISBN 0-612-16446-2

Canada

UNIVERSITÉ D'OTTAWA
UNIVERSITY OF OTTAWA

In the Name of God
the Compassionate, the Merciful

For their patience and prayers
dedicated to my parents
Zahra Ardehali and Ali Asghar Naraghi

and

for her sacrifice and support
dedicated to my wife
Razieh Movahhedin

Abstract

Automated Guided Vehicles (AGV) are important components of modern automated transport systems. Increasing the system efficiency and throughput requires the use of heavy vehicles travelling at high speeds. As the AGV's payload capacity and travelling speed increases, the ensuing increase in lateral acceleration requires thorough dynamic modelling and more sophisticated controller design.

To establish the sufficient level of model complexity necessary for this work, a 3-DOF nonlinear dynamic model comprising yaw, lateral, and roll motions is developed. The suspension, lateral and longitudinal load transfer, nonlinear behaviour of tires, and steering dynamics are included in this model. The model also comprises the effect of actuators, differential gear box, steering and tractive gear boxes. The model is validated through simulations and comparison with other models.

A dynamic-based approach to the control of a typical transport interfactory AGV in a semi structured environment is studied. The 2-DOF side slippage free dynamic model comprising steering, and actuators dynamics is used to design the controller. The input-output feedback linearization technique is employed to linearize the nonlinear dynamics of the vehicle. To improve robustness in the presence of parameter uncertainty, modelling errors and disturbance, a Boundary Layer Sliding Mode (BLSM) controller is adopted. The BLSM controller is later modified to improve performance and enhance robustness, using simultaneous variable boundary layer and multiple sliding surfaces strategies.

Simulations based on the 3-DOF nonlinear model show the satisfactory results for the Modified Boundary Layer Sliding Mode (MBLSM) controller.

Acknowledgments

I would like to express my sincere appreciation and gratitude to my supervisor, Professor Atef Fahim, for his continuous encouragement, guidance, and support throughout the course of this research.

I am grateful to the advisory committee members Professor J. Y. Wong and Professor D. S. Necsulescu for their useful scientific suggestions and discussions.

Study leave and financial support granted from the Islamic Republic of Iran is gratefully acknowledged.

Especial thanks are extended to my parents and immediate family, for their consistent patience and prayers. I must single out my wife who endured the hardship, helped me, and gave all her support and love to our children Houra and Mohammad.

Above all, I thank almighty God for making possible the seemingly impossible.

Table of Contents

Dedication ii

Abstract iii

Acknowledgments iv

Table of Contents v

List of Figures xi

List of Table xv

Nomenclature xvi

Chapter 1 Introduction 1

1.1. Background and State of the Art 1

1.1.1. Historical Development 2

1.1.2. AGV Types and Components 3

1.1.3. AGV Applications 4

1.2. Objectives of Research 6

1.3. Thesis Outline 8

Chapter 2 Literature Survey 10

2.1. Introduction 10

2.2. Wheelbase Configuration 11

2.3. Kinematics and Dynamics 11

2.3.1. Kinematic Modelling 12
2.3.2. Dynamic Modelling 12
2.4. Control 14
2.4.1. Controllability 14
2.4.2. Proportional Controller 15
2.4.3. Kinematic-based Control 15
2.4.4. Dynamic-based Control 17
2.4.4.1. Controllers Based on Rigid Vehicle Dynamics 18
2.4.4.2. Controllers Based on Vehicle Dynamics with Tire Model 20

Chapter 3 Vehicle Dynamics 22
3.1. Introduction 22
3.2. Vehicle Models and Degrees of Freedom 22
3.3. Mechanics of Pneumatic Tires 23
3.3.1. Tire Forces and Moments 23
3.3.2. Rolling Resistance 25
3.3.3. Tractive/Braking Effort 29
3.3.4. Cornering Properties of Tires 29
3.3.4.1. Cornering Force 29
3.3.4.2. Aligning Torque 31
3.3.4.3. Camber Thrust 33

Chapter 4 AGV Dynamic Model 35
4.1. Introduction 35
4.2. Axis System and General Equations of Motion 36
4.3. Assumed Vehicle Model 39
4.3.1. Degrees of Freedom 39
4.3.2. Assumptions 40
4.4. Three DOF Dynamic Model 41

4.5. External Forces and Moments Acting on the AGV 43
4.6. Tire Model 46
4.6.1. Linear Tire Model 46
4.6.2. Nonlinear Tire Model 46
4.7. Tire Slip Angles 47
4.8. Load Transfer 48
4.9. Tractive Force 52
4.10. Steering System 53

Chapter 5 AGV Control 55
5.1. Introduction 55
5.2. Conversion to 2-DOF Side Slippage Free Model 55
5.3. Feedback Linearization 60
5.3.1. Definitions 61
5.3.2. Input-Output feedback Linearization 65
5.3.2.1. Choice of Outputs 65
5.3.2.2. Choice of Coordinates 68
5.3.3. Internal Dynamics 71
5.3.4. Stability of Zero Dynamics 73
5.4. Sliding Mode Control 73
5.4.1. Basic Concepts 74
5.5. Controller Design 76
5.5.1. PD Controller 76
5.5.2. Sliding Mode Controller 77
5.5.3. Boundary Layer Technique 77
5.5.4. Multiple Sliding Surfaces 78
5.5.5. Variable Boundary Layer Thickness 78
5.5.6. Modified Boundary Layer Sliding Mode 79

Chapter 6 Simulations and Results 80
6.1. Introduction 80
6.2. Validation of the Dynamic Model 80
6.2.1. Analysis of the Kinematic Model 81
6.2.2. Analysis of the Dynamic Model 81
6.2.3. AGV Performance Using A Proportional Controller 82
6.2.3.1. Roll DOF and Load Transfer Effect 82
6.2.3.2. Disturbance 83
6.2.3.3. Limitations of the Proportional Controller 83
6.3. Performance Evaluation of the Control Schemes 91
6.3.1. PD Controller 91
6.3.2. SM controller 92
6.3.3. Boundary Layer Sliding Mode Controller 93
6.3.4. Comparison of PD and BLSM Controllers 93
6.3.4.1. Effect of Speed 93
6.3.4.2. Effect of Parameter Change and Model Uncertainty ... 93
6.3.4.3. Effect of Disturbance 94
6.3.4.4. Effect of Path Geometry 95
6.3.4.5. Effect of Initial Conditions 95
6.3.5. Performance of Type VI Outputs 96
6.3.6. Modified BLSM Controller 96
6.4. Discussion of Results 98

Chapter 7 Conclusion and Future Work 115
7.1. Summary 115
7.1.1. Dynamic Modelling 116
7.1.2. Control Design 116
7.2. Contributions 117
7.3. Future Work 118

References 120

Appendix A1 Tractive Motor Dynamics 136

Appendix A2 Steering Motor Dynamics 139

Appendix B1 Input-Output Linearization: Outputs X, Y 141

Appendix B2 Input-Output Linearization: Outputs Y,θ 144

Appendix B3 Input-Output Linearization: Outputs U, δ 146

Appendix B4 Input-Output Linearization: Outputs U, Y 148

Appendix C Path Dependent I/O Linearization 150

Appendix D Diffeomorphic Transformation $\Phi(\chi)$ 153

Appendix E AGV Specifications 155

Appendix F Motor Specifications 157

List of Figures

Figure 3.1 The ISO vehicle dynamics axis system 24

Figure 3.2 Tire axis system 24

Figure 3.3 Tire behaviour when a driving torque is applied (Clark, 1971). 26

Figure 3.4 Typical variation of rolling resistance with inflation pressure for different surface conditions (Taborek, 1975). 26

Figure 3.5 Variation of braking effort with normal load for a truck tire (Ervin, 1975). 28

Figure 3.6 Effect of surface condition on braking effort (Gillespie, 1992, notations are modified for consistency). 28

Figure 3.7 Deformation of a rolling tire due to lateral force (Gillespie, 1992, notations are modified for consistency). 30

Figure 3.8 Typical characteristics of the cornering force (Wong, 1993). 30

Figure 3.9 Typical variation of cornering force with slip angle (Bakker et al., 1987). 32

Figure 3.10 Variation of cornering force with inflation pressure at constant normal load. Note over inflation does not increase the cornering Force due to contact area reduction (Ellis, 1969). 32

Figure 3.11 Typical variation of aligning torque with normal force and slip angle (Ervin, 1975). 34

Figure 3.12 Common variation of camber thrust with camber angle and normal load (Gough, 1956). 34

Figure 4.1 The coordinate system. 36

Figure 4.2 The 3-DOF AGV model 40

Figure 4.3 Plan view of AGV and tire forces 43

Figure 4.4 Forces and moments acting on a simplified AGV model. 45

Figure 4.5 AGV mass distribution. 49

Figure 4.6 Roll axis and AGV mass distribution 50
Figure 5.1 Plane view of bicycle model tire forces. 56
Figure 5.2 AGV's motion with respect to path dependent coordinates. 69
Figure 5.3 PD controller for linearized control subsystem. 77
Figure 6.1 Comparison of kinematic and dynamic models. 84
Figure 6.2 Deviation rate from the path versus speed for dynamic model. 84
Figure 6.3 Comparison of path trace for 2-DOF and 3-DOF AGV models. 85
Figure 6.4 The effect of load on the AGV path trace. 85
Figure 6.5 The effect of cornering stiffness on the AGV path trace. 86
Figure 6.6 The effect of cornering stiffness on deviation rate from the path. 86
Figure 6.7 Path tracking performance of 2-DOF and 3-DOF models. 87
Figure 6.8 Distance error for tracking a line-circle-line path. 87
Figure 6.9 The normal force of front-right tire for tracking a line-circle-line path. 88
Figure 6.10 Cornering force of the front-right tire for tracking a line-circle-line path. 88
Figure 6.11 The effect of step disturbance, Step = 0.3 m. 89
Figure 6.12 The effect of step disturbance, Step = -0.3 m. 89
Figure 6.13 Step response of 3-DOF model using proportional controller for various loading and speed conditions. 90
Figure 6.14 The 3-DOF AGV model tracking a circular path. 90
Figure 6.15 Distance error for tacking a circular path. 91
Figure 6.16 The performance of the PD and the SM controllers for tracking a straight path, utilizing the 2-DOF SSF vehicle model. 99
Figure 6.17 The performance of the PD and the SM controllers for tracking a straight path, utilizing the 3-DOF vehicle model. 99
Figure 6.18 The phase portrait of vehicle's lateral position, utilizing the SM controller. 100

Figure 6.19 Chattering in the steering angle as a result of employing the SM controller. 100
Figure 6.20 The phase portrait of vehicle's lateral position, utilizing the BLSM controller. 101
Figure 6.21 Improved steering activity due to introducing a thin boundary layer around the sliding surface. 101
Figure 6.22 The effect of speed on the tracking performance of the PD controller. 102
Figure 6.23 The effect of speed on the tracking performance of the BLSM controller. 102
Figure 6.24 The effect of change in the payload on the PD controller performance. 103
Figure 6.25 The effect of change in the payload on the BLSM controller performance. 103
Figure 6.26 The effect of change in the tire cornering stiffness on the PD controller performance. 104
Figure 6.27 The effect of change in the tire cornering stiffness on the BLSM controller performance. 104
Figure 6.28 Performance in the presence of step disturbance in the path. 105
Figure 6.29 The performance of the PD and the BLSM controllers in tracking a circular path. 105
Figure 6.30 Comparison of distance error of the PD and the BLSM controllers in tracking a circular path. 106
Figure 6.31 The effect of initial heading on the vehicle response utilizing the PD and the BLSM controllers. 106
Figure 6.32 The effect of initial heading on the vehicle response for the PD and the BLSM controllers. 107
Figure 6.33 Comparison of distance error due to different initial headings for the PD controller. 107

Figure 6.34 Comparison of distance error for the BLSM controller due to different initial conditions. 108
Figure 6.35 Comparison of vehicle's tracking capability implementing PD controllers based on type I and type VI outputs. 108
Figure 6.36 Distance error for PD controllers based on type I and type VI outputs. 109
Figure 6.37 The effect of reducing K_1 and K_2 on the performance of the BLSM controller. 109
Figure 6.38 The effect of reducing K_1 and K_2 on the distance error for the BLSM controller. 110
Figure 6.39 Non-smooth response of the BLSM controller for tracking a straight path at a speed of 3 m/s, due to reducing K_1 and K_2. 110
Figure 6.40 The effect of reducing K_1 and K_2 on the system's trajectory (output Y) for the BLSM controller. 111
Figure 6.41 Performance of the BLSM controller using the VBL strategy. 111
Figure 6.42 Phase portrait of the VBL controller and the BLSM controller with reduced boundary layer thickness. 112
Figure 6.43 Performance of the BLSM and the MBLSM controllers for tracking a straight path. 112
Figure 6.44 The phase portrait of output Y for the BLSM and the MBLSM controllers. 113
Figure 6.45 The performance of the PD, the BLSM and the MBLSM controllers for tracking a circular path. 113
Figure 6.46 Comparison of distance error for the PD, the BLSM, and the MBLSM controllers. 114
Figure 6.47 Response of the MBLSM controller for speed increase of up to 40 percent. 114

List of Table

Table 3.1 Coefficient of rolling resistance (Taborek, 1975). 27

Nomenclature

A_t, B_t, D_t, E_t	nonlinear tire model coefficients
a	distance from c.g. to front axle
a_{abs}	vehicle acceleration
$(a_{abs})_x$	acceleration component along the x axis
$(a_{abs})_y$	acceleration component along the y axis
$(a_{abs})_z$	acceleration component along the x axis
a_O	acceleration of moving frame's origin
a_y	lateral acceleration
b	distance from c.g. to rear axle
C_s, C_t	equivalent gains of steering and tractive motors respectively
$\bar{C}_s, \bar{C}_t$	viscus damping coefficient of steering and tractive motors respectively
C_α	cornering stiffness of tire
C_γ	camber stiffness of tire
$c(s)$	path curvature
c_f, c_r	front and rear suspension roll damping
c_{tot}	total suspension roll damping
E	decoupling matrix
e_i	tracking error of the i^{th} output
$\hat{e}_s$, $\hat{e}_t$	unite vectors in path dependent coordinate
$F(S)$	vector of attractiveness functions $F_i(S)$
F_x	vector of longitudinal forces
F_y	vector of cornering forces
F_c	sprung mass inertia force

F_{cf}, F_{cr}	front and rear sprung mass inertia forces respectively
F_{cuf}, F_{cur}	front and rear unsprung mass inertia forces respectively
F_r	rolling resistance of tire
F_t	combined tractive forces of rear tires
$(F_t)_{xrr}, (F_t)_{xrl}$	tractive forces of rear-right and rear-left tires respectively
F_x, F_y, F_z	force component along the x, y, and z axes respectively
F_{xf}, F_{xr}	combined longitudinal forces of front and rear tires respectively
F_{xfr}, F_{xfl}	longitudinal forces of front-right and front-left tires respectively
F_{xrr}, F_{xrl}	longitudinal forces of rear-right and rear-left tires respectively
F_{yf}, F_{yr}	combined cornering forces of front and rear tires respectively
$F_{y\alpha}$	cornering force of tire
F_{yi}	cornering force of the i^{th} tire
$F_{y\gamma}$	camber thrust of tire
$f(\chi)$	smooth vector field of states
$G(\chi)$	smooth matrix of g_i vector fields
g	gravitational acceleration
H_{1s}, H_{2s}	steering dynamics gains
h	height of unsprung mass cg
$h(\chi)$	smooth vector field of h_i functions
h_s	height of sprung mass cg
h_t	height of vehicle cg
h_f, h_r	front and rear roll centre heights respectively
h_{ra}	distance from sprung mass cg to roll axis
h_{uf}, h_{ur}	front and rear unsprung mass cg heights respectively
I	vehicle moment of inertia about the z axis
I_x, I_y, I_z	moment of inertia about the x, y and z axes
I_{xy}, I_{yz}, I_{zx}	mass product of inertias about the xy, yz, and zx planes respectively

$I_{z,uf}$, $I_{z,ur}$	moment of inertia of the front and rear unsprung masses about the z axis respectively
$\bar{I}_{xs}, \bar{I}_{zs}$	moment of inertia of the sprung mass about the x, and y centroidal axes respectively
J_s, J_t	equivalent mass moment of inertia of steering and tractive motors respectively
$\bar{J}_s, \bar{J}_t$	mass moment of inertia of steering and tractive motors respectively
K_s, K_t	equivalent gains of steering and tractive motors respectively
$\bar{K}_s, \bar{K}_t$	torque constant of steering and tractive motors respectively
k_f, k_r	front and rear suspension roll stiffness
k_{1s}, k_{2s}	steering gains
k_{tot}	combined front and rear suspension roll stiffnesses
L	wheelbase
L_{spring}	moment due to suspension roll stiffness
L_{damper}	moment due to suspension roll damping
M	Inertia matrix
M	total mass of vehicle
M_r	moment of sprung mass inertia force about the roll axis
M_{rf}	front moment of sprung mass inertia force about the roll axis
M_{rr}	rear moment of sprung mass inertia force about the roll axis
M_x, M_y, M_z	moment components about the x, y, and z axes respectively
m_s	sprung mass
m_{uf}, m_{ur}	front and rear unsprung masses
n	order of system
n_s, n_t	gear ratio of steering and tractive motors respectively

R_{as}, R_{at}	armature resistance of steering and tractive motors respectively
R_w	radius of rear tires
r, p, q	angular velocities about the x, y, and z axes respectively
r_t	total relative degree of the system
r_i	relative degree of the i^{th} output
S_i	the i^{th} sliding surface
$\boldsymbol{S}$	vector of S_i sliding surfaces
s, n	path dependent coordinates
$sgn(S_i)$	sign function of the i^{th} sliding surface
$sat\left(\frac{S_i}{\varphi_i}\right)$	saturation function of the i^{th} sliding surface
t	track width
t_f, t_r	front and rear track width
t_p	pneumatic trail of tire
U, V, W	vehicle velocity components along x, y, and z axes respectively
U_{rel}	velocity relative to moving frame along the x axis
U_{xrr}, U_{xrl}	linear velocity of rear-right and rear-left wheels respectively
$\boldsymbol{u}$	control input vector
V_{rel}	velocity relative to moving frame along the y axis
V_s, V_t	terminal voltage of steering and tractive motors respectively
$\boldsymbol{v}$	vehicle velocity expressed in moving frame
$\boldsymbol{v}_O$	velocity of moving frame's origin
$\boldsymbol{v}_{N/O}$	velocity of point N relative to moving frame's origin O
$\boldsymbol{v}_{abs}$	vehicle velocity
$(v_{abs})_x$	velocity component along the x axis

$(v_{abs})_y$	velocity component along the y axis
$(v_{abs})_z$	velocity component along the x axis
W_b	lateral load transfer due to body roll
W_{bf}, W_{br}	front and rear lateral load transfers due to body roll respectively
W_{long}	longitudinal load transfer
W_r	lateral load transfer due to roll centre hight
W_{rf}, W_{rr}	front and rear lateral load transfers due to roll centre hight respectively
W_{rel}	velocity relative to moving frame along the z axis
W_s	lateral load transfer due to change in the cg's hight
W_{sf}, W_{sr}	front and rear lateral load transfers due to change in the cg's hight respectively
W_{tf}, W_{tr}	total front and rear lateral load transfers respectively
W_u	lateral load transfer due to unsprung weight
W_{uf}, W_{ur}	front and rear lateral load transfers due to unsprung weights respectively
X,Y,Z	inertial coordinate system
x,y,z	coordinate system fixed to the vehicle at c.g.
$\bar{x},\bar{y},\bar{z}$	coordinates of vehicle c.g. with respect to moving frame
y	vector of system outputs
y_i	the i^{th} system output
y_{id}	the i^{th} desired output
z	states vector in transformed coordinate
α	slip angle of tire
α_i	slip angle of the i^{th} tire
$\alpha_{ijk}(\chi)$	scalar functions
α_f, α_r	front and rear tire slip angles respectively

γ	camber angle of tire
δ	vehicle steer angle
δ_{fr}, δ_{fl}	steer angle of front-right and front-left tires respectively
δ_{rr}, δ_{rl}	steer angle of rear-right and rear-left tires respectively
ζ	vector of system states in path dependent coordinates
λ_{ij}	positive coefficients of the i^{th} sliding surface
K_i	control gain of the i^{th} sliding surface of the BLSM controller
$\bar{K}_i$	control gain of the i^{th} sliding surface of the SM controller
κ_i	PD control gain vector of the i^{th} output
$\hat{\eta}_i$	positive constant of i^{th} sliding condition
θ	yaw angle
θ_d	desired yaw angle
$\dot{\theta}_{ms}$, $\dot{\theta}_{mt}$	angular speed referred to motor shaft for steering and tractive motors respectively
$\dot{\theta}_s$, $\dot{\theta}_t$	angular speed referred to gear box output for steering and tractive motors respectively
$\dot{\theta}_{rr}$, $\dot{\theta}_{rl}$	angular speed of the rear-right and rear-left wheels respectively
$\tilde{\theta}$	yaw angle deviation from the desired path
ν	decoupling control law
ν_i	the i^{th} output decoupling control law
ξ_i, η_i	normal coordinates

ρ	relative position
ϱ	instantaneous radius of rotation
τ_s, τ_t	torque referred to output shaft of steering and tractive motors respectively
τ_{rr}, τ_{rl}	torque on rear-right and rear-left wheels respectively
$\Phi(\chi)$	diffeomorphism function
ϕ	roll angle of vehicle
χ	vector of system states
ψ_i	the i^{th} boundary layer proportional constant
φ_i	thickness of the i^{th} boundary layer
φ_{i0}	desired thickness of the i^{th} boundary layer near origin
ω	vehicle angular velocity
ω_w	angular velocity of rear wheels

Chapter 1

Introduction

1.1. Background and State of the Art

Whether it is for a wearhousing operation, manufacturing or assembly operation, or even food and supplies delivery in a hospital, material handling is reported to be a major cost of most industries at the present time. Different strategies for transfer of materials have been suggested and used in the past. Among these are hoists, cranes, conveyor belt systems, and automated or manual controlled carriers. However, demand for higher productivity, and increased emphasis on automation, have led to the use of Automated Guided Vehicles (AGVs) as a key element in transportation systems in recent years (Hammond, 1987; Tsumura, 1986).

Although, industrial adoption of AGVs may appear to be an expensive alternative, they offer several advantages over other systems. These include increased control over material movement, better floor-space utilization, increased flexibility in laying new routes, and the ability to operate in hazardous environments. In fact, the full scope of benefits offered by AGVs is yet to be perceived, and there are many that are task specific.

Sometimes called Wheeled Mobile Robots (WMR), Mobile Robots (MR) or Autonomous Vehicles (AV), AGVs are recognized by their extensive use in industry. The Materials Handling Institute (Pittsburgh) defines AGVs as battery powered driverless

vehicles that can be programmed for path selection and positioning and are equipped to follow a flexible guidepath, which can be easily modified and expanded (Bose, 1986).

1.1.1. Historical Development

The first AGVs were developed around 1950's in the USA by Barrett Electronics. Four years later the first Automated Guided Vehicle System (AGVS) was installed at Mercury Motor Freight in Columbia, South Carolina. The controllers in these vehicles were based on vacuum tube technology, and they were guided around their environments by wires buried under the floor. In these types of systems the AGV follows the wire by monitoring the voltage induced between two coils on the vehicle. This information is used to determine the steering action. These early systems were all tugger systems, and used in warehousing applications.

In the next two decades, with the rapid advances in electronic technology the controllers were first transistorized and later replaced with Integrated Circuit (IC) technology. This permitted higher circuit integration and more functional and powerful controllers, and led to a faster improvement of AGV technology. However, it was the European automotive industry this time that used AGVs in manufacturing, 23 years after their inception, and demonstrated their benefits. The first application in manufacturing was in 1974 when Volvo's automated system was installed in Kalmar, Sweden. The system had 260 carriers. Since then, many other companies adopted this technology. In 1985, more than 10,000 vehicles were produced and serviced approximately 450 plants in Europe (Muller, 1987). Based on another survey published in 1986 (Tsumura, 1986), more than 30 companies were researching this field in Japan, and over 15 companies manufactured AGVs.

After the successful implementation of AGV systems in Europe, North American companies gave this technology another chance. From less than twenty-five hundred, within two years the number of AGVs operating in the US increased to four thousand in 1986. Today, GM's operation in Oshawa, Ontario, houses one of the world's largest concentrations of AGVs.

1.1.2. AGV Types and Components

Automated guided vehicles are generally available in five physical forms, towing, pallet trucks, unit-load, fork trucks, and assembly vehicles. All other vehicles in use are either modification of the above five, or application specific. Among different categories the "unit load" types are the most widely used. In fact, they account for 90 percent of the total number of AGVs in Japan (Takahashi, 1988). These vehicles are designed to carry single or multiple loads, and they can interface with conveyors, workstations, machine tools, and a variety of automated systems.

The essential groups of components of an AGV are as follows:

1) Mechanical structure, driving and steering assembly: The mechanical structure embodies all components of the vehicle and provides the space for loading the workpieces. The drive and steering mechanisms are basic components of the vehicle's mechanical system. The drive mechanism causes movement of the vehicle at a desired speed and the steering ensures accurate tracking of the guidepath, usually within a fraction of an inch.

2) Electrical components, electronic components and interfaces, on board power and safety features: Electrical components such as relays, switches and LEDs provide trouble shooting and ease of carrier operation. Electronic components and interfaces such as sensors, servo amplifiers, and digital to analog converters are integral parts of the vehicle control system. Onboard power for computing facilities, steering and drive actuators are normally provided by lead-acid batteries. Safety aspect is also an essential feature for automated guided vehicles. A loaded AGV can weigh several tons and have a maximum speed of about 3 m/s. Therefore, adequate precautions should be taken to provide safety. Some common safety features are, contact and non-contact sensors, warning lights and perhaps horn, software and hardware brakes.

3) Guidance, and communication systems: Besides design variations, what really differentiates vehicles is the means of guidance system they use. Until very recently, the choice of guidance was limited to inductive (imbedded wire) guidepath, and chemical/optical guidepaths. Although wire guidepath is still the most widespread, they suffer from a major drawback of lack of flexibility. This leads to limited ability to change the guide path, and

high installation cost. Chemical and optical guidance technologies are commonly used in light manufacturing and office environments. Although, they offer more flexibility, the maintenance cost due to wear and tear of the guidepath is high, and vehicles' management at junctions is difficult (Premi and Besant, 1983; Boegli, 1985).

In an effort to make AGVs less dependant on fixed guidepaths, and to provide them with greater autonomy, virtual guidepaths are used (Boegli, 1985). In this generation of AGVs, the vehicles' posture (position and orientation) is obtained from sensory information, and is processed using an onboard computer. Recent advances in techniques for obtaining positional information are, dead reckoning, sonic or laser beacons, optical or ultrasonic imaging, inertial navigation, corner-cube and laser scanning (Tsumura, 1986). Often, one technique alone is not enough to obtain satisfactory results, and two, or combination of some should be used.

4) Onboard controller and computing systems: The advances in the AGV technology have been very closely tied to the development of their control system. In fact, the issue is so important, that experts believe, it was only after the developments of sophisticated control systems that AGVs gained new interest in the US (Bose, 1986). The AGV control system usually comprises four levels, factory host, central controller, floor controller, and on board vehicle controls. The vehicle control is managed by a microprocessor and on board controllers. Basic functions involved are; steering, drive, and load handling tasks. The trend in on board controllers is toward smaller physical packages, and more flexible path programming.

1.1.3. AGV Applications

Recent technological advances in guidance systems, and developments of sophisticated control algorithms have increased tremendously the potential application domain of AGVs. Current growth is mainly in the three general areas of distribution, assembly, and manufacturing. The distribution application involves carrying material to and from production process, or within warehouses. The advantages offered in this regard are similar to those provided by a truck over a freight train, that is, independent control and

flexibility. AGVs in manufacturing are mainly used for material movements between manufacturing cells in a Flexible Manufacturing System (FMS). The most impressive growth made in AGVs use has been in support of assembly. At present more than 40 percent of all AGVs work in automotive assemblies.

AGVs have also been used as moving platforms for robots. An example of this type is an AGV from Mentor Products Inc., equipped with a 7.5-ton, 25-ft-high, six axis Cybotech robot for painting aircrafts (Bose, 1986). AGVs are preferred to human operators for use in electronic productions and clean rooms. A "class 100" clean room, contains less than 100 particles of a maximum size of 0.5 μin. per 1 cu ft. A human operator typically emits 150,000 of such particles per minute. Nowadays vehicles are available to meet "class 10" clean room operations (Takahashi, 1988; Hammond, 1987). Although most AGVs have load capacities of 2000-5000 kg, some are specifically produced for heavy duty applications. AGVs with load capacities of 68 tons are being used to automatically load and unload press dies (Hammond, 1987).

Considerable interest has also been shown in using automated guided vehicles in non-manufacturing applications. These applications have a wide range, varying from food, and laundry transfer in hospitals, to carrying mail, messages, and packages in offices (Rajaram, 1988; Klafter, 1988). AGVS are currently being used as a means of transportation in places such as airports, freight stations, and ports where no manufacturing takes place (Evans, 1989). Hostile environments applications form another category where AGVs have potential use. Applications such as nuclear and explosive handling, and mining are contemplated as natural candidates for the AGV technology (Stone and Edmonds, 1992; Anderson and Donna, 1989). Military, security, space, and under water applications where the vehicle has to operate in almost entirely unstructured environment are also active research areas in the United States (Aviles et al., 1991; Schultz et al., 1991; Wilcox and Gennery, 1987; Rodseth and Hallset, 1991). AGVs and mobile robots are also developed for disabled mobility (Treherne, 1990), and patient care (Borenstein and Koren, 1987).

Given the range of applications and advantages offered by AGVs, there still remains many engineering problems to be addressed, and many potential applications to be investigated. The installation and maintenance costs are still high, and demand is for systems

to operate in structured environments, with reliable guidance and control, and reasonable path redesign costs.

1.2. Objectives of Research

Advanced automated factories require an unmanned transport system that assures efficient and flexible transfer of material in a semi-structured environment. Automated guided vehicles are important components of this modern automated transport system. Increasing the system efficiency and throughput requires the use of heavy vehicles travelling at high speeds. The main objective of this research is to contribute to the fundamental understanding of the dynamics and control of automated guided vehicles for high speed and high load applications.

A survey of pertinent literature reveals that experimental AGVs and WMRs with maximum weight of 120 kg and very low speeds have been the focus of research in the past (Petrov, 1991; Borenstein and Koren, 1987). Wheelbase designs of these vehicles are either simple differential drives or steerable wheels. However, a typical industrial AGV weighs around 350 kg and is capable of carrying 500 kg loads at its centre. These vehicles can typically travel at the maximum speed of 1 m/sec. In this research a transport interfactory AGV with one ton capacity is considered. The unloaded vehicle including the lifter weighs 700 kg, and is provided with pneumatic tires and suspension for high load applications. The vehicle has a maximum speed of 3 m/s.

Dynamics

To validate the controller performance, a suitable vehicle model that can accurately describe the behaviour of the AGV is required. The models used in the surveyed literature are mainly kinematic models (Sordalen and Canudas, 1992; Kanayama et al., 1990; Sung et al., 1989). This is due to the imposed simplification of low speed and light load conditions under which these vehicles operate. However, for practical AGVs designed to transport heavy loads and travel at high speeds, dynamic modelling of the vehicle is essential. A few researchers have derived dynamic models for AGVs (Hamdy and Badreddin, 1992; Saha and

Angeles, 1989). These models however, are not valid for heavily loaded vehicles due to simplifying assumptions, and inaccurate tire modelling. In this work, a 3-DOF nonlinear dynamic model that represents the behaviour of the real vehicle under imposed condition is developed. The tire model is also considered. The effects of roll degree of freedom, suspension, lateral and longitudinal load transfer are also taken into account. In order to investigate the relevance of the dynamics in the AGV model, simulations of the performance of a kinematic model are compared to those of the dynamic model. Also, 3-DOF and 2-DOF dynamic models are compared for a 90-degree left turn.

Control

The main problem in controlling AGVs lies in the fact that these systems possess less control inputs than system outputs. A review of literature reveals that dynamic models of AGVs have scarcely been investigated in connection with control design. Previous works on the controller design of such systems are generally based on the kinematic models. However, dynamic-based control of these vehicles is the subject of recent research (d'Andrea et al., 1992; Hemami et al., 1992). Linearization by feedback is investigated for the simple wheel base configurations with solid tire models. However, the problem is not completely resolved for AGV's with complicated wheel base configurations and realistic models. In a different approach, linearized dynamic model of Automated Transient Vehicles (ATV) with pneumatic tires is used for control design (Smith and Starkey, 1994; Jurie et al., 1994). Though, in this approach, the problem of suitable dynamic-based controller for emergency manoeuvres and curved routes with small radii is still the subject of more research.

Limitations of proportional controllers under different conditions are shown in this thesis. Clearly, a proportional controller based on mere information of heading and orientation errors is not adequate for the particular conditions under study. A dynamic-based approach for a car-like AGV has been sought. For the controller design, a slippage free dynamic model comprising the steering dynamics and the effect of actuators is considered. The multi-input multi-output feedback linearization technique is employed to transform the given nonlinear system into two subsystems. The choice of different output functions is

studied, and a number of controllers for the linearized control subsystem are designed. The sliding mode control structure is adopted to improve the robustness of system in the presence of parameter uncertainty, modelling errors, and disturbance. To eliminate undesirable chattering, the boundary layer technique is employed. The robustness of the boundary layer sliding mode controller is further enhanced by utilizing simultaneous variable boundary layer and multiple sliding surfaces strategies.

1.3. Thesis Outline

This thesis consists of seven chapters. A review of the general concept of automated guided vehicles, and historical advances made in this field is presented in this chapter. Related issues like classification of types, comprising components and their functions, and different application areas are also discussed. The objective of the proposed research is also included.

Chapter 2 is devoted to the review of existing literature. A particular emphasis is given to the areas most relevant to the proposed study. In this respect, recent works on kinematic and dynamic modelling are presented. The Control problem of these vehicles is presented. Different approaches to the design of the control law for vehicle's motion about a geometrical path, a time-index trajectory, or fixed points in posture space are also discussed. Kinematic and dynamic-based approaches to control design are reviewed separately.

Some general notation usually used in vehicle dynamics, and description of mechanisms of force and moment generation by pneumatic tires are discussed in Chapter 3.

The general equations of motion are presented in Chapter 4. Assumptions applicable to the particular case under study are discussed. Two models are presented: the first is a 3-DOF nonlinear model comprising yaw, lateral, and roll degrees of freedom, considering a nonlinear tire model, and load transfer. The second is a 2-DOF model comprising yaw and lateral degrees of freedom, and linear tire model. The models also incorporate steering dynamics, the effect of actuators, differential gear box, steering and tractive gear boxes.

Dynamic-based control of AGVs is presented in Chapter 5. The 2-DOF nonlinear model is used to design a new control strategy for 4-wheel front steering AGVs. Exact input-output feedback linearization is applied to linearize the slippage free vehicle model. The boundary layer sliding mode technique is used to guarantee the robustness, and account for disturbances and modelling errors. This controller is later modified to enhance its performance and robustness by applying simultaneous variable boundary layer and multiple sliding surfaces strategies.

Chapter 6 deals with the computer simulations and discussion of results. The kinematic model, 2-DOF, and 3-DOF dynamic models are compared to demonstrate the necessity of proper dynamic modelling. The path tracking performance of the vehicle under different control schemes has been studied. By comparing proportional derivative, sliding mode and modified sliding mode controllers it is illustrated that by implementing the new control strategy significant improvement in tracking performance can be achieved.

Finally, Chapter 7 concludes with a summary and general discussion of results. An outlook for future work is also presented in this chapter.

Chapter 2

Literature Survey

2.1. Introduction

The studies of Automated Guided Vehicles and Wheeled Mobile Robots are fundamentally multi disciplinary, incorporating technologies from different disciplines like: mechanical engineering, electrical engineering, control theory, computer vision, robotics, estimation theory, artificial intelligence, operation research, programming languages, and physics (Cox and Wilfonge, 1990). Consequently a vast scope of knowledge is directly or indirectly relevant to this area of research. A classification of research works on AGVs follows:

- Task level planning, decision making and control
- Navigation
    - Map making and real world modelling
    - Path planning, and motion planning
    - Kinematics, dynamics and control
    - Intelligent AGVs and WMRs
- Sensors and sensing strategies
- Applications
    - Flexible manufacturing system
    - Systems and successful applications

A survey of papers discussing relevant approaches and techniques in areas that contribute most to kinematics, dynamics and control of AGVs and WMRs is presented in this chapter.

2.2. Wheelbase Configuration

This section emphasis is on mechanical configurations mostly used in industry. Wheelbase design of most wheeled land vehicles falls into one of two categories, steered wheeled vehicles or differential drive (powered wheel steering) vehicles (Cox and Wilfonge, 1990).

The configuration of the first class typically consists of a fixed rear axle and steered (or sometimes driven) front wheels. The tricycle wheelbase, with only one front steered wheel, is a common example in mobile robots and automated guided vehicles. A general four wheeled vehicle is another example of this category, where steering is done by an Ackerman steering linkage. While four wheel vehicles offer more stability and more traction when all wheels are driven, three wheels offer less complex steering, and the possibility of suspension elimination.

The familiar example of a differentially driven vehicle is a military tank, in which steering is performed by differences in the two tracked wheels velocities or torques. Differentially driven AGVs, are commonly equipped with one or more castors in order to provide stability. An advantage of a differential drive vehicle is the ability to turn with zero turn radius. This is a marked advantage since physical limits on the steering angle of a steered wheeled vehicle can cause a large turning radius, and make manoeuvring more difficult in a cluttered environment.

2.3. Kinematics and Dynamics

The study of kinematic and dynamic modelling of automated guided vehicles and wheeled mobile robots is very recent, though research on such vehicles dates back to the late 1960's. In this section the issue of kinematic and dynamic modelling is considered briefly.

2.3.1. Kinematic Modelling

The kinematic modelling of automated guided vehicles differs from that of manipulators in several aspects. Among these: a) AGVs are closed-chain mechanisms, b) for AGVs, only some degrees of freedom are actuated, c) both lower and higher joints (surface and point joints) are present in an automated guided vehicle, whereas a stationary robot arm has only lower joints (McKerrow, 1991). Consequently, AGVs cannot be modelled using Denavit-Hartenberg convention, which is commonly used to model robot arms.

Muir and Neuman (1986, 1987) presented a kinematic modelling methodology for wheeled mobile robots using the transformation approach. Sheth-Uicker (1971) convention is used to model the kinematics. This method can be thought of as a complement to the transformation modelling technique employed for robot manipulators. Although, the proposed method may increase complexity in the modelling for some cases (Saha and Angeles, 1989), the merit lays in its ability to be generalized into any wheelbase pattern, with different number of wheels and various combination of driving/driven, steerable/nonsteerable wheels.

Alexander and Maddocks (1989) examined the questions of what planar rigid body trajectories are accessible for a given wheel pattern, and what steering and drive rates are required to reach these trajectories, assuming an ideal rolling of all wheels. The authors also addressed the analysis of slippage, which may occur for incompatible steering and wheel velocities.

2.3.2. Dynamic Modelling

Although, much work has been done on some aspects of AGVs such as navigation (Tsumura et al., 1981; Fujiwara and Kawashima, 1981; Koren and Borenstein, 1991), and path planning (Graettinger and Krogh, 1989; Barraquand et al., 1990; Shiller and Gwo, 1991), very little attention is being given to the dynamic modelling of AGVs and WMRs (Cyril et al., 1989; Boyden and Velinsky, 1994).

Muir and Neuman (1988) presented a modelling scheme that is based on Newtonian dynamics, force/torque propagation notion, frictional coupling, and the kinematic transformation approach. This modelling technique can be applied to multibody robotic mechanisms having the following characteristics: (1) closed-chains, (2)friction, (3)higher pair joints, (4) unactuated joints and (5) unsensed joints.

In another approach, Saha and Angeles (1989), and Cyril et al. (1989) presented a general methodology for dynamic modelling of wheeled mobile robots and AGVs of arbitrary wheelbase configurations. The method is based on the Hybrid Newton-Euler, Euler-Lagrangian and Natural Complement methods.

Using Lagrangian formalism and differential geometry approach, d'Andrea-Novel et al. (1991) derived a general dynamical model for three wheeled mobile robots with nonholonomic constraints. The authors demonstrated that static feedback allows reduction of the system to the stage that stabilizing input-output linearization is possible.

Agullo et al. (1989) considered the dynamics of AGVs with directionally sliding wheels. Such wheels can freely slide along a direction at a definite angle from wheel plane. The virtual work method is used to derive the dynamic equations of motion.

Hamdy and Badreddin (1992) presented the dynamic modelling of a WMR to estimate the occurrence of slip, and slip magnitude. Once this is done, the results are used to correct sensed forward navigation.

All these approaches are based on solid tire assumptions. However, dynamic modelling can be accomplished using the classical techniques based on D'Alembert's principal. This approach is usually used to model road and off-road vehicle dynamics considering the pneumatic tire model (Ellis, 1994; Wong, 1993). The simulation package of Huang (1991) employs a dynamic model for a 2-DOF AGV which is based on classical method. However, this approach is not general in nature.

Boyden and Velinsky (1994) discussed the necessity of dynamic modelling of AGVs and WMRs for high load applications. The authors show that the use of kinematic models must be limited to vehicles that operate under very low speeds, very low accelerations and under lightly loaded conditions.

2.4. Control

Based on the type of constraints, one can classify mechanical systems as holonomic or nonholonomic systems. A mechanical system in which all joints are the result of holonomic constraints is called holonomic mechanical system. On the other hand, if the mechanical system has at least one nonholonomic constraint, it is known as a nonholonomic mechanical system. Wheeled vehicles are typical examples of mechanical systems with nonholonomic constraints. Though, the theory of mechanical systems with nonholonomic constraints has been developed at the end of the last century by authors such as Appell and Hamel (Campion et al., 1990), the control of these systems has only been studied very recently.

2.4.1. Controllability

Similar to robot manipulators, commonly used wheeled vehicles subject to nonholonomic constraints are usually completely controllable in their configuration space. This is true when the number of actuators is equal to the number of degrees of freedom. (Bloch and McClamroch, 1989; Samson, 1991b; d'Andrea-Novel et al., 1992; Zhao and BeMent, 1992). However, unlike manipulators, the controllability of these systems does not imply the existence of stabilizing feedback. (Bloch and McClamroch, 1989; Samson and Ait-Abderrahim, 1991c). This negative result can be explained by a theorem in the nonlinear control theory due to Brockett (1983).

Bloch and McClamroch (1989) first demonstrated that smooth feedback cannot stabilize a nonholonomic system to a single equilibrium point. Bloch et al. (1990) also showed that these systems are small-time locally controllable at the origin. In later publications, the authors explain a general procedure for constructing piecewise analytic state feedback to stabilize the systems about a point (Bloch et al., 1992).

Campion et al. (1990) showed that nonholonomic systems are strongly accessible despite the structure of the constraints. Although, smooth pure feedback cannot asymptotically stabilize these systems, it can globally marginally stabilize them.

2.4.2. Proportional Controller

Sometimes referred to as sensor-based controllers, in this approach usually some information about position and heading errors are analysed to decide the steering action of AGVs.

Rajagopalan et al. (1992), proposes a dual camera guidance for an AGV with pneumatic tires, where accurate path tracking, and faster alignment of the front and rear ends of the vehicle with the path is required. Both front and rear position and orientation information are used to obtain different control schemes for straight and curved paths. The controller gains are changed on-line, based on vehicle location relative to the track. Simulation is used to compare the results with the case of single camera guidance.

Usually a proportional gain is used to feedback the sensory information, though nonlinear control laws are also reported. Hemami et al. (1990) present a nonlinear controller to adjust the steering of a front drive/front steering vehicle. The dynamics of the vehicle with pneumatic tires is simulated to compare the tracking capability of the system with the one using linear proportional feedback of orientation and distance errors. Based on the simulation results, improvement in performance is reported. However, practical difficulty to measure the yaw rate term included in the nonlinear controller is not addressed.

2.4.3. Kinematic-based Control

The problem of designing a control law to stabilize motion about a desired trajectory, $P_d(t)$, where t is the time, is specified as trajectory tracking. Samson and Ait-Abderrahim (1991a) investigated trajectory tracking of a powered wheel steering mobile robot. The authors show that by introducing a virtual reference cart, which has a predefined trajectory, feedback stabilization in both position and orientation becomes possible as long as the reference cart is moving.

Kanayama et al. (1990) developed a stable control law for precise trajectory tracking of autonomous vehicles. The method is suitable for vehicles capable of dead reckoning and distinct specification of the reference path and its position. Lyapunov function is used to

prove the stability of the control law. A condition for critical damping has been obtained through linearizing the systems differential equations. Then, this condition is used to find appropriate parameters for the specific controller. In order to handle non-smooth paths and avoid slippage, a velocity/acceleration limiting scheme is introduced. Simulation and experiments of the Yamabico-11 mobile robot are carried out. Close agreement between theory and experimental results is reported.

The design of a control law to stabilize motion about a desired geometric path, $P_d(s)$, where s is any convenient path parameter, is referred to as path following or path tracking in the literature. Among existing path tracking schemes, some approaches obtain the steering angle based on vehicle orientation and position errors. Usually, gains for these errors are chosen by trial and error (Kanayama et al., 1988; Nelson and Cox, 1988). Other methods continuously generate paths that converge to the reference path from the deviated vehicle position, then using simple kinematics the generated paths are converted into steering angles and wheel velocities (Shin et al. 1992; Pears and Bumby, 1991).

Nelson and Cox (1988) described a path control system for Blanch, an autonomous robot cart. The on-board navigation system comprises a reference state generator, an error feedback controller, and odometers to sense cart's location. The cart controller consists of path and motor controllers. At the path control level, a feedback controller based on normal and heading errors is used for steering control, and one based on tangential and speed error is used for drive control. Simulation and experimental results are reported.

Kim (1987) presented a theoretical optimal (and suboptimal) steering control of a wire-guided AGV. Since for tracking a circular reference path steady state error cannot be eliminated by simple proportional control law, an optimal proportional plus integral (PI) controller is employed. Also, the effect of design parameters of the AGV, such as forward velocity, wheel radius, and sensor position is studied.

Pears and Bumby (1991) formulated a steering control method for steering control of a differential drive AGV. The control law is based on generating a local demand heading pointing toward the vehicle's current reference path, with a gradient proportional to the local normal distance error. This demand heading is used to generate a command turning curvature in proportion to the heading error. To have the vehicle's performance independent

of velocity, controller parameters are derived as functions of velocity. Both, simulation and experimental tests for tracking straight and circular paths are done. The steady state offset error observed for a curved path, is compensated for by treating the reference curvature as an input.

Work on designing a control law for stabilizing the vehicle about a fixed point in the configuration space is another issue which has been addressed recently (Canudas de Wit et al., 1993). As explained earlier, the study of this class of problems show that the kinematic and dynamic model properties such as: controllability, linearization, decoupling, and stabilization, depend on the selected coordinates. Also, the kinematic and dynamic model of nonholonomic wheeled vehicles derived in the posture space cannot be stabilized by smooth pure state space feedback laws. To solve this problem, the following three approaches have attracted more attention, time-varying feedback laws (Samson, 1990b), discontinuous or piecewise smooth controllers (Bloch et al., 1990; Canudas de Wit and Sordalen, 1992), and hybrid strategy (Pomet et al., 1992).

2.4.4. Dynamic-based Control

A survey of the literature published on AGVs and WMRs shows a significant amount of research is being done on their kinematic modelling and control. Whereas the dynamics and control of these systems are subject of more recent investigations, and are not fully studied (Sarkar et al., 1994; Canudas de Wit and Roskam, 1991). Dynamic-based control is not only a natural extension of the kinematic approach, but it is also essential for the proper control of these systems (Deng and Brady, 1993a, Mehrabi et al., 1993). This is true specially in practical applications where load, required drive power, and dynamic constraints for feasible trajectories have to be considered (Boyden and Velinsky, 1994; Canudas de Wit and Roskam, 1991; Fraichard, 1993).

In the following sections, the dynamic-based control is considered. Among existing schemes, some approaches design controllers based on rigid vehicle dynamics. The tire model is usually ignored in these methods. Other approaches are based on the vehicle

dynamics considering the pneumatic tire model and characteristics. These two strategies are separately discussed.

2.4.4.1. Controllers Based on Rigid Vehicle Dynamics

Trajectory tracking of a three wheeled vehicle is considered by d'Andrea-Novel et al. (1991). Using Lagrangian dynamics, the authors show that a static feedback can reduce system dynamics to a form for which stabilizing input-output feedback linearization is possible. No simulation of a practical application is presented.

Iida and Yuta (1991) proposed a controller structure for steered wheeled mobile robots. A feed forward compensator comprising the inverse dynamics of the vehicle, is used to cancel vehicle dynamics, and control the wheels' angular velocities. Simulations with 10 percent errors between controller parameters and vehicle dynamics, and experiment on the Yamabico mobile robot has been performed. Improved results for a feedforward controller are reported.

Deng and Brady (1993a, 1993b) applied Lagrange formalism and the feed back linearization method for trajectory tracking of a wheeled vehicle. The model is a 2-DOF, front driven and steered tricycle. Kinematic constraints are treated as a part of the control model. However, no simulation or comparison of results is reported to validate the method.

When the input output linearization is used to design controllers for nonlinear dynamic systems, the effectiveness of the control design based on the reduced order model depends on the stability of the internal dynamics (Slotine and Li, 1991). Yun and Yamamoto (1993) addressed the stability of internal dynamics and zero dynamics of a differential drive mobile robot. Using a novel Lyapunov function, the authors prove that the zero dynamics is always stable. However, the internal dynamics of the system is asymptotically stable when the reference point is commanded to move straight forward, and unstable for backward motion of the reference point. Both simulations, and experimental tests on a TRC LABMATE mobile platform were done to verify the results.

The input-output linearization and zero dynamics of a differential drive mobile robot is discussed by Sarkar et al. (1994). It is shown that the zero dynamic of the system is

Lagrange stable. Using simulations, control algorithms for trajectory tracking and path following are compared. It is concluded that, while trajectory tracking is preferred for situations where the vehicle must follow a curve in space-time coordinates, path following is a more realistic control strategy for vehicle control applications. However, the approach to controller design of path following is not general, and it depends on the tracking path.

Path tracking of a carlike mobile robot is considered by DeSantis (1993). Both kinematics and Newtonian dynamics are considered for planar motion with no side slippage. It is shown that a controller capable of tracking an assigned path may be computed in terms of the lateral, heading, and velocity offsets. A linearized, time invariant model is developed for the special case where the path is straight or circular curve, and the tracking velocity is constant. The author suggests a decoupled structure controller based on classical techniques such as PID or pole placement for the case where the offset is kept small. Nevertheless, no simulation or practical application is addressed to support the results. In more recent works, a similar approach is applied to controller design of double steered car-like robots (DeSantis, 1995a), and differential drive WMRs (DeSantis, 1995b).

When a nonlinear system cannot be stabilized at an equilibrium point by smooth state feedback, one alternative is to consider discontinuous feedback, as explained earlier. However, another possibility consists of considering smooth time-varying feedback was first introduced by Samson (1990b). Assuming the inputs to the system are wheels torque, Samson and Ait-Abderrahim (1991c) show that time-varying feedback can be applied to the dynamic model of a 2-DOF differential drive mobile robot. However, no simulation or experimental application of torque control is reported.

Some works on dynamic-based control design are motivated by the need for planning velocity profiles along the path so that these profiles comply with torque limitations, or verification of wheel-ground contact forces. Canudas de Wit and Roskam (1991), consider path following of a 2-DOF WMR, taking into account path and input torque constraints. Dahl and Nielsen (1989) on-line reference profile generation method is employed to reshape a nominal velocity profile to comply with the input torque constraints. Dynamic-based control is used for the motion control problem. The dynamic model has been transformed into a two-dimensional sub space (tangential velocity and orientation), then used to design

a computed torque type feedback law. Improvement of performance under input torque saturation is reported based on experiments with micro-WMR KITBORD. However, when the cart slips the feedback law cannot correct the induced path error. Also, the problem of path admissibility remains to be studied. This study is restricted only to path generation by straight segments.

To verify wheel-terrain contact forces and avoid slippage, Necsulescu et al. (1994) use Newtonian dynamics for a 2-DOF, three wheeled mobile robot. Motion control is done by the input-output linearization for the dynamic model of the system in two-dimensional operational space. The system is linearized with respect to the third differentiation of outputs (x, y). However, problems of practical measurement of acceleration, and stability of internal dynamics have not been addressed.

Since the exact model of the nonlinear vehicle system is not available when doing input-output linearizations, these approaches suffer form the fact that "no robustness is guaranteed in the presence of parameter uncertainty and unmodeled dynamics" (Slotine and Li, 1991).

2.4.4.2. Controllers Based on Vehicle Dynamics with Tire Model

The lateral and yaw motion dynamics of a vehicle are significantly governed by parameters such as vehicle speed and road tire interactions. These parameters are not constant during vehicle operation and must be considered in controller design for a more realistic speed and load ranges (Matsumoto and Tomizuka, 1992).

An approach to obtain optimal gains for a controller based on feedback of the position and orientation is proposed by Hemami et al. (1992). A linearized vehicle dynamic model is considered to derive the optimal control law. Minimization is based on a quadratic performance index of the offset, orientation errors, and the steering angle. Simulations for path tracking of an AGV with front wheel steering are depicted. However, performance of the designed controller is limited to straight line trajectories, and compared with other works, the effectiveness of the proposed method is not investigated.

Mehrabi et al. (1991), considered path following of a double steered AGV with pneumatic tires. A control law based on position and orientation errors of the mass centre is implemented. Simulations for straight line path tracking were conducted. In a more recent paper (Mehrabi et al., 1993) the authors report results on the CONCIC III experimental vehicle. Using dead reckoning reasonably good performance is reported except for the case of curvatures with sharp changes.

Makino (1993) studies hunting reduction of an automated guided vehicle. The three wheeled AGV has a total weight of 1700 kg with a maximum speed of 60 m/min. Navigation is based on guiding tapes along a straight line. Linearized dynamic model of the vehicle was used to design a control system. Controller gains were obtained based on simulation and experiments. Reduction in hunting motion is observed, but the problem of motion control along curved routes is not addressed.

To decide between 2-DOF model and 3-DOF models of WMRs, and Automated Transit Vehicles (ATVs) for control purpose, Cheng and Mehrabi (1992) proposed a dimensionless number called roll number. Two degrees of freedom models incorporates lateral and yaw motions, whereas 3-DOF includes roll motion also. The linearized dynamic model is used for this study; however, the suspension dynamics and the lateral load transfer are not considered.

Other studies available in the literature focus on the handling characteristics and directional stability of the Automated Highway Vehicles (AHV), and automated transit vehicles (Jurie et al., 1994; Matsumoto and Tomizuka, 1992; Shladover et al., 1991; Fenton and Mayhan, 1991). Vehicle dynamics becomes very important in designing controllers for AHVs, due to the higher speeds and accelerations at which they operate (Smith, 1991). However, unlike AGVs, a linearized dynamic model is often used to describe the structure of AHV controllers. This is mainly due to their operational environment where only large curvature routes or straight paths are encountered.

Among model-based approaches to controller design of AHVs, two have attracted more attention in the literature, one involving classical control theory (Fenton et al., 1976; Cormier and Fenton, 1980), and the other optimal control theory (Shladover, 1978; Johnston and Assefi, 1979; Hatwal and Mikulcik, 1986).

Chapter 3

Vehicle Dynamics

3.1. Introduction

Among different approaches to model the dynamics of automated vehicles, two have been considered more frequently, the Lagrangian formalism for nonholonomic systems (d'Andrea-Novel et al., 1991; Saha and Angeles, 1989; Cyril et al., 1989), and the Newtonian dynamics (Jurie et al., 1994; Muir and Neuman, 1989; Nisonger and Wormley, 1979). While the first method is based on rigid body assumption of the vehicle and wheels, the second is commonly used to model the vehicle incorporating pneumatic tires. Throughout this study the second approach has been implemented for the purpose of motion analysis, then simplified to allow controller synthesis.

Due to reliance of the adopted dynamic technique upon the understanding of the pneumatic tire and ground interactions, this chapter is devoted to review some general notation usually used in vehicle dynamics, and description of mechanisms of force and moment generation by pneumatic tires.

3.2. Vehicle Models and Degrees of Freedom

As a rigid body a vehicle has six degrees of freedom, translation along the x, y, and z axes and rotation about these axes as represented in Figure 3.1. By inclusion of these motions in the analysis, complex dynamic models can be developed for simulation purposes.

Fortunately, the literature in this regard indicate that dealing with the whole complete model is not usually required (Jurie et al., 1994; Wong, 1993). Simplified versions of dynamic models are being proposed for certain conditions that are reasonably accurate. Within the scope of present study it is well accepted that a dynamic model that takes into account the lateral, yaw, and roll motions of the vehicle is quiet adequate to represent the vehicle's motion (Xia and Law, 1992; Shladover et al., 1978). Even simpler models that consider yaw and lateral motion are reported to give satisfactory results for controller design purposes under certain condition (Jurie et al. 1994; Fenton and Selim, 1988).

3.3. Mechanics of Pneumatic Tires

It has often been said that "the critical control forces that determine how a vehicle turns, brakes, and accelerates are developed in four contact patches no bigger than a man's hand" (Gillespie, 1992). Apart from gravitational and aerodynamic forces, all other major forces acting on a vehicle result from tire-ground interaction. Extensive research has been devoted to analyse the mechanism of this interaction (Pacejka and Bakker, 1993; Palkovics and Elgindy, 1993; Bakker et al., 1987; Dugoff et al., 1977). Thus, an understanding of the tire mechanics on hard surfaces is essential to study the dynamic behaviour of ground vehicles (Wong, 1993). In what follows some basic properties of pneumatic tires, and the resulting forces and moments developed at the contact patches are discussed.

3.3.1. Tire Forces and Moments

To assist precise description of tire characteristics, forces, and moments, a set of axes with the origin located at the centre of the tire to road contact is adopted. The X axis is pointing in the forward direction, and the Z axis perpendicular to the road pointing upward.

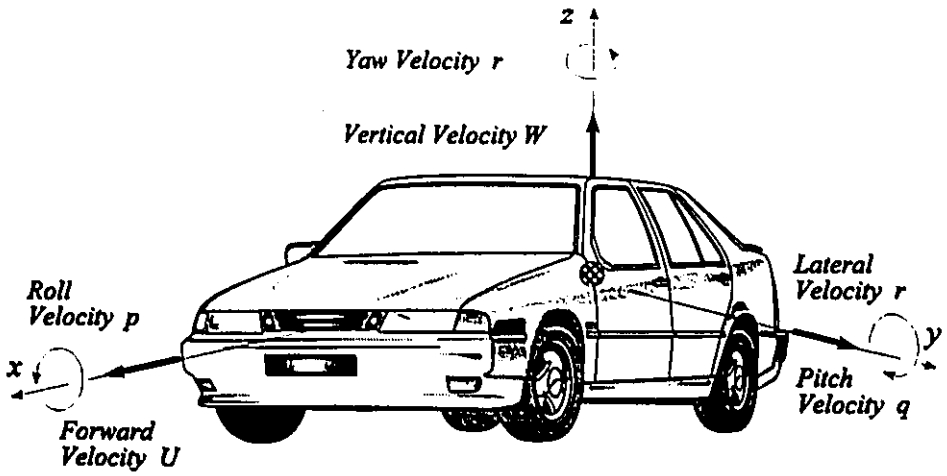

Figure 3.1 The ISO vehicle dynamics axis system

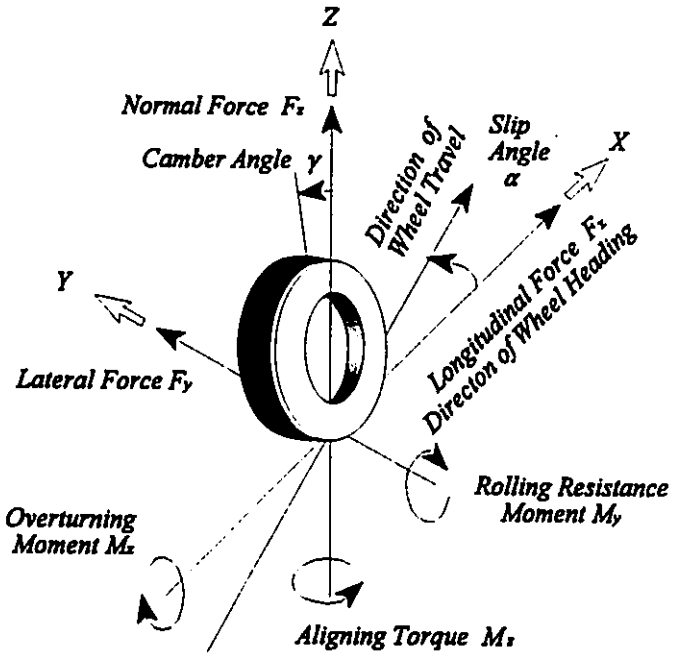

Figure 3.2 Tire axis system

The ground reactions on the tire are described by three forces and three moments as shown in Figure 3.2, and are defined as:

- Longitudinal Force (F_x): The components of the resultant force acting on the tire by the road, in the X-direction. The force component in the direction of wheel travel is called Tractive force. Tractive forces are generated during acceleration and braking.

- Lateral Force (F_y): The components of the force acting on the tire by the road, in the Y-direction. Lateral forces are developed when the wheel is steered at an angle, and they have a dominant role on vehicle control.

- Normal Force (F_z): The components of the force acting on the tire by the road, in the Z-direction.

- Overturning Moment (M_x): Moment acting on the tire by the road, about the X-axis.

- Rolling Resistance Moment (M_y): Moment acting on the tire by the road, about the Y-axis.

- Aligning Moment (M_z): Moment acting on the tire by the road, about the Z-axis.

Also, two important angles are associated with the rolling tire, defined as:

- Slip Angle (α): The angle formed between the direction of wheel heading and the direction of travel.

- Camber Angle (γ): The angle formed between the Wheel plane and XZ plane.

More detailed description of these forces is given in the following sections.

3.3.2. Rolling Resistance

One of the major resistance forces acting on a vehicle is the rolling resistance of tires. In fact at low speeds, on level and hard pavements the rolling resistance is the primary motion resistance force. At least, seven mechanisms are responsible for the rolling resistance, these are energy losses due to deflection of the tire side walls and tread elements,

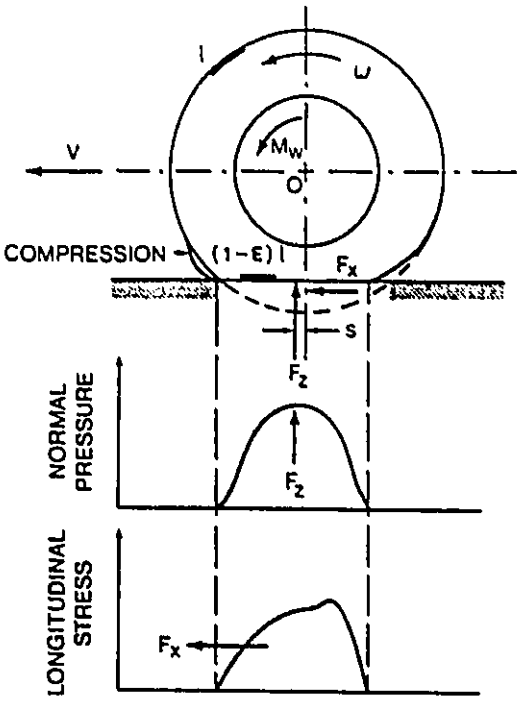

Figure 3.3 Tire behaviour when a driving torque is applied (Clark, 1971).

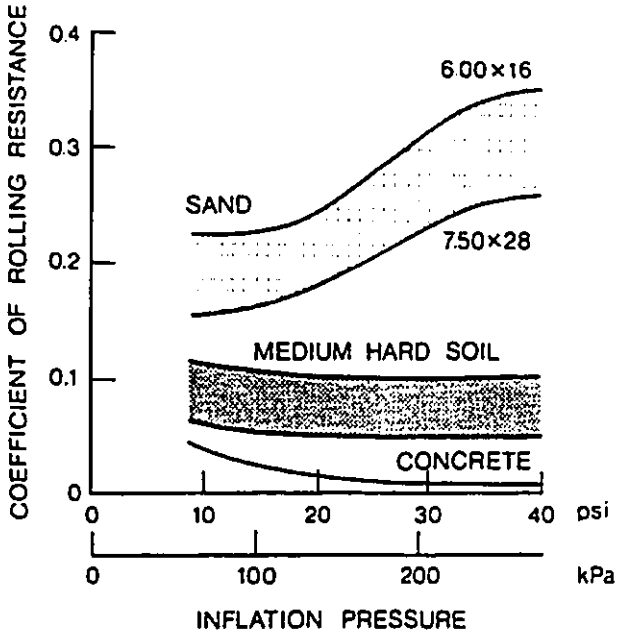

Figure 3.4 Typical variation of rolling resistance with inflation pressure for different surface conditions (Taborek, 1975).

scrubbing in the contact area, air drag on the inside and outside of the tire, tire slips in longitudinal and lateral directions, and energy loss on bumps (Gillespie, 1992).

When a tire is rolling, the front tire treads in ground contact are deflected. This results in a higher normal pressure at the front half of the contact patch than in rear half as shown in Figure 3.3. Thus, the centre of normal pressure is shifted to the front, causing a moment about the axis of rotation called the rolling resistance moment. In a free-rolling tire, to satisfy equilibrium condition, this moment should be balanced with a force known as the rolling resistance. The ratio of rolling resistance to the normal load is a dimensionless factor, and defined to be the coefficient of rolling resistance.

Several factors affect the rolling resistance of a tire (Wong, 1993): a) The tire structure, that is, material and design, and b) tire operating conditions such as tire temperature, inflation pressure, velocity, and diameter. For instance, variation of rolling resistance coefficient with inflation pressure is shown in Figure 3.4.

The complex relationship between rolling resistance, structural, and operational parameters of a tire makes it difficult to obtain an analytical method for predicting the rolling resistance. However, based on experimental results many empirical formulas have been proposed. At lower speeds this relationship can be represented as

$$F_r = .01(1+U/223.7) \tag{3.1}$$

where U is speed expressed in m/s.

For the AGVs at the speed range of this study the effect of speed may be ignored, and the average value of F_r for a specific operating condition may be used. Table 3.1 lists some typical values for rolling coefficient (Wong, 1993; Gillespie, 1992).

Tire Type	Surface		
	Concrete	Medium Hard Surface	Sand
Passenger Car	0.015	0.08	0.30
Truck	0.010	0.06	0.25
Tractor	0.020	0.04	0.20

Table 3.1 Coefficient of rolling resistance (Taborek, 1975).

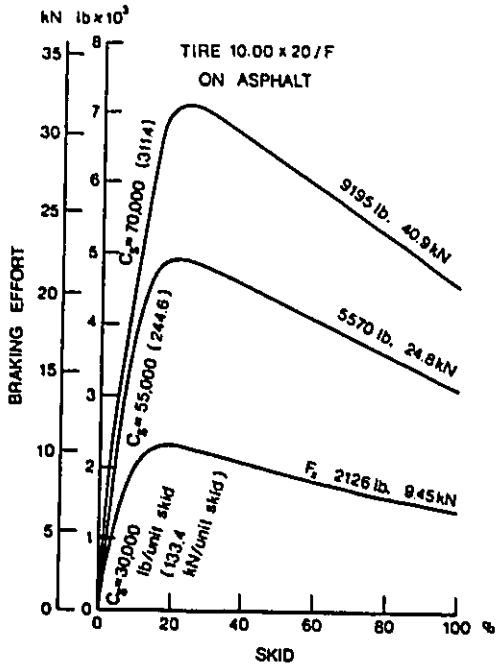

Figure 3.5 Variation of braking effort with normal load for a truck tire (Ervin, 1975).

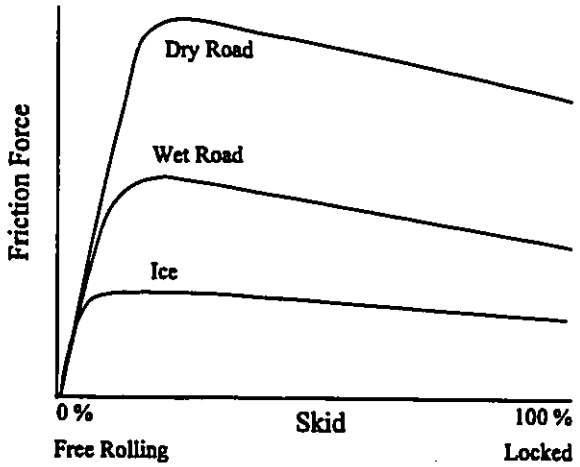

Figure 3.6 Effect of surface condition on braking effort (Gillespie, 1992, notations are modified for consistency).

3.3.3. Tractive/Braking Effort

When a driving torque is applied to a tire and the vehicle accelerates, a tractive force is developed at the tire-ground patch. The tread elements are compressed as they enter the contact area, resulting in a distance travelled by the tire less than that in free rolling Figure 3.3. This is usually referred to as longitudinal slip. Whereas in braking, the tread elements stretch before entering the contact area causing a distance travel by the tire greater than that of a free wheel. This phenomenon is called the skid. The severity of tractive and braking effort

are measured by the longitudinal slip and skid. Several parameters affect the tractive and braking effort of a tire these are; road characteristics, surface condition, normal load, and vehicle speed (Wong, 1993). The variation of braking effort with the normal load and surface condition are shown in Figure 3.5-3.6.

3.3.4. Cornering Properties of Tires

Vehicle handling characteristics mostly depend on the cornering properties of the tire. In fact, the tire should develop the lateral forces necessary to control the vehicle direction during turns and lane change manoeuvre.

3.3.4.1. Cornering Force

When a rolling tire is not subjected to any side force, it will move in a direction coinciding with the wheel plane. However, if a lateral force is applied to the tire, it drifts to the side, and moves along a path at angle α with the wheel plane. This angle is known as slip angle. The side slip of a tire is mainly due to the elastic properties of the tire, and the mechanism responsible for that is better perceived considering the Figure 3.7.

For a rolling tire the tread elements that are not in contact with the ground are undeflected, and they have the same direction as the heading. However, as the tire advances the tread elements reach the contact surface, and deflect toward the direction of travel

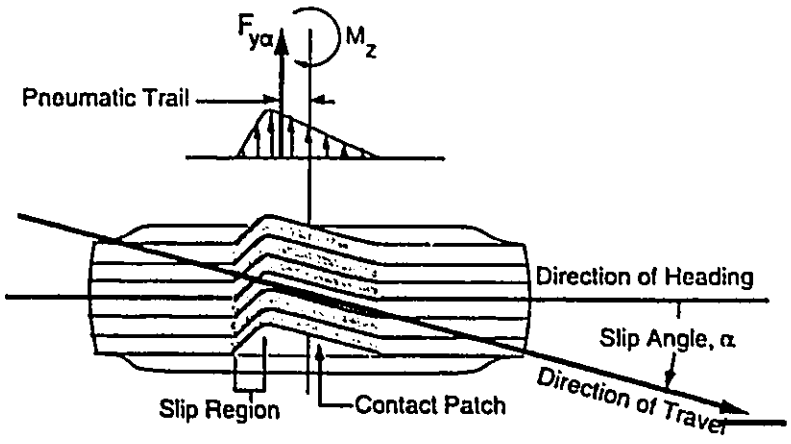

Figure 3.7 Deformation of a rolling tire due to lateral force (Gillespie, 1992, notations are modified for consistency).

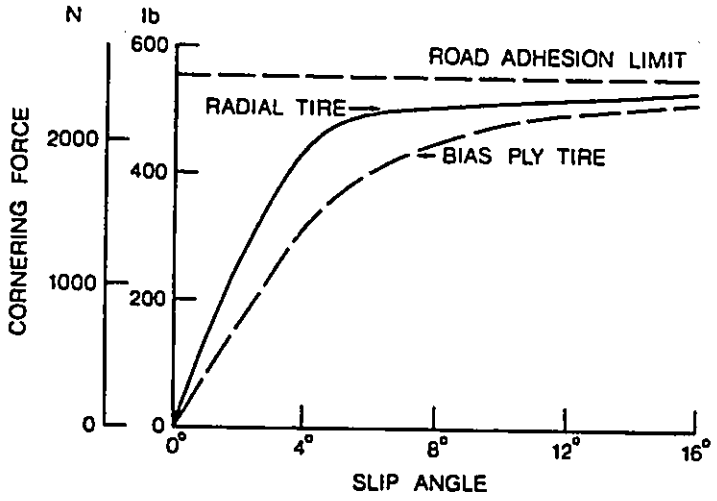

Figure 3.8 Typical characteristics of the cornering force (Wong, 1993).

producing a lateral force. Further advancement of the tire generates larger forces, up to a point where the lateral force overcomes the friction available and a slip occurs. (The slip region is in the rear edge of the contact patch). The point of action of the resultant force, $F_{y\alpha}$ is behind the contact patch at a distance called the pneumatic trail, t_p. The resultant force at zero camber angle is called the cornering force (Wong, 1993; Gillespie, 1992).

Extensive studies have been done to explain the relationship between the cornering force and slip angle for various tires. Most analyses suggest a typical characteristic as shown in Figure 3.8. It can be seen that for slip angles less than 4 degrees the cornering force is proportional to the slip angle, beyond that, the cornering force reaches a maximum value where the tire begins sliding laterally. The slope of this curve at zero slip angle is called cornering stiffness C_α, and is a measure for comparing the cornering behaviour of different tires.

The effect of normal loads on the cornering ability of tires is evaluated using the cornering coefficient. The cornering coefficient is defined as the ratio of the cornering stiffness to the normal load.

Different factors affect the cornering behaviour of pneumatic tires; and these are, the type of tire, the normal load, the inflation pressure, and the tread design (Wong 1993). Typical variations of the cornering force with the normal load and inflation pressure are shown in Figure 3.9-3.10.

3.3.4.2. Aligning Torque

As a result of uneven force distribution in the contact patch, the cornering force acts toward the rear of the contact patch. This produces a moment called the self aligning torque, which tends to align the wheel plane with the direction of motion. The aligning torque is given as

$$M_z = t_p F_{y\alpha} \tag{3.2}$$

The contribution of this moment to the overall yaw moments is small. It does, however, contribute to the reactions in the steering system. A carpet plot of the aligning torque versus

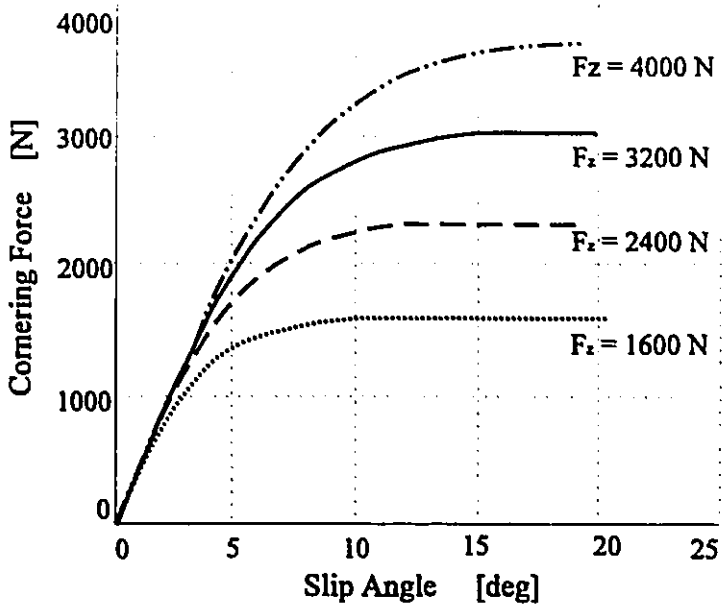

Figure 3.9 Typical variation of cornering force with slip angle (Bakker et al., 1987).

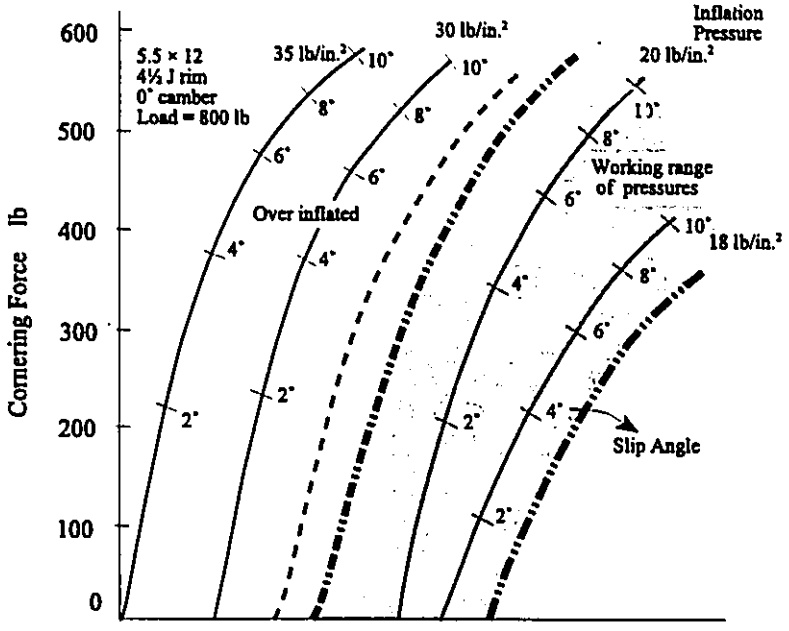

Figure 3.10 Variation of cornering force with inflation pressure at constant normal load. Note over inflation does not increase the cornering Force due to contact area reduction (Ellis, 1969).

the slip angle and normal load is shown in Figure 3.11. Path curvature, normal load, and inflation pressure of tires are some factors affecting the aligning torque (Gillespie, 1992).

3.3.4.3. Camber Thrust

Another factor contributing to the lateral force in a tire is the camber thrust. Camber thrust, $F_{y\gamma}$, is produced as a result of non-vertical tire orientation. As shown in Figure 3.2, the inclination angle is known as the camber angle. The variation of camber thrust with the camber angle is shown in Figure 3.12. The initial slope of this curve is called camber stiffness, C_γ, and is typically in the range of 10 to 20 percent of the cornering stiffness. Similar to the cornering force, the camber thrust has linear properties for small camber angles and it is affected by a few of parameters such as type of tire, normal load, and inflation pressure (Wong, 1993; Gillespie, 1992).

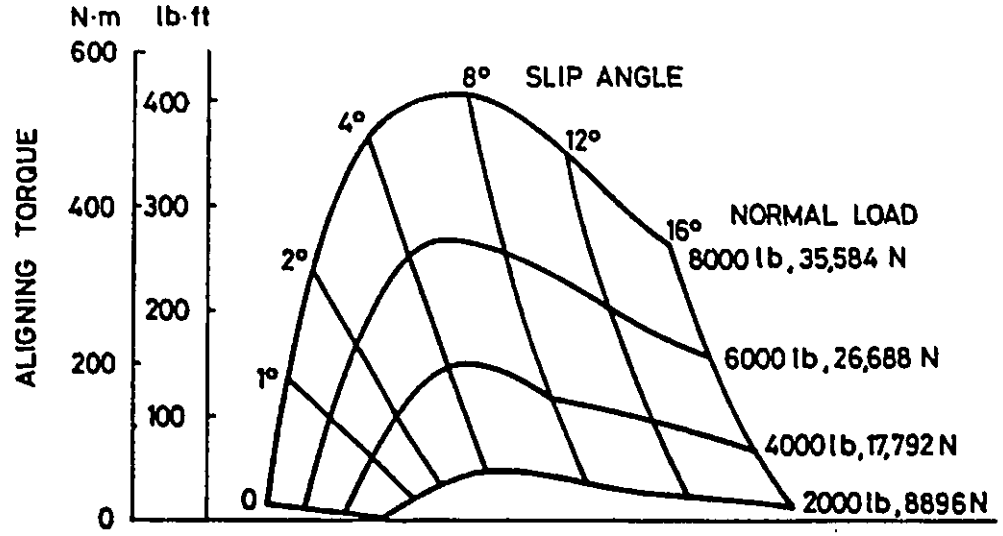

Figure 3.11 Typical variation of aligning torque with normal force and slip angle (Ervin, 1975).

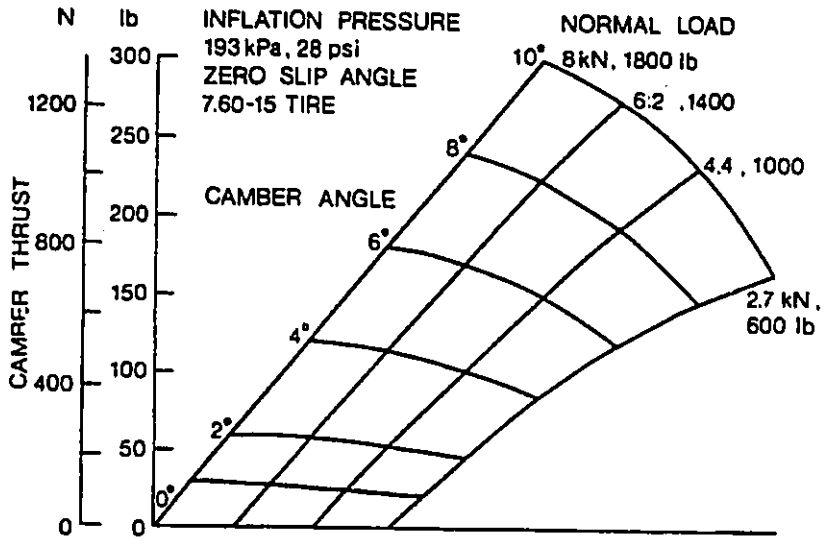

Figure 3.12 Common variation of camber thrust with camber angle and normal load (Gough, 1956).

Chapter 4

AGV Dynamic Model

4.1. Introduction

A common tendency in the modelling and control of Automated Guided Vehicles and Autonomous Vehicles is to develop the required kinematic equations, but to ignore a precise description of the vehicle dynamics. Other works exist, which compensate for the dynamics using "fudge factors" (Singh et al., 1991). However, having a suitable dynamic model is important for the following reasons:

1) An accurate dynamic model of the vehicle is required for simulation purposes. This model can be used to verify the control algorithms, before having to experiment directly on the vehicle.

2) Dynamic modelling is particularly important when the inertia forces, and load transfer due to heavy load and/or high velocities are significant.

3) Whenever wheel-ground forces are needed to confirm the dynamic constraints, a dynamic model of the vehicle should be used.

4) Dynamics is required when the input torque constraints due to power limitations in the motor actuators are to be verified.

Various dynamic models with different ranges of complexities have been introduced in the literature to investigate the handling characteristics and directional stability of autonomous vehicles (Yu and Moskwa, 1994; Xia and Law, 1992; Allen et al., 1987). The

focus of this chapter is to develop a model that accurately represents the behaviour of the vehicle, taking into account various parameters such as pneumatic tire model and load transfer. However, care should be taken to avoid an unduly complicated model by introducing only necessary characteristics relevant to the particular AGV under study. First the general equations of motion are developed, employing an approach similar to Ellis (1994). The equations are then simplified for the 3-DOF vehicle model of interest. Finally, the external forces and moments resulting from tire-ground interactions are derived.

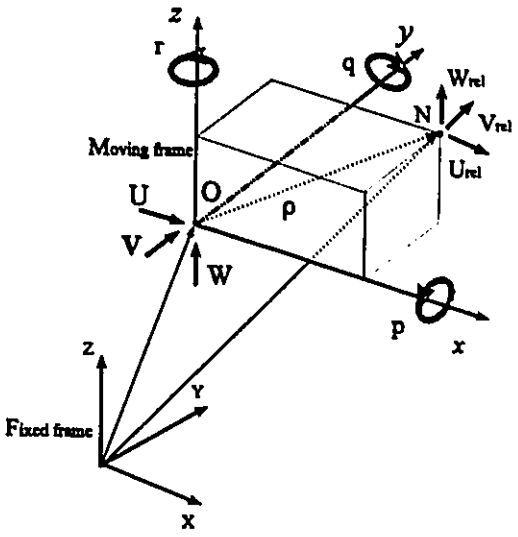

Figure 4.1 The coordinate system.

4.2. Axis System and General Equations of Motion

Common practice in vehicle dynamic analysis is to use two sets of coordinate axes. One set is attached to the vehicle with the origin of the axes usually fixed at the mass centre of the total vehicle (moving frame), and the second set fixed to a stationary inertial frame (fixed frame).

With reference to Figure 4.1, consider a point $N(x, y, z)$ on the vehicle body having linear velocities U_{rel}, V_{rel}, W_{rel} relative to the moving origin O, along the axes x, y, z, respectively, as well as rotational velocities p, q, r about x, y, z axes, respectively. The

positive sense of rotation is defined by the right-hand rule. The absolute velocity of point N with respect to the fixed frame is given by:

$$v_{abs} = v_O + v_{N/O} + \omega \times \rho \tag{4.1}$$

where

$$v_O = \begin{Bmatrix} U \\ V \\ W \end{Bmatrix} \qquad v_{N/O} = \begin{Bmatrix} U_{rel} \\ V_{rel} \\ W_{rel} \end{Bmatrix} \qquad \omega = \begin{Bmatrix} p \\ q \\ r \end{Bmatrix} \qquad \rho = \begin{Bmatrix} x \\ y \\ z \end{Bmatrix}$$

the velocity components of point N parallel to the x, y, z axes, are given by $(v_{abs})_x$, $(v_{abs})_y$, $(v_{abs})_z$, respectively. These are given by

$$\begin{aligned} (v_{abs})_x &= U + U_{rel} - ry + qz \\ (v_{abs})_y &= V + V_{rel} - pz + rx \\ (v_{abs})_z &= W + W_{rel} - qx + py \end{aligned} \tag{4.2}$$

For a rigid body vehicle in which the axes' origin is fixed relative to the body, $v_{N/O} = 0$ (i.e., $U_{rel}=V_{rel}=W_{rel}=0$). Thus, Equation 4.1 reduces to,

$$v_{abs} = v_O + \omega \times \rho \tag{4.3}$$

The acceleration of point N is expressed as

$$\begin{aligned} \frac{d}{dt}(v_{abs}) &= \frac{d}{dt}(v_O) + \frac{d}{dt}(\omega \times \rho) \\ a_{abs} &= a_O + \omega \times v_O + \dot{\omega} \times \rho + \omega \times (\omega \times \rho) \\ &= a_O + \dot{\omega} \times \rho + \omega \times v_{abs} \end{aligned} \tag{4.4}$$

where

$$a_O = \begin{bmatrix} \dot{U} & \dot{V} & \dot{W} \end{bmatrix}^T$$

It should be noted that v_O is expressed in terms of moving frame axes. Therefore, the first term on the right-hand side of Equation 4.4 is due to change in magnitude of v_O, and the second term is due to change in direction of v_O. $(a_{abs})_x$, $(a_{abs})_y$, and $(a_{abs})_z$ are the acceleration components of point N parallel to the x, y, z axes, respectively, and are given by

$$
\begin{aligned}
(a_{abs})_x &= \dot{U} - rV + qW - (q^2+r^2)x + (pq-\dot{r})y + (pr+\dot{q})z \\
(a_{abs})_y &= \dot{V} - pW + rU - (p^2+r^2)y + (qr-\dot{p})z + (pq+\dot{r})x \\
(a_{abs})_z &= \dot{W} - qU + pV - (p^2+q^2)z + (pr-\dot{q})x + (qr+\dot{p})y
\end{aligned} \tag{4.5}
$$

Applying D'Alembert's principle, the sum of all external forces and moments must be in equilibrium with the sum of the inertial forces, i.e.,

$$
\begin{aligned}
\sum X &= \sum \delta m \ (a_{abs})_x \\
\sum Y &= \sum \delta m \ (a_{abs})_y \\
\sum Z &= \sum \delta m \ (a_{abs})_z \\
\sum L &= \sum \delta m \ [y\,(a_{abs})_z - z\,(a_{abs})_y] \\
\sum M &= \sum \delta m \ [z\,(a_{abs})_x - x\,(a_{abs})_z] \\
\sum N &= \sum \delta m \ [x\,(a_{abs})_y - y\,(a_{abs})_x]
\end{aligned} \tag{4.6}
$$

Substituting the accelerations from Equation 4.5 into Equation 4.6 gives

$$
\begin{aligned}
\sum X &= M(\dot{U}-rV+qW) - M\bar{x}(q^2+r^2) + M\bar{y}(pq-\dot{r}) + M\bar{z}(rp+\dot{q}) \\
\sum Y &= M(\dot{V}-pW+rU) + M\bar{x}(pq+\dot{r}) - M\bar{y}(p^2+r^2) + M\bar{z}(rq-\dot{p}) \\
\sum Z &= M(\dot{W}-qU+pV) + M\bar{x}(pr-\dot{q}) + M\bar{y}(qr+\dot{p}) - M\bar{z}(p^2+q^2) \\
\sum L &= I_x\dot{p} - (I_y-I_z)qr + I_{yz}(r^2-q^2) - I_{xz}(pq+\dot{r}) + I_{xy}(pr-\dot{q}) \\
&\quad + M\bar{y}(\dot{W}-qU+pV) - M\bar{z}(\dot{V}-pW+rU) \\
\sum M &= I_y\dot{q} - (I_z-I_x)pr + I_{xz}(p^2-r^2) - I_{xy}(qr+\dot{p}) + I_{yz}(pq-\dot{r}) \\
&\quad + M\bar{z}(\dot{U}-rV+qW) - M\bar{x}(\dot{W}-qU+pV) \\
\sum N &= I_z\dot{r} - (I_x-I_y)pq + I_{xy}(q^2-p^2) - I_{yz}(pr+\dot{q}) + I_{xz}(qr-\dot{p}) \\
&\quad + M\bar{x}(\dot{V}-pW+rU) - M\bar{y}(\dot{U}-rV+qW)
\end{aligned} \tag{4.7}
$$

where

$$
\begin{aligned}
\sum \delta m &= M \\
\sum \delta m\, x &= M\bar{x} \\
\sum \delta m\, y &= M\bar{y} \\
\sum \delta m\, z &= M\bar{z}
\end{aligned} \tag{4.8}
$$

and moments of inertias are defined as,

$$
\begin{aligned}
I_x &= \sum \delta m\ (y^2+z^2) \\
I_y &= \sum \delta m\ (x^2+z^2) \\
I_z &= \sum \delta m\ (x^2+y^2) \\
I_{xy} &= \sum \delta m\ (xy) \\
I_{yz} &= \sum \delta m\ (yz) \\
I_{xz} &= \sum \delta m\ (xz)
\end{aligned}
\qquad (4.9)
$$

Equation 4.7, is given in the most general form, later the salient assumptions for the AGV under study will be used to simplify the equation.

4.3. Assumed Vehicle Model

The complexity of the dynamic model is influenced by the AGV model, system's degrees of freedom, and the simplifying assumptions considered. In this section these issues will be examined.

4.3.1. Degrees of Freedom

Equation 4.7 is used to develop the dynamic model of vehicles with varying complexities. Considering certain conditions that are not far from reality (Nalecz and Bindemann, 1989; Nisonger and Wormley, 1979; Allen et al., 1987), the simplified versions of these equations are often used for simulation and steering control studies of automated transit vehicles. Among the different models, the 2-DOF and 3-DOF models have been the focus of more attention. The 2-DOF bicycle model combines left and right wheels at the front and rear of the vehicle and includes lateral and yaw degrees of freedom. On the other hand, the 3-DOF models using lateral, yaw, and roll degrees of freedom has shown to be quite accurate for manoeuvres where the lateral acceleration is less than 0.3 g (Nisonger and Wormley, 1979). For this study the three degrees of freedom AGV model is considered. The model consists of a sprung mass and the two unsprung masses of front and rear with the centre of masses located as shown in Figure 4.2.

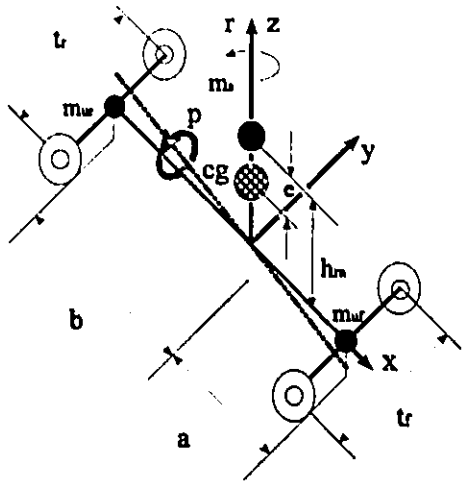

Figure 4.2 The 3-DOF AGV model

4.3.2. Assumptions

To derive the dynamic model for the AGV under study, the following assumptions are made:

1) The AGV is moving on a horizontal plane surface.
2) Pitch and bounce degrees of freedom are not considered due to the above assumption.
3) External disturbances like road irregularities, and aerodynamics are not considered.
4) Only steering and speed command inputs are allowed.
5) The sprung mass and the two unsprung masses are positioned such that the sum of their moment about the centre of gravity of the whole vehicle is zero.
6) The sprung mass will roll about the x axis (Segel, 1956). This axis is defined with respect to the unsprung masses, rather than the actual dynamic roll axis, which is generally defined using suspension deformations.
7) The effects of inertia properties of the wheels are considered negligible.
8) Front and rear track widths are equal.

4.4. Three DOF Dynamic Model

Unsymmetrical load distribution about the xz plane will slightly deform the wheels on one side more than the other. This will cause the vehicle to tend to travel along an arc rather than along a straight line (Borenstein and Koren, 1987). Therefore, it is a common practice in vehicle modelling to consider symmetry about xz plane. This results in $M\bar{y}=0$, $I_{xy}=0$, and $I_{zy}=0$. Also, in the operating environment where the plane surface assumption is valid, vertical movements of the vehicle and pitch motions are ignored. In the absence of movement along the z axis, $W=0$, and rotation about the y axis $q=0$. Thus for the centre of the sprung mass at $\bar{x}=0$, $\bar{y}=0$, *and* $\bar{z}\neq 0$ Equation 4.7 simplifies to:

$$\begin{aligned} \sum X &= M(\dot{U}-rV) + M\bar{z}\,pr \\ \sum Y &= M(\dot{V}+rU) - M\bar{z}\,\dot{p} \\ \sum L &= I_x\dot{p} - I_{xz}\dot{r} - M\bar{z}(\dot{V}+rU) \\ \sum N &= I_z\dot{r} - I_{xz}\dot{p} \end{aligned} \qquad (4.10)$$

Similar equations can be derived for the case where the centre of mass is at $\bar{x}\neq 0$, $\bar{y}=0$, and $\bar{z}=0$ (unsprung masses). Again, ignoring pitch and bounce movements, and considering symmetry about the xz plane Equation 4.7 reduces to

$$\begin{aligned} \sum X &= M(\dot{U}-rV) - M\bar{x}\,r^2 \\ \sum Y &= M(\dot{V}+rU) + M\bar{x}\,\dot{r} \\ \sum L &= I_x\dot{p} - I_{xz}\dot{r} \\ \sum N &= I_z\dot{r} - I_{xz}\dot{p} + M\bar{x}(\dot{V}+rU) \end{aligned} \qquad (4.11)$$

Referring to Figure 4.2, and using the x components of Equation 4.10 for sprung mass (m_s), and Equation of 4.11 for the unsprung masses (m_{uf} and m_{ur}) the following set of equations will result,

$$\begin{aligned} (\sum X)_s &= m_s(\dot{U}-rV) + m_s h_{ra}\,pr \\ (\sum X)_{uf} &= m_{uf}(\dot{U}-rV) - m_{uf}\,ar^2 \\ (\sum X)_{ur} &= m_{ur}(\dot{U}-rV) + m_{ur}br^2 \end{aligned}$$

Summing these equations gives,

$$\sum X = (m_s+m_{uf}+m_{ur})(\dot{U}-rV) + m_s h_{ra} rp + r^2(m_{ur}b - m_{uf}a)$$

where a, b and h_{ra} are positive constants. Using the 5th assumption in Section 4.3.2, which stipulates that $m_{ur}b=m_{uf}a$, the above equation reduces to

$$\sum X = M(\dot{U}-rV) + m_s h_{ra}\, pr$$

The other components of the equation of motion for the AGV are derived similarly. The entire equation of motion for the AGV is given by:

$$\begin{aligned}
\sum X &= M(\dot{U}-rV) + m_s h_{ra}\, pr \\
\sum Y &= M(\dot{V}+rU) - m_s h_{ra}\, \dot{p} \\
\sum L &= I_x \dot{p} - I_{xz}\dot{r} - m_s h_{ra}(\dot{V}+rU) \\
\sum N &= I_z \dot{r} - I_{xz}\dot{p}
\end{aligned} \tag{4.12}$$

The moments of inertias in Equation 4.12, are given by

$$\begin{aligned}
I_x &= \bar{I}_{x,s} + m_s h_{ra}^2 \\
I_z &= \bar{I}_{z,s} + I_{z,uf} + I_{z,ur} \\
I_{xz} &= 0
\end{aligned} \tag{4.13}$$

where

$\bar{I}_{x,s}$ is the moment of inertia of the sprung mass about the x centroidal axis

$\bar{I}_{z,s}$ is the moment of inertia of the sprung mass about the z centroidal axis

$I_{z,uf}$ is the moment of inertia of the front unsprung mass about the z axis

$I_{z,ur}$ is the moment of inertia of the rear unsprung mass about the z axis

Substituting for the moments of inertias, the final form of the equation of motion for the 3-DOF AGV model follows

$$\begin{aligned}
\sum X &= M(\dot{U}-rV) + m_s h_{ra}\, pr \\
\sum Y &= M(\dot{V}+rU) - m_s h_{ra}\, \dot{p} \\
\sum L &= I_x \dot{p} - m_s h_{ra}(\dot{V}+rU) \\
\sum N &= I_z \dot{r}
\end{aligned} \tag{4.14}$$

The expressions for the external forces in the left-hand side equation 4.14 are derived in the next section.

Two DOF Dynamic Model

The 2-DOF model is derived by ignoring the terms related to roll motion in Equation 4.14. This model will be used for controller design and comparison purposes in coming chapters, and is given by

$$\begin{aligned} \sum X &= M(\dot{U}-rV) \\ \sum Y &= M(\dot{V}+rU) \\ \sum N &= I_z\dot{r} \end{aligned} \tag{4.15}$$

4.5. External Forces and Moments Acting on the AGV

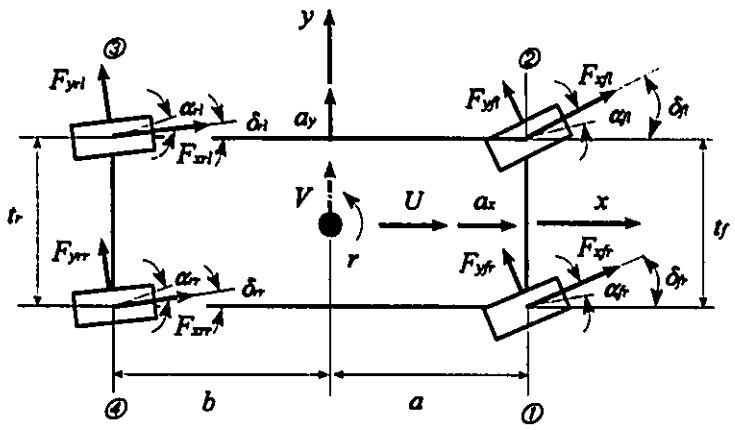

Figure 4.3 Plan view of AGV and tire forces

The desired mathematical model is obtained by equating the inertia reactions to their respective external forces and moments. External longitudinal and side forces, and yaw moments acting on the AGV are created in the ground plane and are derived from the tire-ground force interactions. The moment about the x axis, on the other hand, results from the suspension springs, the dampers, and the gravitational forces.Referring to Figure 4.3, the force summation in the x, and the y directions are

$$\begin{aligned}\sum F_x &= F_{xfl}\cos(\delta_{fl}) + F_{xfr}\cos(\delta_{fr}) + F_{xrl}\cos(\delta_{rl}) + F_{xrr}\cos(\delta_{rr}) \\ &\quad - F_{yfl}\sin(\delta_{fl}) - F_{yfr}\sin(\delta_{fr}) - F_{yrl}\sin(\delta_{rl}) - F_{yrr}\sin(\delta_{rr}) \\ \sum F_y &= F_{yfl}\cos(\delta_{fl}) + F_{yfr}\cos(\delta_{fr}) + F_{yrl}\cos(\delta_{rl}) + F_{yrr}\cos(\delta_{rr}) \\ &\quad + F_{xfl}\sin(\delta_{fl}) + F_{xfr}\sin(\delta_{fr}) + F_{xrl}\sin(\delta_{rl}) + F_{xrr}\sin(\delta_{rr})\end{aligned} \tag{4.16}$$

In the above equations δ_{ij} is the vehicle steering angle, where the first subscript denotes the front/rear steering angle, and the second subscript denotes the right/left wheels. Also, F_{ijk} represents wheel ground forces, where the subscripts denote the force directions, front/rear wheels, and right/left wheels, respectively. The longitudinal wheel forces are F_{xfl}, F_{xfr}, F_{xrl} and F_{xrr} and are given by

$$\begin{aligned}F_{xfl} &= (-F_r + F_t)_{xfl} \\ F_{xfr} &= (-F_r + F_t)_{xfr} \\ F_{xrl} &= (-F_r + F_t)_{xrl} \\ F_{xrr} &= (-F_r + F_t)_{xrr}\end{aligned} \tag{4.17}$$

where

F_r is the rolling resistance

F_t is the tractive force

The moment summation about the x and z axes are

$$\begin{aligned}\sum L &= m_s g \bar{h} - L_{spring} - L_{damper} \\ \sum N &= a\,[F_{yfl}\cos(\delta_{fl}) + F_{yfr}\cos(\delta_{fr}) + F_{xfl}\sin(\delta_{fl}) + F_{xfr}\sin(\delta_{fr})] \\ &\quad - b\,[F_{yrl}\cos(\delta_{rl}) + F_{yrr}\cos(\delta_{rr}) + F_{xrl}\sin(\delta_{rl}) + F_{xrr}\sin(\delta_{rr})] \\ &\quad + \frac{t_f}{2}[F_{yfl}\sin(\delta_{fl}) - F_{yfr}\sin(\delta_{fr}) - F_{xfl}\cos(\delta_{fl}) + F_{xfr}\cos(\delta_{fr})] \\ &\quad + \frac{t_r}{2}[F_{yrl}\sin(\delta_{rl}) - F_{yrr}\sin(\delta_{rr}) - F_{xrl}\cos(\delta_{rl}) + F_{xrr}\cos(\delta_{rr})]\end{aligned} \tag{4.18}$$

where, referring to Figure 4.4 for small angles ϕ

$$\begin{aligned}\bar{h} &= h_{ra}\phi \\ L_{spring} &= (k_f + k_r)\phi = k_{tot}\phi \\ L_{damper} &= [c_f + c_r]p = c_{tot}p\end{aligned}$$

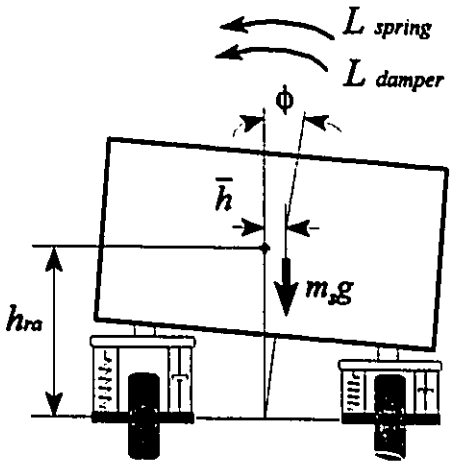

Figure 4.4 Forces and moments acting on a simplified AGV model.

Simplification for the Two Wheel Steering AGV

For the rear drive, front wheel steering AGV, assuming the following,

$$\begin{aligned} \delta_{rl} &= \delta_{rr} = 0 \\ \delta_{fl} &= \delta_{fr} = \delta \\ t_f &= t_r = t \\ (F_t)_{xfl} &= 0 \\ (F_t)_{xfr} &= 0 \end{aligned} \tag{4.19}$$

then, Equations 4.16 and 4.18 simplifies to

$$\begin{aligned} \sum F_x &= (F_{xfl}+F_{xfr})\cos\delta + F_{xrl} + F_{xrr} - (F_{yfl}+F_{yfr})\sin\delta \\ \sum F_y &= (F_{yfl}+F_{yfr})\cos\delta + F_{yrl} + F_{yrr} + (F_{xfl}+F_{xfr})\sin\delta \\ \sum L &= (m_s g\, h_{ra} - k_{tot})\,\phi - c_{tot} p \\ \sum N &= a\,[(F_{yfl}+F_{yfr})\cos\delta + (F_{xfl}+F_{xfr})\sin\delta] - b\,(F_{yrl}+F_{yrr}) \\ &\quad + \frac{t}{2}[(F_{yfl}-F_{yfr})\sin\delta + (F_{xfr}-F_{xfl})\cos\delta - F_{xrl} + F_{xrr}] \end{aligned} \tag{4.20}$$

Equation 4.20, is the final form of the relationships for the external forces and moments acting on the AGV. The lateral tire forces in this equation will be determined based on the tire model.

4.6. Tire Model

For the dynamic model to be reliable, an accurate representation of the wheel-ground interaction is necessary. The following tire models are used in the present work for dynamic modelling and simulation purposes.

4.6.1. Linear Tire Model

The simplest tire model that gives good results in many applications is the linear model. This model stipulates that the side forces do vary linearly with side slip angle and the camber angle and is valid if these angles are restricted to small magnitudes of about 4 degrees (Wong, 1993). The model assumes that the cornering stiffness is constant within this range, and is given as

$$F_{yi} = C_\alpha \alpha_i \tag{4.21}$$

where

F_{yi} is the cornering (lateral) force (N)

C_α is the cornering stiffness (N/rad)

α_i is the slip angle (rad)

The subscript i denotes the wheel number as illustrated in Figure 4.3. This tire model is used for the 2-DOF AGV. The load transfer effect is not considered in this model.

4.6.2. Nonlinear Tire Model

Many publications exist on the subject of nonlinear modelling of tire mechanics. Bakker et al. (Bakker, 1987) approach contains equations that are not unduly complicated, and can be programmed to provide tire forces and moments. In addition the results agree quite well with experimental data (Brach, 1991). The following set of equations is a simplification of the model presented by Bakker.

$$\begin{cases} A_i = (-0.0221\times10^{-3} F_{zi} + 1.011) F_{zi} \\ B_i = -0.354\times10^{-3} F_{zi} + 0.707 \\ D_i = \dfrac{C_\alpha}{(1.30 A_i)} \\ E_i = (1-B_i)\,\alpha_i + \left(\dfrac{B_i}{D_i}\right) \arctan(\alpha_i D_i) \end{cases} \tag{4.22}$$

$$F_{yi} = A_i \sin(1.30 \arctan(D_i E_i))$$

where

F_{zi} is the normal force on each tire, (N)

F_{yi} is the cornering force on each tire (N)

Similar to the linear model, the subscript i denotes the wheel number. Also, units for C_α and α_i are N/deg and deg respectively. Cornering stiffness, C_α , is constant, and the effect of tractive and braking forces are ignored.

4.7. Tire Slip Angles

Due to the elastic deformation of the tire, the velocity vector of the wheel does not lie in the wheel plane. The angle between the velocity vector and the wheel plane is called the slip angle. With reference to Figure 4.3, the slip angles are given by

$$\begin{aligned} \alpha_{fr} &= \delta_{fr} - \arctan\left(\frac{V+a r}{U+\frac{l}{2} r}\right) \\ \alpha_{fl} &= \delta_{fl} - \arctan\left(\frac{V+a r}{U-\frac{l}{2} r}\right) \\ \alpha_{rl} &= \delta_{rl} - \arctan\left(\frac{V-b r}{U-\frac{l}{2} r}\right) \\ \alpha_{rr} &= \delta_{rr} - \arctan\left(\frac{V-b r}{U+\frac{l}{2} r}\right) \end{aligned} \tag{4.23}$$

For a front wheel steering AGV, the slip angles of the front and the rear tires are given by

$$\begin{aligned}
\alpha_{fr} &= \delta - \arctan\left(\frac{V+ar}{U+\frac{t}{2}r}\right) \\
\alpha_{fl} &= \delta - \arctan\left(\frac{V+ar}{U-\frac{t}{2}r}\right) \\
\alpha_{rl} &= -\arctan\left(\frac{V-br}{U-\frac{t}{2}r}\right) \\
\alpha_{rr} &= -\arctan\left(\frac{V-br}{U+\frac{t}{2}r}\right)
\end{aligned} \tag{4.24}$$

4.8. Load Transfer

When the vehicle is turning, or changing speed, the effect of load transfer is to change the distribution of the normal load on the tires, which in turn changes the cornering forces. This will affect the vehicle directional stability (Wong, 1993). The change in the wheel normal load caused by lateral acceleration is referred to as lateral load transfer, while the change in the wheel normal load caused by longitudinal accelerations is known as longitudinal load transfer.

The total lateral load transfer on the front and rear tires of the vehicle are

$$\begin{aligned}
W_{tf} &= W_{bf} + W_{rf} + W_{uf} + W_{sf} \\
W_{tr} &= W_{br} + W_{rr} + W_{ur} + W_{sr}
\end{aligned} \tag{4.25}$$

where the four components of lateral load transfer are

W_b is the lateral load transfer due to body roll

W_r is the lateral load transfer due to roll centre height

W_u is the lateral load transfer due to unsprung weight

W_s is the lateral load transfer due to change in the centre of gravity's height

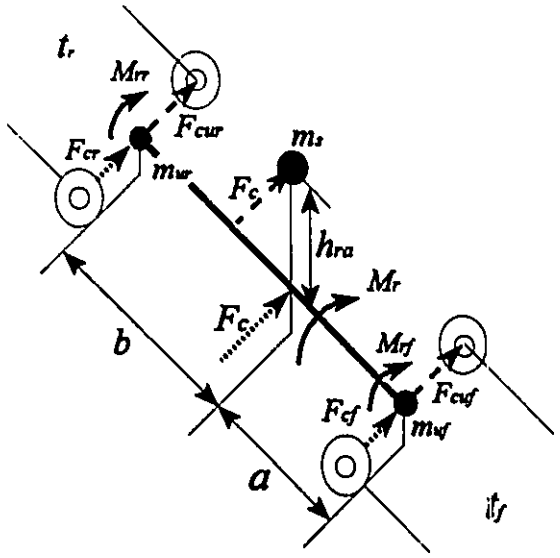

Figure 4.5 AGV mass distribution.

A quasi-static approximation of the dynamic load transfer effect is employed in this work. As shown in Figure 4.5, the total lateral inertia force acting on the vehicle during a turn consists of the sprung mass inertia force, F_c and the unsprung mass inertia forces of front and rear suspensions represented by F_{cuf} and F_{cur}, given by

$$F_c = m_s a_y$$
$$F_{cuf} = m_{uf} a_y$$
$$F_{cur} = m_{ur} a_y$$

The inertia force of sprung mass acting on its centre of gravity, can be transferred to the vehicle roll axis with the addition of a roll couple of magnitude

$$M_r = F_c h_{ra}$$

This roll couple causes the sprung mass to rotate about the roll axis. This motion is resisted by the roll stiffness of the vehicles suspension. The portions of the roll couple resisted by the front and rear suspensions are proportional to the their suspension's roll stiffness, and given by

$$M_{rf} = M_r \frac{k_f}{k_{tot}}$$

$$M_{rr} = M_r \frac{k_r}{k_{tot}}$$

The load transfer due to the vehicle body roll is given by

$$W_{bf} = \frac{M_{rf}}{t_f}$$

$$W_{br} = \frac{M_{rr}}{t_r}$$

The vehicle's parameters and mass distribution for a general roll axis are shown in Figure 4.6, however, as explained earlier for the AGV under consideration the roll axis is considered to coincide with the x axis.

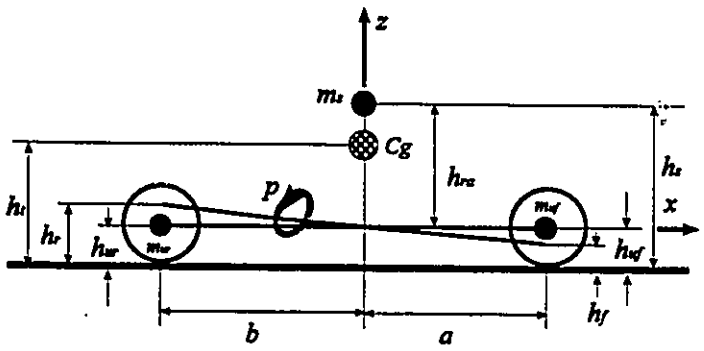

Figure 4.6 Roll axis and AGV mass distribution

The second elements of the total load transfer are due to the portions of sprung mass inertia force carried by each axle, and given by

$$W_{rf} = F_{cf} \frac{h_f}{t_f}$$

$$W_{rr} = F_{cr} \frac{h_r}{t_r}$$

where

$$F_{cf} = F_c \frac{b}{L}$$

$$F_{cr} = F_c \frac{a}{L}$$

The third components of the total lateral weight transfer result from inertia forces of the unsprung masses, and are given by

$$W_{uf} = F_{cuf} \frac{h_{uf}}{t_f}$$

$$W_{ur} = F_{cur} \frac{h_{ur}}{t_r}$$

Again, with reference to Figure 4.4, the last terms of the total load transfer expression are due to the change in location of the centre of mass of the sprung mass

$$W_{sf} = m_s g h_{ra} \phi \frac{b}{Lt_f}$$

$$W_{sr} = m_s g h_{ra} \phi \frac{a}{Lt_r}$$

With reference to assumptions 6 and 8 in Section 4.3.2, the following is true:

$$h_{uf} = h_{ur} = h$$
$$h_f = h_r = h$$
$$t_f = t_r = t$$

using the above set of equations the terms of the total lateral load transfer in Equation 4.25, reduce to

$$
\begin{aligned}
W_{bf} &= m_s h_{ra}(\dot{V}+Ur)\ \frac{k_f}{tk_{ot}} \\
W_{br} &= m_s h_{ra}(\dot{V}+Ur)\ \frac{k_r}{tk_{ot}} \\
W_{rf} &= m_s h\ (\dot{V}+Ur)\ \frac{b}{Lt} \\
W_{rr} &= m_s h\ (\dot{V}+Ur)\ \frac{a}{Lt} \\
W_{uf} &= h(\dot{V}+Ur)\ \frac{m_{uf}}{t} \\
W_{ur} &= h(\dot{V}+Ur)\ \frac{m_{ur}}{t} \\
W_{sf} &= m_s g h_{ra}\,\phi\ \frac{b}{Lt} \\
W_{sr} &= m_s g h_{ra}\,\phi\ \frac{b}{Lt}
\end{aligned}
\qquad (4.26)
$$

The magnitude of the longitudinal load transfer due to speed change is computed using the following relation

$$
W_{long} = \frac{m_s \dot{U} h_s}{2L} + \frac{m_{uf}\,\dot{U} h}{2L} + \frac{m_{ur}\,\dot{U} h}{2L} \qquad (4.27)
$$

The normal ground reactions on the four tires required in Equation 4.22, are hence given by

$$
\begin{aligned}
F_{zfl} &= \frac{Mgb}{2L} + W_{long} - W_{tf} \\
F_{zfr} &= \frac{Mgb}{2L} + W_{long} + W_{tf} \\
F_{zrl} &= \frac{Mga}{2L} - W_{long} - W_{tr} \\
F_{zrr} &= \frac{Mga}{2L} - W_{long} + W_{tr}
\end{aligned}
\qquad (4.28)
$$

4.9. Tractive Force

It is assumed that the entire effort of the motion is provided by the forces between the driving wheels and the working surface. For the case where the wheels roll without slipping, and the rear wheels are driven by an electric motor through a gear box and differential gear, the total tractive forces of rear tires are given by (Appendix A1),

$$F_t = K_t V_t - J_t \dot{U} - C_t U \tag{4.29}$$

where

$$K_t = \frac{n_t \bar{K}_t}{R_w R_{at}}$$

$$J_t = \frac{n_t^2 \bar{J}_t}{R_w^2}$$

$$C_t = \frac{n_t}{R_w^2}\left(\frac{\bar{K}_t^2}{R_{at}} + n_t \bar{C}_t\right)$$

Using Equation 4.17, and substituting for F_t ($F_t = F_{xrl} + F_{xrr}$) in Equation 4.20, will result in the AGV dynamic equations, including the effect of tractive motor dynamics, gear boxes.

4.10. Steering System

Different models are suggested to represent the steering dynamics of AGVs, WMRs, and ATVs. Some authors use a second order system to model the dynamics of the steering system (Deng and Brady, 1993a; Makino, 1993), others, argue that the effect of steering inertia is negligible, and have used a simple proportional model, $\tau_s = \dot{\delta}$ (DeSantis, 1995a; Yu and Moskwa, 1994). However, for all practical purposes of this work a first order lag system (damper and spring) is used to represent the dynamics of steering system. This later model is often practically implemented for simulation and design controllers for ATVs, AGVs, and WMRs (Smith and Starkey, 1994; Shin et al., 1992; Fenton et al., 1988; Shladover et al., 1978). The steering dynamics is represented by

$$\tau_s = H_{1s}(\dot{\delta} + H_{2s}\delta) \tag{4.30}$$

Referring to Appendix A2, for the case where steering system is actuated by a DC motor the steering torque is given by

$$\tau_s = K_s V_s - C_s \dot{\delta} \tag{4.31}$$

where

$$K_s = \frac{n_s \bar{K}_s}{R_{as}}$$

$$C_s = n_s \left(\frac{\bar{K}_s^2}{R_{as}} + n_s \bar{C}_s \right)$$

Substituting for τ_s into Equation 4.30 results in the steering dynamics

$$\dot{\delta} = \frac{1}{k_{1s}} V_s - k_{2s} \delta \tag{4.32}$$

where

$$k_{1s} = \frac{H_{1s} + C_s}{K_s}$$

$$k_{2s} = \frac{H_{1s} H_{2s}}{H_{1s} + C_s}$$

Chapter 5

AGV Control

5.1. Introduction

In order to obtain satisfactory performance for an automated guided vehicle, an efficient control scheme is required to generate the control signals. This controller should be capable of correcting the errors in a stable manner, in a reasonable time, and without oscillations about the path (hunting). Controllers based on mere feedback information of position and orientation errors are shown to be incapable of proper tracking. Even the kinematic-based controllers are not adequate for this purpose, as payload and travelling speed increases. In this chapter other alternatives are being investigated, and in particular a dynamic-based controller that takes into account the vehicle's dynamic behaviour is explored. A 2-DOF nonlinear model is used to design the controller. The vehicle model is first transformed into a Side Slippage Free (SSF) model, then exact input-output feedback linearization is used to linearize the nonlinear system. A sliding mode controller is applied to guarantee the robustness, and deal with disturbances and unmodeled dynamics.

5.2. Conversion to 2-DOF Side Slippage Free Model

2-DOF Bicycle Model Dynamics

While in practice using a more complicated model for simulation studies is quite acceptable (Allen et al., 1987; Elgindy and Ilosvai, 1983; Brach, 1991), a simpler model is

preferred for control purposes. For non-emergency operations, where lateral accelerations are less than 0.3 g, 2-DOF models are often used to develop steering controllers (Smith and Starkey, 1994; Jurie et al.,1994; Fenton and Selim, 1988). Since, the AGV's under normal industrial operating conditions experience accelerations that are usually less than 0.3 g, a 2-DOF bicycle model that neglects the vehicle body roll is used in this study to develop the AGV controller. Furthermore, the motion of the vehicle is assumed to be free of side slippage. The 3-DOF model developed in Chapter 4 will ultimately be used for simulation purposes (Chapter 6).

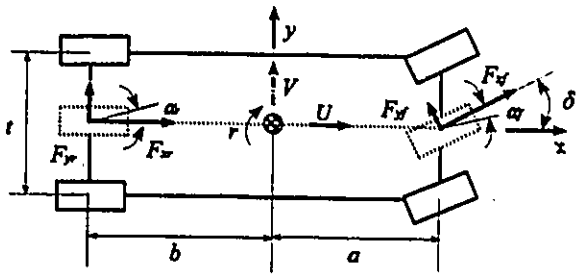

Figure 5.1 Plane view of bicycle model tire forces.

With reference to Figure 5.1, and Equations 4.15, 4.17, and 4.20 the motion equations of the 2-DOF bicycle model can be written as,

$$\begin{aligned} M\dot{U} &= MVr + F_{xf}\cos\delta - F_{yf}\sin\delta + F_t + F_{xr} \\ M\dot{V} &= -MUr + F_{xf}\sin\delta + F_{yf}\cos\delta + F_{yr} \\ I\dot{r} &= aF_{xf}\sin\delta + aF_{yf}\cos\delta - bF_{yr} \end{aligned} \tag{5.1}$$

where

F_{xf} is the combined rolling resistance force of front tires

F_{xr} is the combined rolling resistance force of rear tires

F_{yf} is the combined lateral force of front tires

F_{yr} is the combined lateral force of rear tires

F_t is the combined tractive force of rear tires

I is I_z, the total moment of inertia about z axis

Substituting for the relevant terms related to the effect of tractive motor dynamics, gear box, and the differential gear box given by Equation 4.29, Equation 5.1 can be rewritten in matrix notation as

$$M\dot{\mathbf{v}} = M\mathbf{G}_0 + \mathbf{G}_x\mathbf{F}_x + \mathbf{G}_y\mathbf{F}_y + \mathbf{G}_t V_t \tag{5.2}$$

where the parameters are given by

$$\mathbf{G}_x = \begin{bmatrix} \cos\delta & 1 \\ \sin\delta & 0 \\ a\sin\delta & 0 \end{bmatrix};\ \mathbf{G}_y = \begin{bmatrix} -\sin\delta & 0 \\ \cos\delta & 1 \\ a\cos\delta & -b \end{bmatrix};\ \mathbf{G}_0 = \begin{bmatrix} Vr - \frac{C_t U}{M} \\ -Ur \\ 0 \end{bmatrix};\ \mathbf{G}_t = \begin{bmatrix} K_t \\ 0 \\ 0 \end{bmatrix}$$

$$\mathbf{M} = \begin{bmatrix} M+J_t & 0 & 0 \\ 0 & M & 0 \\ 0 & 0 & I \end{bmatrix};\ \dot{\mathbf{v}} = \begin{bmatrix} \dot{U} \\ \dot{V} \\ \dot{r} \end{bmatrix};\ \mathbf{F}_x = \begin{bmatrix} F_{xf} \\ F_{xr} \end{bmatrix};\ \mathbf{F}_y = \begin{bmatrix} F_{yf} \\ F_{yr} \end{bmatrix}$$

Recalling the steering actuator dynamics given in Equation 4.32, the dynamics of 2-DOF model is formulated as

$$\begin{aligned} \dot{\mathbf{v}} &= \mathbf{M}^{-1}[M\mathbf{G}_0 + \mathbf{G}_x\mathbf{F}_x + \mathbf{G}_y\mathbf{F}_y + \mathbf{G}_t V_t] \\ \dot{\delta} &= \frac{1}{k_{1s}} V_s - k_{2s}\delta \\ \dot{\theta} &= r \\ \dot{X} &= U\cos\theta - V\sin\theta \\ \dot{Y} &= U\sin\theta + V\cos\theta \end{aligned} \tag{5.3}$$

Side Slippage Free Motion

For the purposes of controller design a motion free from side slippage, which corresponds to setting front and rear slip angles equal to zero, is assumed. Although, this assumption may not be true for highway applications, it has been proven to be quite realistic for AGV applications where the maximum speed is usually small (DeSantis 1995a, 1995b).

In the absence of slippage the angular and lateral velocities can be expressed in terms of the steering angle and forward velocity. This interdependency greatly simplifies the dynamic equations of the vehicle.

Recalling Equation 4.24, the tire slip angles for the bicycle model are given by

$$\begin{aligned} \alpha_f &= \delta - \arctan\left(\frac{V+ar}{U}\right) \\ \alpha_r &= \arctan\left(\frac{V-br}{U}\right) \end{aligned} \tag{5.4}$$

Setting $\alpha_f = \alpha_r = 0$, leads to the nonholonomic constraints

$$\begin{aligned} V &= \frac{Ub\tan\delta}{L} \\ r &= \frac{U\tan\delta}{L} \end{aligned} \tag{5.5}$$

Differentiating Equation 5.5 gives

$$\begin{aligned} \dot{V} &= \frac{b\tan\delta}{L}\dot{U} + \frac{Ub}{L\cos^2\delta}\dot{\delta} \\ \dot{r} &= \frac{\tan\delta}{L}\dot{U} + \frac{U}{L\cos^2\delta}\dot{\delta} \end{aligned} \tag{5.6}$$

In matrix notation, Equations 5.5 and 5.6 are represented as

$$\begin{aligned} \nu &= J_1 U \\ \dot{\nu} &= J_1 \dot{U} + J_2 \dot{\delta} \end{aligned} \tag{5.7}$$

where

$$J_1 = \begin{Bmatrix} 1 \\ \frac{b\tan\delta}{L} \\ \frac{\tan\delta}{L} \end{Bmatrix}; \qquad J_2 = \begin{Bmatrix} 0 \\ \frac{bU}{L\cos^2\delta} \\ \frac{U}{L\cos^2\delta} \end{Bmatrix}$$

Using an approach similar to that of DeSantis (1995b), both sides of the first equality in Equation 5.3 are pre-multiplied by $J_1^T M$. Since, $J_1^T G_y = 0$ the following results

$$J_1^T M \dot{\nu} = M J_1^T G_0 + J_1^T G_x F_x + J_1^T G_t V_t \tag{5.8}$$

Substituting for $\dot{\nu}$ and $\dot{\delta}$ from Equations 5.7 and 5.3 respectively it follows that

$$\dot{U} = M(J_1^T M J_1)^{-1} J_1^T G_0 + (J_1^T M J_1)^{-1} J_1^T G_x F_x + (J_1^T M J_1)^{-1} J_1^T G_t V_t - k_{1s}^{-1} (J_1^T M J_1)^{-1} J_1^T M J_2 V_s + k_{2s} (J_1^T M J_1)^{-1} J_1^T M J_2 \delta \quad (5.9)$$

Equation 5.9 can be written in a general form as follows:

$$\dot{U} = g_x F_x + g_t V_t + g_s V_s + g_0$$

where the g coefficients are defined as follows:

$$g_p = (J_1^T M J_1)^{-1}$$
$$g_x = (J_1^T M J_1)^{-1} J_1^T G_x$$
$$g_t = (J_1^T M J_1)^{-1} J_1^T G_t$$
$$g_s = -k_{1s}^{-1} (J_1^T M J_1)^{-1} J_1^T$$
$$g_0 = M(J_1^T M J_1)^{-1} J_1^T G_0 + k_{2s} (J_1^T M J_1)^{-1} J_1^T M J_2 \delta$$

Substituting for the matrices M, J_1, J_2, G_x, G_t, and G_0 in the above equation, the complete dynamics of the vehicle under side slip free condition is given by

$$\begin{aligned}
\dot{U} &= g_x F_x + g_t V_t + g_s V_s + g_0 \\
\dot{\delta} &= \frac{1}{k_{1s}} V_s - k_{2s} \delta \\
\dot{\theta} &= \frac{U \tan\delta}{L} \\
\dot{X} &= \frac{U}{\cos\delta} \left(\cos\theta \cos\delta - \frac{b}{L} \sin\theta \sin\delta \right) \\
\dot{Y} &= \frac{U}{\cos\delta} \left(\sin\theta \cos\delta + \frac{b}{L} \cos\theta \sin\delta \right)
\end{aligned} \quad (5.12)$$

where

$$g_p = \left[M + J_t + \frac{\tan^2\delta}{L^2}(Mb^2 + I) \right]^{-1}$$

$$g_x = \left[\frac{1}{\cos\delta} \quad 1 \right] g_p$$

$$g_t = g_p K_t$$

$$g_s = \left[-\frac{U\tan\delta}{k_{1s} L^2 \cos^2\delta}(Mb^2 + I) \right] g_p$$

$$g_0 = -g_p C_t U - k_{1s} k_{2s} g_s \delta$$

The nonlinear dynamic system in Equation 5.12 can finally be described in the general state space form as

$$\dot{\chi} = f(\chi) + g(\chi)u \tag{5.13}$$

where

$$\chi = [\, U \;\; \delta \;\; \theta \;\; X \;\; Y \,]^T$$

$$u = [\, V_t \;\; V_s \,]^T$$

$$f(\chi) = \left[g_x F_x + g_0 \quad -k_{2s}\delta \quad \frac{U\tan\delta}{L} \quad \frac{UD_1}{\cos\delta} \quad \frac{UD_2}{\cos\delta} \right]^T$$

$$g(\chi) = \begin{bmatrix} g_t & 0 & 0 & 0 & 0 \\ g_s & \frac{1}{k_{1s}} & 0 & 0 & 0 \end{bmatrix}^T$$

the parameters D_1 and D_2 are defined as

$$D_1 = (\cos\theta\cos\delta - \frac{b}{L}\sin\theta\sin\delta)$$

$$D_2 = (\sin\theta\cos\delta + \frac{b}{L}\cos\theta\sin\delta)$$

5.3. Feedback Linearization

Feedback linearization is an approach for the controller design of a nonlinear system which has received considerable attention in recent years in areas such as high performance aircraft and industrial robots (Hedrick, 1993; Jagannathan et al. 1994). The central idea in

this approach is to algebraically transform the nonlinear system into a linear or partially linear system by exact state transformation and feedback. Linear control techniques are then used to design the controller for the linearized system. This method is entirely different from approximate linearization approach known as the Jacobian linearization, where Taylor expansion is used to linearize the system about equilibrium point (Slotine and Li, 1991). The remainder of this chapter deals with the linearization and the synthesis of the feedback control laws for the nonlinear system given in Equation 5.13.

5.3.1. Definitions

This section introduces some useful definitions for understanding the methodology used in this chapter. The presentation is primary based on Iisidori (1995, 1989), Slotine and Li (1991), Khalil (1992) and Vidyasagar (1993).

In what follows the Multi-Input Multi-Output (MIMO) nonlinear control systems with n states χ_i, m inputs u_k, and m outputs y_i (i.e., square systems) are studied. The MIMO systems are described in the state space form as

$$\begin{aligned} \dot{\chi} &= f(\chi) + \sum_{k=1}^{m} g_k(\chi) u_k \\ y_i &= h_i(\chi) \qquad\qquad 1 \le i \le m \end{aligned} \tag{5.14}$$

in which $f, g_1, g_2, \ldots, g_m$ are smooth vector fields, and $h_1, h_2, \ldots, h_m$ are smooth functions defined on an open set of R^n. Whenever possible and convenient, these equations will be written in the short form

$$\begin{aligned} \dot{\chi} &= f(\chi) + g(\chi)u \\ y &= h(\chi) \end{aligned} \tag{5.15}$$

where

- χ is the $n\times1$ state vector
- u is the $m\times1$ control input vector of components u_i
- y is the $m\times1$ vector of system outputs of components y_i
- f, h are smooth vector fields

g is a $n \times m$ matrix whose columns are smooth vector fields g_i

Definition 1 *Smooth Vector Field: Based on differential geometry terminology a vector function* $f: R^n \to R^n$ *is called a smooth vector field, if* $f(\chi)$ *has continuous partial differential of any order.* Also, a scalar function $h: R^n \to R$ having continuous partial differential of any order is called a *smooth scalar function.*

Definition 2 *Lie Derivative: Suppose* $h: R^n \to R$ *and that* $f: R^n \to R^n$ *denote smooth scalar and vector functions on* R^n*, respectively. Then the Lie derivative of h with respect to f is also a scalar function and is defined as*

$$L_f h = \nabla h \, f$$

In other words, the resulting function is the directional derivative of h along f. Of course repeated use of this operation is possible and defined recursively as

$$L_f^0 h = h$$
$$L_f^i h = L_f (L_f^{i-1} h) = \nabla (L_f^{i-1} h) f \qquad i=1,2,...$$

Definition 3 *Lie Bracket: Let two vector fields f and g be defined on* R^n*. The Lie bracket (or Lie product) of f and g is a new smooth vector field defined by*

$$[f,g] = \nabla g \, f - \nabla f \, g$$

Repeated bracketing of a vector field g with the same vector field f is also possible. Whenever this is needed, it is a common practice to show the Lie bracket of $[f,g]$ with $ad_f g$, where *ad* stands for "adjoint."

$$ad_f^0 g = g$$
$$ad_f^i g = [f, ad_f^{i-1} g] \qquad i=1,2,...$$

Definition 4 *Involutivity: Suppose* $\{f_1, f_2, ..., f_m\}$ *denotes a set of linearly independent vector fields. The set is involutive if, and only if, there are scalar functions* $\alpha_{ijk}: R^n \to R$ *such that*

$$[f_i, f_j] = \sum_{k=1}^{m} \alpha_{ijk}(\chi) f_k(\chi) \qquad \forall\ i,j$$

Thus, the Lie bracket of any pairs of vector fields f_i and f_j from an involutive set can be expressed as a linear combination of the original set of vector fields.

Definition 5 *Diffeomorphism: A function* Φ: $R^n \to R^n$, *defined in a region* Ω, *is called a diffeomorphism if its inverse exists, and if both* Φ *and* Φ^{-1} *are smooth. A transformation of this type is called global diffeomorphism, if* Ω *is the whole space of* R^n. Sometimes, to find a transformation defined for all χ is difficult. Thus, in most cases one rather looks for *local diffeomorphisms* that are defined only in a neighbourhood of a given point.

Definition 6 *Relative Degree: A multi variable nonlinear system of the form given in Equation 5.15 has a (vector) relative degree* $\{ r_1, r_2, ..., r_m \}$ *at* χ_0, *and the scalar* $r_t = r_1 + r_2 + ... + r_m$ *is called the total relative degree of the system at* χ_0. *Where,* r_i *is the number of times one has to differentiate the* i^{th} *output* y_i *in order to have at least one component of the input vector* u *to explicitly appear.*

Definition 7 *Input-State Linearization: Given a set of vector fields f and* $g_1, g_2, ..., g_m$ *being smooth in* $\Omega \subset R^n$. *The MIMO system in Equation 5.15 (without output) is said to be input-state linearizable in a neighbourhood* Ω *of* χ_0, *if there exists a diffeomorphism* $\phi : \Omega \to R^n$ *and, a nonlinear feedback control law*

$$u = \alpha(\chi) + \beta(\chi)\upsilon$$

such that the new variable $z = \phi(\chi)$ *and the new input* υ *satisfy a linear time invariant relation*

$$\dot{z} = Az + B\upsilon$$

where A and B are controllable.

Definition 8 *Input-Output Linearization: The system in Equation 5.15 is said to be input-output linearizable if it is possible to generate a linear differential relation between the output* y_i *and inputs* u_k *such that*

$$y_i^{(r_i)} = L_f^{r_i} h_i + \sum_{k=1}^{m} (L_{g_k} L_f^{r_i-1} h_i) u_k \tag{5.16}$$

with r_i being the minimum order of derivative of y_i where the coefficient of at least one u_k is not zero.

Performing the above procedure for each output y_i yields

$$\Upsilon = b(\chi) + E(\chi)\, u \tag{5.17}$$

where

$$\Upsilon = \begin{bmatrix} y_1^{(r_1)} & \dots & \dots & y_m^{(r_m)} \end{bmatrix}^T$$

$$b(\chi) = \begin{bmatrix} L_f^{r_1} h_1(\chi) & \dots & \dots & L_f^{r_m} h_m(\chi) \end{bmatrix}^T$$

Also the $m \times m$ matrix $E(\chi)$ is called the *decoupling matrix* of the system and defined as

$$E(\chi) = \begin{bmatrix} L_{g_1} L_f^{r_1-1} h_1 & L_{g_2} L_f^{r_1-1} h_1 & \dots & L_{g_m} L_f^{r_1-1} h_1 \\ L_{g_1} L_f^{r_2-1} h_2 & L_{g_2} L_f^{r_2-1} h_2 & \dots & L_{g_m} L_f^{r_2-1} h_2 \\ \dots & \dots & \dots & \dots \\ L_{g_1} L_f^{r_m-1} h_m & L_{g_2} L_f^{r_m-1} h_m & \dots & L_{g_m} L_f^{r_m-1} h_m \end{bmatrix}$$

Using transformations similar to that of the Single Input Single Output (SISO) case yields m equations of the simple form

$$y_i^{(r_i)} = v_i \tag{5.18}$$

Definition 9 *Normal form: Let a system has a relative degree of*

$$r_1 + r_2 + \dots + r_m \le n$$

and

$$\xi_i = \begin{bmatrix} \xi_1^1 & \xi_2^1 & \dots & \xi_{r_i}^1 \end{bmatrix}^T = \begin{bmatrix} h_i(\chi) & L_f h_i(\chi) & \dots & L_f^{r_i-1} h_i(\chi) \end{bmatrix}^T$$

Then the normal form of the system in a neighbourhood Ω of a point χ_0. *can be written as*

$$\begin{cases} \dot{\xi}_1^i = \xi_2^i \\ \cdots \\ \dot{\xi}_{r_i-1}^i = \xi_{r_i}^i \\ \dot{\xi}_{r_i}^i = b_i(\xi,\eta) + \sum_{j=1}^{m} a_{ij}(\xi,\eta)\, u_j \\ y_i = \xi_1^i \end{cases} \qquad 1 \le i \le m$$

$$\dot{\eta} = q(\xi,\eta)$$

The ξ_i, and η_i are referred to as normal coordinates or normal states in Ω (or at χ_0).

Definition 10 *Internal Dynamics: The part of the system dynamics rendered unobservable by the process of input-output Linearization.* This is called internal dynamics because it cannot be seen from external input-output relation.

Definition 11 *Zero Dynamics: The zero dynamics is defined to be the internal dynamics of the system when the system outputs are kept at zero by the inputs.* The zero dynamics is an intrinsic feature of the nonlinear system which does not depend on the choice of the control law or the desired trajectories. Also, examining the stability of the zero dynamics is much easier than examining the stability of the internal dynamics.

5.3.2. Input-Output feedback Linearization

The development of a linear differential relation that describes the input-output relationship of the dynamic model under consideration follows.

5.3.2.1. Choice of Outputs

While the state Equations 5.13 are determined by the dynamic characteristics of the vehicle, the output functions $y_i = h_i(\chi)$ are chosen in such a way to achieve a desired task performance and would result in a convenient controller design. Moreover, different choices of output functions will result in different internal dynamics. Thus, it is quite possible to have stable internal dynamics for a certain choice of output variables, while another choice

of outputs leads to an unstable one. In this section some possible choices of output variables are presented and discussed separately.

For a system having two inputs, any choice of two functions or variables is possible. The following options are considered in this work.

Type I: $y = h(\chi) = [\ X \quad Y\ ]^T$

Type II: $y = h(\chi) = [\ Y \quad \theta\ ]^T$

Type III: $y = h(\chi) = [\ U \quad \delta\ ]^T$

Type IV: $y = h(\chi) = [\ U \quad Y\ ]^T$

Type I Output

The input-output linearization can be achieved only when the decoupling matrix E is nonsingular in the region Ω. For the case under study the outputs are a function of state variables only, and the decoupling matrix for the system is 2×2. The mathematical derivation of E for the type I output is presented in Appendix B1, and the final result is given by

$$E(\chi) = \begin{bmatrix} \dfrac{g_t D_1}{\cos\delta} & \dfrac{g_s D_1}{\cos\delta} - \dfrac{Ub\sin\theta}{Lk_{1s}\cos^2\delta} \\ \dfrac{g_t D_2}{\cos\delta} & \dfrac{g_s D_2}{\cos\delta} + \dfrac{Ub\cos\theta}{Lk_{1s}\cos^2\delta} \end{bmatrix}$$

Substituting for g_t, D_1, and D_2, the determinant of decoupling matrix simplifies to

$$\begin{aligned} \det E &= \frac{g_t Ub}{k_{1s} L\cos^2\delta} \\ &= \left\{ M+J_t + \sin^2\delta \left[\frac{I+M(b^2-L^2)}{L^2} \right] \right\}^{-1} \frac{K_t bU}{k_{1s} L} \end{aligned} \tag{5.19}$$

This system has a total relative degree of four at any point χ_0 provided that E^{-1} is not singular. The determinant of Equation 5.19 is singular if and only if $b=0$, or $U=0$. The first condition indicates that the trajectory tracking of a representative point (in this case the centre of gravity) on the rear wheel axle is not possible. This is due to the presence of the nonholonomic constraints and has already been pointed out by Samson and Ait-Abderrahim

(1990a). Where as the presence of U in the determinant is a result of the particular wheel base configuration under study. Had the AGV been powered by a differential drive, for the same outputs, the decoupling matrix would have been independent from U (Jagannathan et al. 1994.)

Type II Outputs

Here the desired outputs to be controlled are Y, and θ. Following the same procedure as for type I, the decoupling matrix determinant is obtained as shown in Appendix B2 and is given by

$$\det \boldsymbol{E} = \frac{g_t U b \sin\theta}{k_{1s} L \cos^2\delta}$$

The system has a relative degree of four. The matrix $\boldsymbol{E}$ is singular if $b=0$, $U=0$, or $\sin\theta=0$. Thus, the system is linearizable only in portions of the entire state space region. Due to this limitation type II outputs are not of practical value, further, it is difficult to specify control tasks having these outputs.

Type III Outputs

Here instead of controlling the positional variables, the forward velocity U, and the steering angle δ, are controlled. The decoupling matrix determinant derived in Appendix B3 is given by

$$\det \boldsymbol{E} = \frac{g_t}{k_{1s}}$$

This determinant is nonsingular for the entire region of state space. However, the total relative degree of the system is two for this choice of outputs, resulting in a complex nonlinear internal dynamics of order three. Moreover, due to selecting δ as one of the outputs, it is not convenient to compensate for the tracking error in vehicle position.

Type IV Outputs

When a human driver controls a vehicle along a road, the two primary consideration are

1) To maintain a desired forward velocity.

2) To follow the road by staying as close as possible to a reference path.

Based on these observations, and considering straight routes for the time being, it is desired to define the outputs as the forward velocity U, and the lateral error from the reference line Y. This is some times referred to as dynamic path following (Shin et al., 1992; Sarkar et al. 1994; DeSantis, 1994), and differs from trajectory tracking, where the longitudinal error along the path, and time history of position are of paramount concern. The determinant of the decoupling matrix for this case is derived in Appendix B4 and given by

$$\det \boldsymbol{E} = \frac{g_t U b \cos\theta}{k_{1_s} L \cos^2\delta} \tag{5.20}$$

This system has a total relative degree of three, leading to a more involved internal dynamics compared to type I outputs. The determinant in Equation 5.20 is singular if and only if $b=0$, $U=0$, and $\cos\theta = \frac{\pi}{2}$. The first condition implies that the trajectory tracking of a representative point on the rear wheel axis is not possible, which is due to the presence of the nonholonomic constraints. Whereas the presence of U in the determinant is a result of the particular wheel base configuration under study. The third condition occurs when the vehicle is normal to the path. This is because the direction along the path is not explicitly specified in the function $h_1(\chi)=Y$.

5.3.2.2. Choice of Coordinates

The nonlinear state equations of the AGV, Equation 5.13, can be described in different coordinate systems. One can express these equations in inertial coordinates, vehicle's fixed coordinates, or path dependent coordinates. Often, for a particular choice of output equations it is more meaningful to deal with one coordinate system rather than the others. In what follows Equation 5.13 is first transformed into the path dependent

coordinates, then the input output (I/O) linearization for different choice of outputs is carried out.

Path Dependent Coordinates

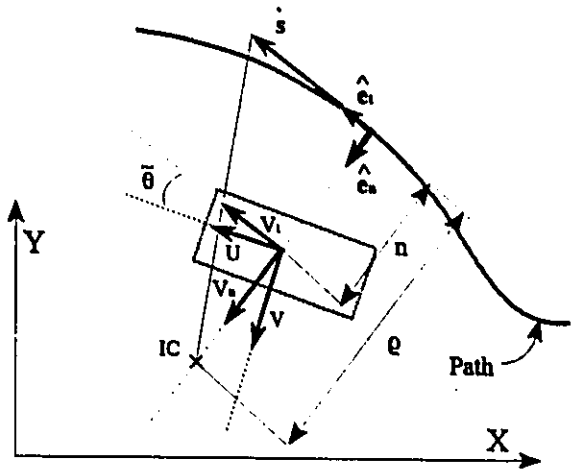

Figure 5.2 AGV's motion with respect to path dependent coordinates.

Referring to Figure 5.2, the two components of velocity in the AGV's fixed coordinates are depicted as forward, U and lateral, V. Thus, the total vehicle velocity v in the path dependent coordinates is given by

$$\begin{aligned} v &= V_t \hat{e}_t + V_n \hat{e}_n \\ v &= (U\cos\tilde{\theta} - V\sin\tilde{\theta})\hat{e}_t + (U\sin\tilde{\theta} + V\cos\tilde{\theta})\hat{e}_n \end{aligned} \tag{5.21}$$

where $\tilde{\theta} = \theta - \theta_d$ is the yaw angle deviation from the desired path.
Moreover, using simple trigonometry yields the following relations

$$\begin{aligned} \dot{s} &= \left[\frac{\varrho}{\varrho - n}\right] V_\theta = \frac{V_\theta}{1 - c(s)} \\ \dot{n} &= V_n \\ \dot{\theta}_d &= \frac{\dot{s}}{\varrho} = \frac{c(s)V_\theta}{1 - c(s)} \end{aligned} \tag{5.22}$$

where

ϱ is the instantaneous radius of rotation

c(s) is the curvature of path

n is the normal distance from the path

Using Equation 5.21 and 5.22, the dynamics of the vehicle in the path dependent coordinates can be represented as

$$\dot{\zeta} = f(\zeta) + g(\zeta)u$$

where

$$\zeta = [\ \omega_w \quad \delta \quad \dot{\theta} \quad s \quad n\ ]^T$$

$$u = [\ V_t \quad V_s\ ]^T$$

$$f(\zeta) = \begin{Bmatrix} \frac{1}{R_w}(g_x F_x + g_0) \\ -k_{2s}\delta \\ \frac{R_w\omega_w}{\cos\delta}\left[\frac{\sin\delta}{L} - \frac{c(s)D_1}{1-c(s)}\right] \\ \frac{R_w\omega_w D_1}{\cos\delta} \\ \frac{R_w\omega_w D_2}{\cos\delta} \end{Bmatrix}; \qquad g(\zeta) = \begin{bmatrix} \frac{g_t}{R_w} & \frac{g_s}{R_w} \\ 0 & \frac{1}{k_{1s}} \\ 0 & 0 \\ 0 & 0 \\ 0 & 0 \end{bmatrix}$$

R_w and ω_w are the radius and angular velocity of the rear wheels respectively. Also, the values for g_x, g_n, g_s, g_0, D_1, and D_2 are obtained using a similar approach to that used for the inertial coordinate case and are given in Appendix C.

I/O Linearization for Path Dependent Coordinates

The output choices considered are

Type V Outputs

The desired outputs in this case are the path coordinates *s* and n. Following the same procedure of differentiating the variables will result in decoupling matrix determinant derived in Appendix C and is given by

$$\det E = \frac{g_t R_w \omega_w b}{k_{1s} L \cos^2\delta}$$

The result is very similar to the decoupling matrix in Equation 5.19, for the type I outputs. The total relative degree of the linearized subsystem system is four, and the order internal dynamics is one.

Type VI Outputs

The wheels angular velocity[1] ω_w, and normal distance from the path, n are chosen as the desired outputs. The decoupling matrix determinant for this case is derived in Appendix C and is given by

$$\det E = \frac{g_t \omega_w b \cos\delta}{k_{1s} L \cos^2\delta}$$

Comparable to the type IV outputs, the linearized subsystem has a total relative degree of three, and results in a second order internal dynamics.

5.3.3. Internal Dynamics

Since the total relative degree of the system r_t, is less than the system's order n, the input output linearization technique decomposes the AGV's nonlinear dynamics into two parts, external and internal. The external part results in a linear differential relation between y_i and υ_i, where a suitable design of υ_i yields the desired behaviour of y_i. However, the internal behaviour or unobservable part of the system has to be investigated to assure the internal states remain bounded. Referring to Definition 10, in the normal coordinates the internal dynamics corresponds to the last n-r_t equations of the normal form.

---

[1]Analogous result is obtained if the forward linear velocity, U, is selected instead of angular velocity ω_w.

For a discussion of the internal dynamics and the zero dynamics, first, a diffeomorphism is constructed to transform the whole system into the normal form of the nonlinear systems, then the stability issue is discussed.

Since the total relative degree of the system is four for this choice of output, the dimension of internal dynamics is one, that is

$$\text{Dim(Internal Dyn)} = n - \text{Dim(I/O)}$$

where n=5 is the order of original system. To transform the system into normal form, the first four components of the required diffeomorphism are constructed as

$$\begin{aligned}
\xi_1^1 &= h_1(\chi) = X \\
\xi_2^1 &= L_f h_1(\chi) = \frac{UD_1}{\cos\delta} \\
\xi_1^2 &= h_2(\chi) = Y \\
\xi_2^2 &= L_f h_2(\chi) = \frac{UD_2}{\cos\delta}
\end{aligned}$$

Since the distribution spanned by the vector fields $g_1(\chi)$ and $g_2(\chi)$ is involutive, it is possible to choose the remaining new coordinate in such a way that

$$L_{g_j}\eta_i = 0 \qquad \forall \ 1 \le i \le n-r_i \ ; \ \forall \ 1 \le j \le m$$

thus having $L_{g_1}\eta_1 = 0$ and $L_{g_2}\eta_1 = 0$ results in

$$\begin{aligned}
&\frac{\partial \eta_1}{\partial U} g_t = 0 \\
&\frac{\partial \eta_1}{\partial U} g_s + \frac{\partial \eta_1}{\partial \delta} \frac{1}{k_{1s}} = 0
\end{aligned} \tag{5.24}$$

To satisfy the partial differential Equations 5.24, one possible choice is $\eta_1 = \theta$. Thus, the proposed diffeomorphic transformation would be $\Phi(\chi)$, where for simplicity new notations z_i's are being adopted[1]

$$\Phi(\chi) = \begin{bmatrix} \xi_1^1 & \xi_1^2 & \xi_2^1 & \xi_2^2 & \eta_1 \end{bmatrix}^T = \begin{bmatrix} z_1 & z_2 & z_3 & z_4 & z_5 \end{bmatrix}^T$$

---

[1]If the distribution is not involutive then one can always look for η_i's, such that the Jacobian matrix of $\Phi(\chi)$ is nonsingular.

To verify that $\Phi(\chi)$ is indeed a diffeomorphism, one has to check that $\nabla\Phi(\chi)$ has full rank(Appendix D). The inverse transformation is given by

$$
\begin{aligned}
U &= z_2\cos z_5 + z_4\sin z_5 \\
\delta &= \arctan\left(\frac{z_4\cos z_5 - z_2\sin z_5}{\frac{b}{L}(z_2\cos z_5 + z_4\sin z_5)}\right) \\
\theta &= z_5 \\
X &= z_1 \\
Y &= z_3
\end{aligned}
$$

Therefore, the internal dynamics in the normal form is given by

$$\dot{z}_5 = \frac{1}{b}(z_4\cos z_5 - z_2\sin z_5) \tag{5.25}$$

5.3.4. Stability of Zero Dynamics

The zero dynamics of a control system is defined as the dynamics of the system when the outputs are identically zero. If the outputs are identically zero, for this case this implies that

$$\dot{z}_5 = 0 \tag{5.26}$$

The zero dynamics in this case is stable, but not asymptotically stable.

5.4. Sliding Mode Control

A variety of control laws can be designed for the linearized control subsystem given in Equation 5.18 to track the desired outputs X_d and Y_d. However, due to the model imprecision, parameter uncertainty, and the disturbances inherited in the vehicle systems, a robust controller is preferred. In what follows the attractive features of variable structure control system are being used to achieve this purpose. This technique is shown to be successful in other applications (Richards and Ready, 1991; Ro and Kim, 1994; Yu and Moskwa, 1994). First, some preliminary concepts are explained. Later on, the boundary layer sliding mode technique is used to design a suitable controller.

5.4.1. Basic Concepts

The basic idea in the sliding mode technique is to first describe the desired closed loop behaviour of the system by a hyper surface, called the sliding surface. Then, to force the dynamic system to restrict its motion to this user defined surface. This is achieved by altering the control structure in such a way to direct the system trajectories toward the sliding surface. The main advantages of Sliding Mode (SM) control are its invariant properties and the ability to replace n^{th} dimensional system by an equivalent lower order problem.

Sliding Surface

Define S_i, the i^{th} sliding surface element of the vector S as (Fernandez and Hedrick, 1987)

$$S_i = \sum_{j=0}^{r_i-1} \lambda_{ij} \frac{d^j e_i}{dt^j} = \sum_{j=0}^{r_i-1} \lambda_{ij} e_i^{(j)} \qquad 1 \le i \le m \qquad (5.27)$$

where r_i is the relative order of the i^{th} output and

$$e_i = y_i - y_{id} \qquad 1 \le i \le m$$

The m surfaces S_i, of Equation 5.27 are defined such that they are decoupled from one another, that is S_i is only function of e_i. Then, differentiating S_i will result in

$$\begin{aligned} \dot{S}_i &= \sum_{j=1}^{r_i} \lambda_{i(j-1)} e_i^{(j)} \\ &= \lambda_{i(r_i-1)} e_i^{(r_i)} + \sum_{j=1}^{r_i-1} \lambda_{i(j-1)} e_i^{(j)} \qquad 1 \le i \le m \end{aligned} \qquad (5.28)$$

Without loss of generality $\lambda_{i(r_i-1)}$ can be set to unity. Substituting 5.16 into Equation 5.28 gives

$$\dot{S}_i = -\bar{Y}_i + L_f^{r_i} h_i + \sum_{k=1}^{m} (L_{g_k} L_f^{r_i-1} h_i) u_k \qquad 1 \le i \le m \qquad (5.29)$$

where

$$\bar{Y}_i = y_{id}^{(r_i)} - \sum_{j=1}^{r_i-1} \lambda_{i(j-1)} e_i^{(j)}$$

Equation 5.29 can be rewritten in vector form as follows

$$\dot{S} = -\bar{Y} + b(\chi) + E(\chi)u \tag{5.30}$$

where

$$\bar{Y} = \left[\bar{Y}_1 \quad \bar{Y}_2 \quad \ldots \quad \bar{Y}_m \right]^T$$

Sliding Condition

To guarantee that all the surfaces $S_i=0$, will be reached in a finite time, and that sliding will occur on all surfaces, the sliding condition is defined as

$$\frac{1}{2}\frac{d}{dt} S_i^2 \le -\hat{\eta}_i |S_i| \tag{5.31}$$

Where $\hat{\eta}_i$ is a strictly positive constant. Satisfying Equation 5.31 implies that the squared distance to the sliding surfaces, quantified by S_i^2, will decrease with movement along all system trajectories (Slotine and Li, 1991).

The attraction condition to the sliding surface as defined by Equation 5.31 is assured by a suitable choice of

$$\dot{S}_i = F_i(S) \tag{5.32}$$

One obvious choice for $F_i(S)$ is

$$F_i(S) = -\bar{K}_i sgn(S_i)$$

Substituting Equation 5.32 into 5.30 yields the control input as

$$u = E^{-1}(\chi)\left[\bar{Y} + F(S) - b(\chi)\right] \tag{5.33}$$

where

$$F(S) = \left[F_1(S) \quad F_2(S) \ldots F_m(S)\right]$$

5.5. Controller Design

In this section a suitable controller for the linearized system with the type I outputs is designed. The decoupling matrix and internal dynamics for this case are given in Equations 5.19 and 5.25 respectively. Differentiating the outputs twice will results in

$$\Upsilon = b(\chi) + E(\chi)u \tag{5.34}$$

where

$$\Upsilon = \begin{bmatrix} \ddot{y}_1 & \ddot{y}_2 \end{bmatrix}^T$$

$$u = \begin{bmatrix} V_t & V_s \end{bmatrix}^T$$

$$b(\chi) = \begin{Bmatrix} \frac{D_1}{\cos\delta}\left(g_x F_x + g_0\right) + \frac{U}{L\cos^2\delta}\left(b\delta k_{2s}\sin\theta - UD_2\sin\delta\right) \\ \\ \frac{D_2}{\cos\delta}\left(g_x F_x + g_0\right) - \frac{U}{L\cos^2\delta}\left(b\delta k_{2s}\cos\theta - UD_1\sin\delta\right) \end{Bmatrix}$$

Identifying the following nonlinear feedback

$$u = E^{-1}(\chi)\left[\upsilon - b(\chi)\right] \tag{5.35}$$

Substituting Equation 5.35 into Equation 5.34 yields the simple linear relation

$$\Upsilon = \upsilon \tag{5.36}$$

5.5.1. PD Controller

For the linear system thus obtained and described by Equation 5.36, υ can be designed in different ways to achieve a desirable performance for y_i outputs. For instance, one can impose a new feedback control laws like

$$\upsilon_i = -\kappa_{i0}e_i - \kappa_{i1}\dot{e}_i - \ldots - \kappa_{i(r_i-1)}e_i^{(r_i-1)} + y_{id}^{(r_i)} \qquad 1 \le i \le m \tag{5.37}$$

Where

$$e_i = y_i - y_{id} \qquad 1 \le i \le m$$

and

$$\kappa_i = [\kappa_{i0}, \kappa_{i1}, \ldots, \kappa_{i(r_i-1)}] \qquad 1 \le i \le m$$

can be chosen in such a way to assign a specific set of eigenvalues, or to satisfy an optimality criterion. The schematic diagram of a PD controller for the linearized control subsystem is shown in Figure 5.3.

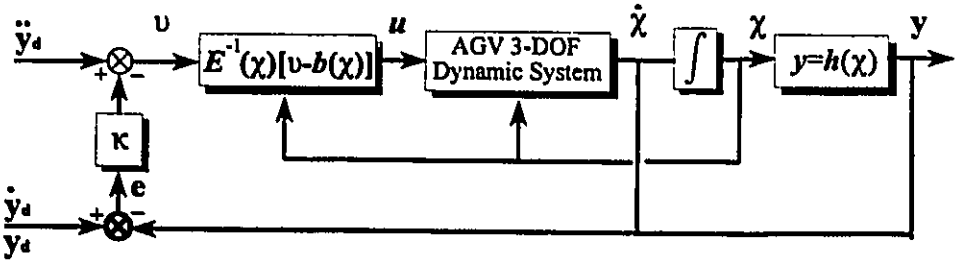

Figure 5.3 PD controller for linearized control subsystem.

5.5.2. Sliding Mode Controller

For the case where X and Y are the desired outputs (i.e., type I outputs), using Equation 5.33, the controller outputs are given by

$$u = -E^{-1}(\chi)b(\chi) + E^{-1}\begin{bmatrix} \ddot{y}_{1d} - \lambda_{10}\dot{e}_1 - \bar{K}_1 sgn(S_1) \\ \ddot{y}_{2d} - \lambda_{20}\dot{e}_2 - \bar{K}_2 sgn(S_2) \end{bmatrix} \tag{5.38}$$

5.5.3. Boundary Layer Technique

The control laws that satisfy Equation 5.31 are discontinuous across $S_i(t)$ and lead to "perfect" tracking. However, this is obtained at the cost of high control activity (i.e., control chattering). In general chattering is undesirable and should be eliminated. As proposed by Slotine (1984), this can be achieved using a thin boundary layer φ_i and having the $sgn(S_i)$ replaced by the function $sat(S_i)$. Where

$$sat(S_i) = \begin{cases} sgn(S_i), & |S_i| \ge \varphi_i \\ \dfrac{S_i}{\varphi_i}, & |S_i| \le \varphi_i \end{cases} \qquad 1 \le i \le m \tag{5.39}$$

modified sliding condition given by

$$\frac{1}{2}\frac{d}{dt}S_i^2 \le (\dot{\varphi}_i - \hat{\eta}_i)|S_i| \tag{5.40}$$

Inside the boundary layer the continuous control gives smooth S_i dynamics. This leads to tracking within a precision zone rather than perfect tracking. The controller output u for this case is given by

$$u = -E^{-1}(\chi)b(\chi) + E^{-1}\begin{bmatrix} \ddot{y}_{1d} - \lambda_{10}\dot{e}_1 - K_1 sat\left(\frac{S_1}{\varphi_1}\right) \\ \ddot{y}_{2d} - \lambda_{20}\dot{e}_2 - K_2 sat\left(\frac{S_2}{\varphi_2}\right) \end{bmatrix} \tag{5.41}$$

5.5.4. Multiple Sliding Surfaces

Since the desirable properties of variable structure systems exist only in the sliding mode, it is required to converge to this mode as quickly as possible. If a high value of λ_{i0} is used, the system may not be in sliding mode for a long portion of transient time. This makes the system susceptible to parameter variations and disturbance. Although, the robustness could be improved using high feedback gains, this could be impractical to implement (Richards and Reay, 1991; El-Sharkawi and Huang, 1989). Another alternative is to use non-stationary sliding surface, or Multiple Sliding Surfaces (MSS). The system initially slides on the surface with small value of λ_{i0} then switches to the next surface which can be incremented as a function of time. The concept is useful where a system is subjected to large variations in parameters (Kaynak et al., 1982). Improved results are reported applying this strategy to a dc motor (Alasty and Naraghi, 1991; El-Sharkawi and Hung, 1989).

5.5.5. Variable Boundary Layer Thickness

Due to the $sat(S_i)$ function given in Equation 5.38, the system trajectory is directed toward the sliding surface for the condition of $|S_i| \ge \varphi_i$, however, for $|S_i| \le \varphi_i$ the attraction to the sliding surface is not guaranteed by the proposed method. Thus, the introduction of a saturation function restricts the system trajectory to remain in a

neighbourhood of sliding surface. The larger the boundary layer thickness the less chattering is expected. However, if the boundary layer thickness is too large, besides large tracking error, the system's trajectory may never reach the equilibrium point (Yeung and Chen, 1988), and in some cases even non-smooth responses are expected. To benefit from the advantages of a boundary layer and the same time reduce the boundary layer thickness specially near the equilibrium point (i.e., is the origin of phase plane), a Variable Boundary Layer (VBL) strategy is adopted. The boundary layer is set to be proportional to the error but has a minimum desired thickness at the origin to avoid chattering at the equilibrium point, i.e.,

$$\varphi_i = \varphi_{i0} + \psi_i |e_i|$$

Where φ_{i0} is the desired boundary layer thickness at origin, and ψ_i is boundary layer proportional constant. A constant reduction of boundary layer thickness does not have this advantage, and will result in chattering.

5.5.6. Modified Boundary Layer Sliding Mode

In this case, the MSS and the VBL strategies are simultaneously implemented to improve the BLSM controller. In the proposed controller, robustness in the presence of parameter changes and modelling errors is further enhanced by applying the MSS. Whereas, using the VBL scheme restricts the system trajectories within the boundary layer to stay in the vicinity of sliding regime. The reduction of the boundary layer thickness in proportion to the tracking error results in a diminished tracking error, improved tracking responses, and reduced chattering. This new controller is referred to as Modified Boundary Layer Sliding Mode (MBLSM) for the remaining part of this thesis.

Chapter 6

Simulations and Results

6.1. Introduction

In this chapter the controllers designed in the preceding chapter will be evaluated through simulations. The 3-DOF dynamic model is used as a simulation testbed for this purpose. Since, it is important that the model accurately represents the vehicle behaviour for practical conditions. The first part of this chapter is devoted to the validation of the dynamic model. Then a thorough study of the AGV control schemes is presented. The numerical integration routine used to solve the equations of motion is based on the fourth order Runge-Kutta method. MATLAB has been used for the different simulation programs and the input data for the vehicle are presented in Appendix E.

6.2. Validation of the Dynamic Model

In order to emphasize the significance of dynamic modelling for the problem under study, the performance of the kinematic model of the vehicle is compared to the dynamic model through computer simulations. Also, to assess the level of sophistication of the required dynamic model, the 3-DOF model is compared with the 2-DOF dynamic model. For the sake of comparison with other studies, the electrical motors' equations are ignored only for the simulations in this section.

6.2.1. Analysis of the Kinematic Model

In an approach similar to Boyden (Boyden and Velinsky, 1994), the open loop model of the AGV is simulated for a 90-degree left turn. In the first set of simulations the kinematic model and dynamic model are compared, in order to demonstrate the limitations of the kinematic model. Forward speed is maintained constant. The steering angle is increased sinusoidally to 30 degrees, and maintained constant for a certain period, then returned to zero. This experiment is repeated for forward speeds of 0.3, 0.5, 1, 2 m/sec.

Results of this test are shown in Figure 6.1. With reference to this figure the kinematic model is evidently independent of speed and always predicts the perfect 90-degree left turn. However, the response of the dynamic model is highly speed dependent, and at 2 m/s the difference is significant. The difference increases considerably with speed. The deviation rate from the path due to speed increase is shown in Figure 6.2.

6.2.2. Analysis of the Dynamic Model

A similar strategy is used to compare the 2-DOF and 3-DOF dynamic models. The rear wheels' tractive forces are controlled to obtain the desired constant forward speed. The steering angle is increased sinusoidally to 30 degrees, and maintained constant for a certain period, then returned to zero.

Simulation results for comparing the path trace of the 2-DOF and the 3-DOF dynamic models are presented in Figure 6.3. The difference in the path trace for a left turn manoeuvre is due to including the roll degree of freedom, and the lateral load transfer in the dynamic model.

The effect of weight on the path trace for the unloaded AGV (700 Kg), and when it is fully loaded (1700 Kg) is shown in Figure 6.4. The vehicle's path traces differ considerably under unloaded and loaded conditions.

The pneumatic tires and their characteristics are often neglected in the reported dynamic modelling of AGVS and WMRs. Figure 6.5 shows the effect of tire cornering stiffness C_α on the AGV performance. As expected from vehicle dynamic theory, the

increase in cornering stiffness results in a more damped system. Referring to Figure 6.6, the deviation rate from the path due to the change in cornering stiffness is shown.

6.2.3. AGV Performance Using A Proportional Controller

The ability of the 2-DOF and 3-DOF models to accurately track a specific path is studied in this section. A proportional controller based on position and distance errors is used for this purpose. Although this control strategy is often used in practice, no systematic analysis exists on how to obtained the controller's gains. This control strategy has also other limitations that will be elaborated on in Section 6.2.3.3.

6.2.3.1. Roll DOF and Load Transfer Effect

The tracking ability of the 3-DOF dynamic model comprising yaw, lateral and roll motions is compared in Figure 6.7 with the 2-DOF model using a proportional controller based on position and orientation errors. The test track consists of a "line-circle-line" path. The load transfer across the wheels, which was not considered in the AGV dynamic models reported in the literature, has also been included. The maximum tracking error for the two, and the three degrees of freedom model in Figure 6.7 are shown in Figure 6.8. The results show this maximum error to be 22 cm and 27 cm for the 2-DOF and 3-DOF models respectively.

The tire normal forces as the AGV navigates the line-circle-line path, are shown in Figure 6.9, for a front-right tire. The 2-DOF model has a constant normal force throughout the path, while the normal force increases as the 3-DOF model enters the curve and it is governed by the vehicle's load transfer.

Based on the tire models, the cornering forces vary for the two and three degrees of freedom models. Figure 6.10, shows the increase in front-right tire cornering force for the 3-DOF model due to the load transfer. An increase in cornering force can initiate earlier saturation of the tire force in the presence of braking, acceleration, or slippery floor (a track with lower coefficient of friction).

6.2.3.2. Disturbance

The ability of a vehicle to converge to its path after being subjected to disturbances is generally referred to as a vehicle's directicnal stability. A directionally stable vehicle will return to a steady state condition upon removal of the disturbances. This is not the case for a directionally unstable vehicle (Wong, 1993). In practice, the disturbances to a control system are not known ahead of time but are random in nature. However, suitable test signals are frequently used to compare the performance of different control systems. This is of particular interest for analysing and designing a suitable controller. Many design criteria are based on performance of systems to these test inputs (Ogata, 1990).

The response of the AGV due to a step input in the steering angle is evaluated. To create such an input a 0.3 m shift in the path is considered. Performances of the 2-DOF and 3-DOF models travelling at a constant speed of 2 m/sec are illustrated in Figure 6.11 and Figure 6.12. The lateral deviation due to step input is higher for a 3-DOF model, indicating the effect of terms included in this model.

6.2.3.3. Limitations of the Proportional Controller

Trial and error methods are generally used to obtain suitable gains for proportional controllers. Hemami et al. (1992) proposed a systematic approach for gain adjustment of such controllers. However, the proposed approach is limited to a vehicle with linearized model travelling on a straight paths.

Although proportional controllers are simple to implement, they have numerous drawbacks. These controllers are highly speed, load, and path dependent, and suffer from steady state error in tracking circular paths. Referring to Figure 6.13, the performance of the 3-DOF AGV model using the proportional controller is shown for various load and speed conditions. The gains that are tuned for mid load and speed ranges are not suitable for other conditions and result in overdamped response for lower loads and speeds and under damped response for higher loads and speeds. Figure 6.14, shows the performance of the controller used in the case shown in Figure 6.13 when tracking a circular path. Using gains tuned for step response the distance error is notable (Figure 6.15).

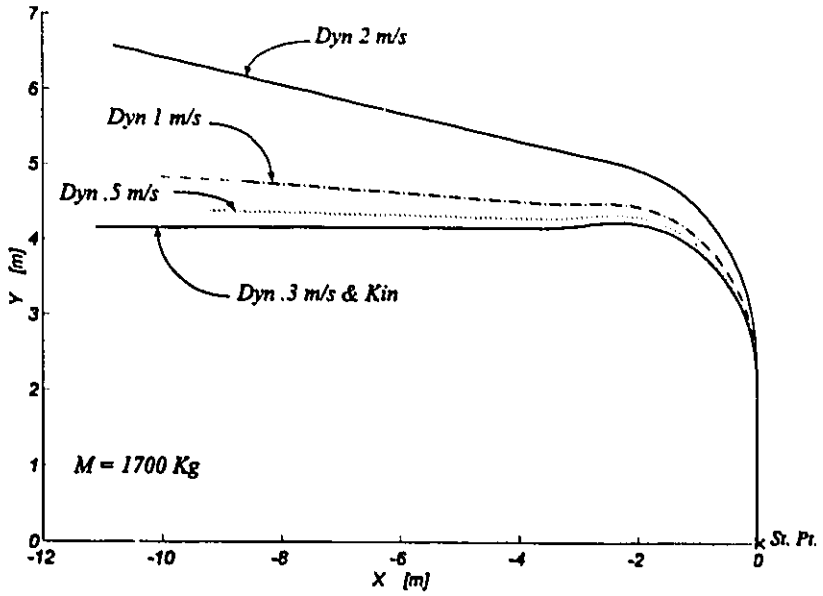

Figure 6.1 Comparison of kinematic and dynamic models.

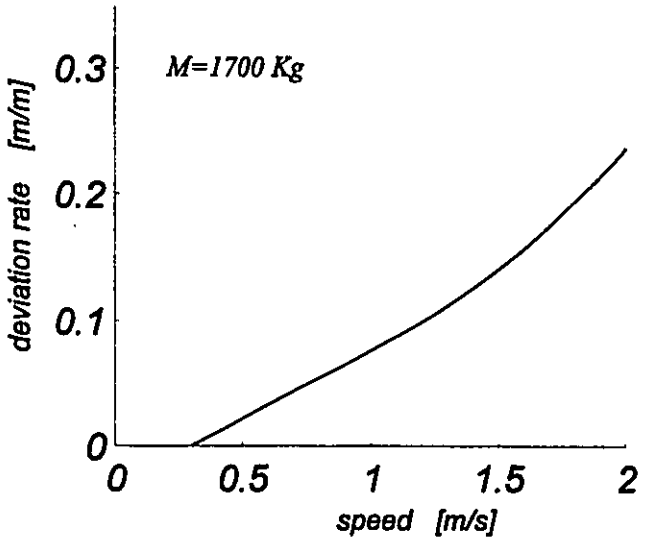

Figure 6.2 Deviation rate from the path versus speed for dynamic model.

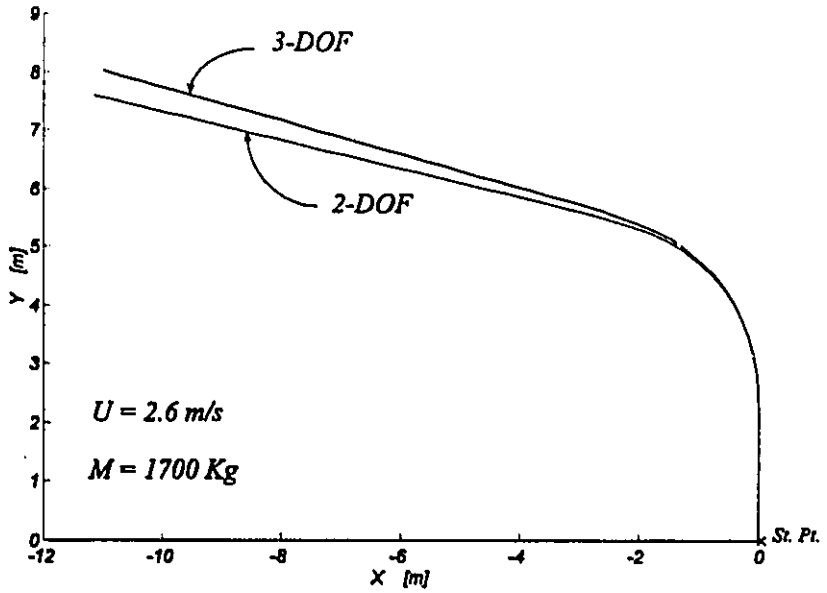

Figure 6.3 Comparison of path trace for 2-DOF and 3-DOF AGV models.

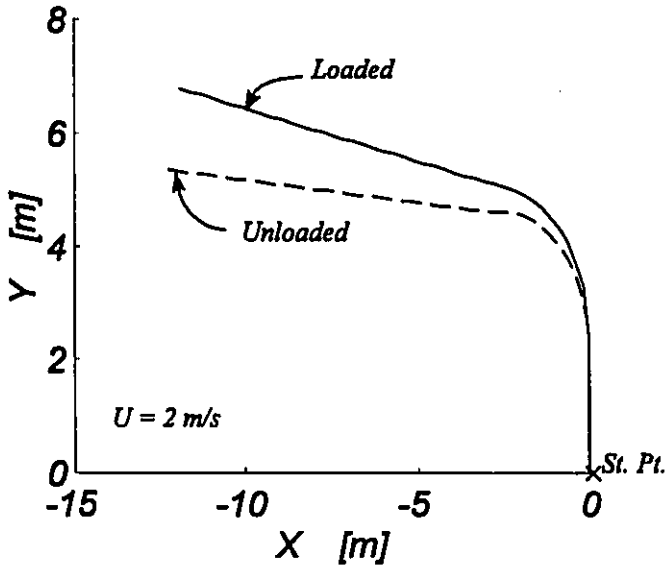

Figure 6.4 The effect of load on the AGV path trace.

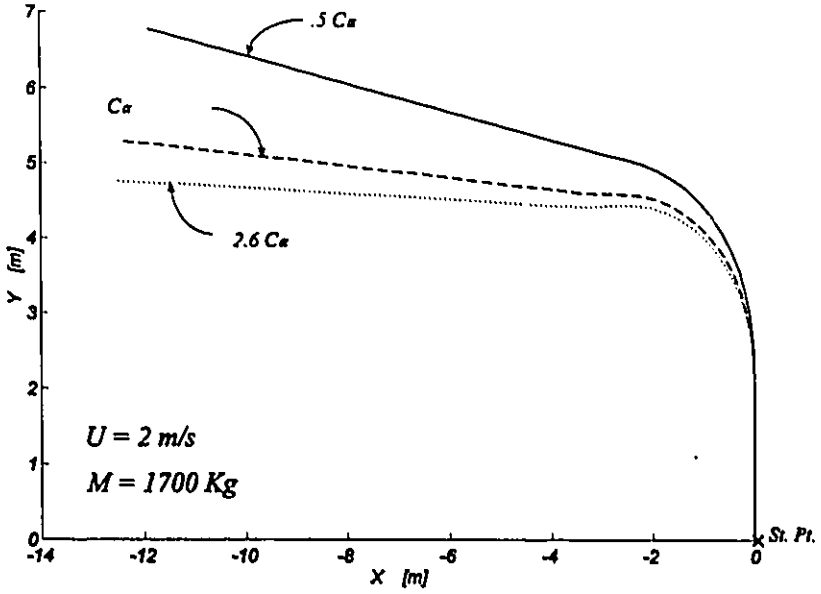

Figure 6.5 The effect of cornering stiffness on the AGV path trace.

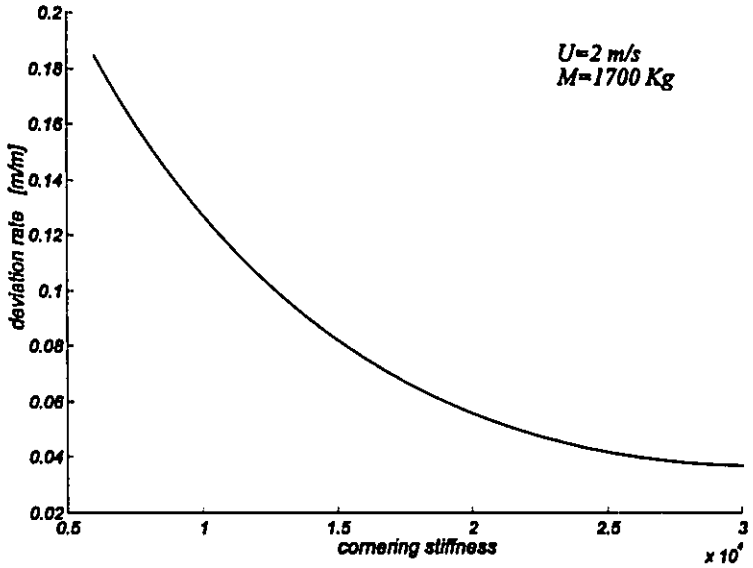

Figure 6.6 The effect of cornering stiffness on deviation rate from the path.

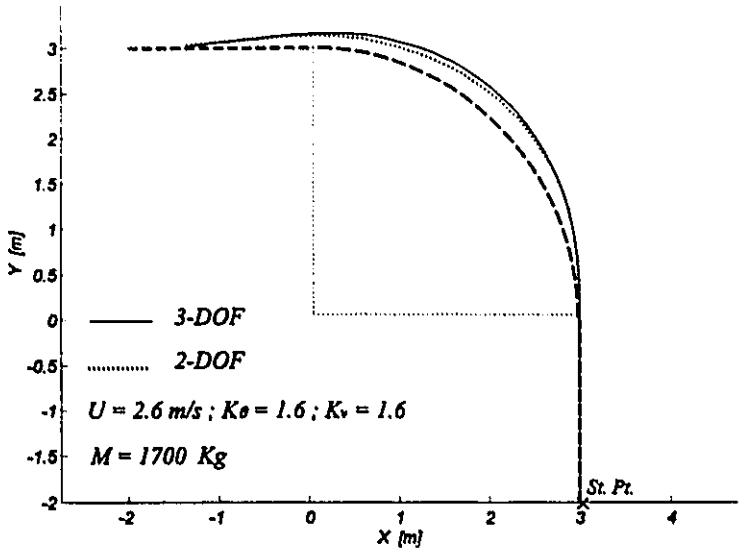

Figure 6.7 Path tracking performance of 2-DOF and 3-DOF models.

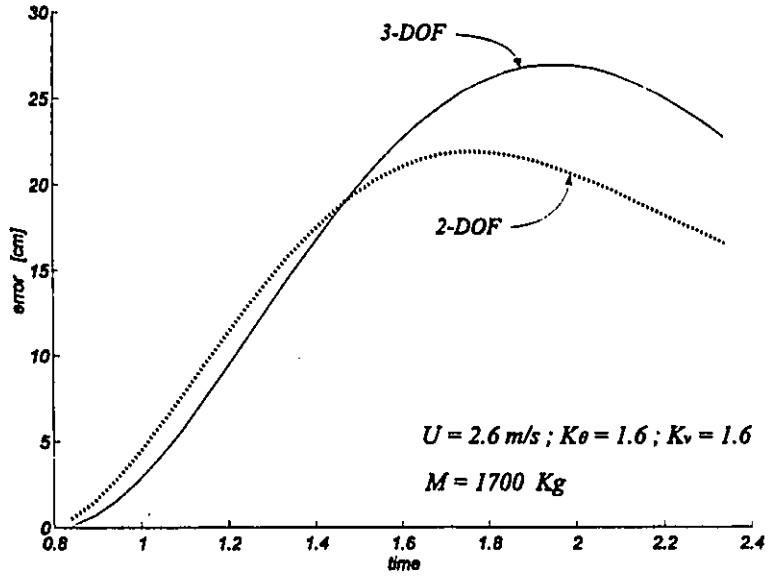

Figure 6.8 Distance error for tracking a line-circle-line path.

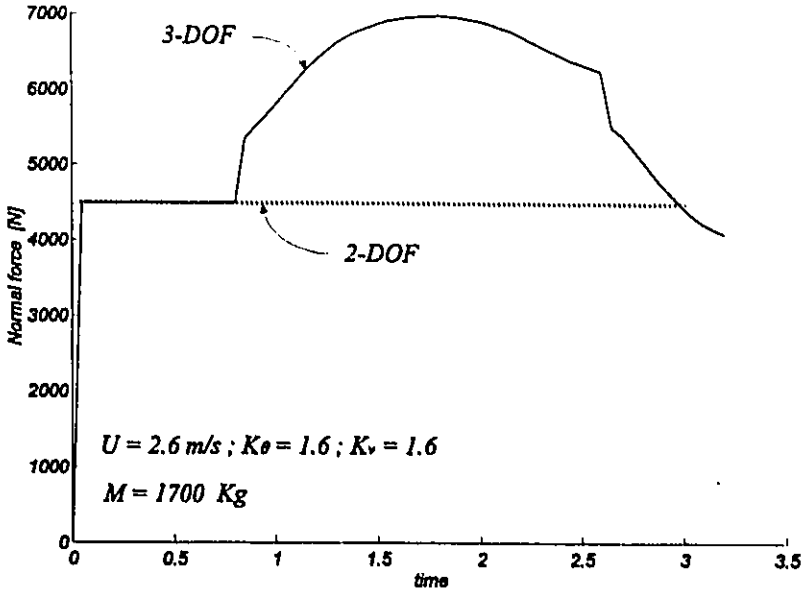

Figure 6.9 The normal force of front-right tire for tracking a line-circle-line path.

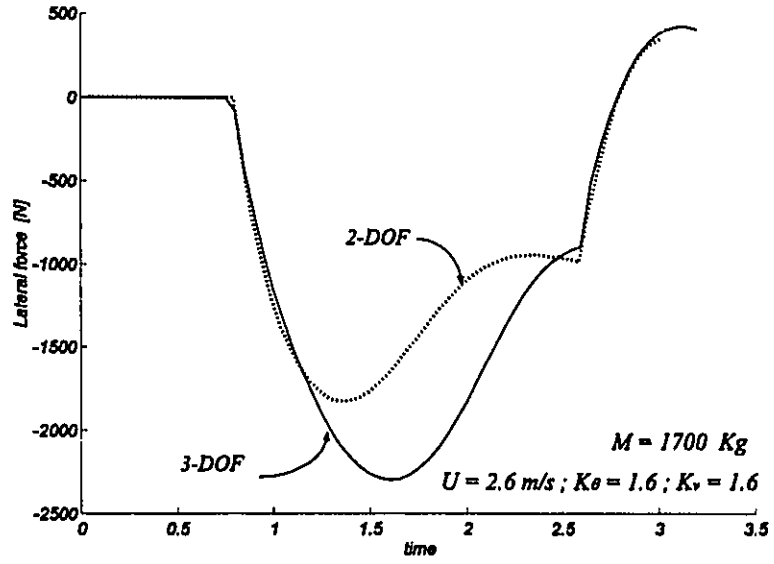

Figure 6.10 Cornering force of the front-right tire for tracking a line-circle-line path.

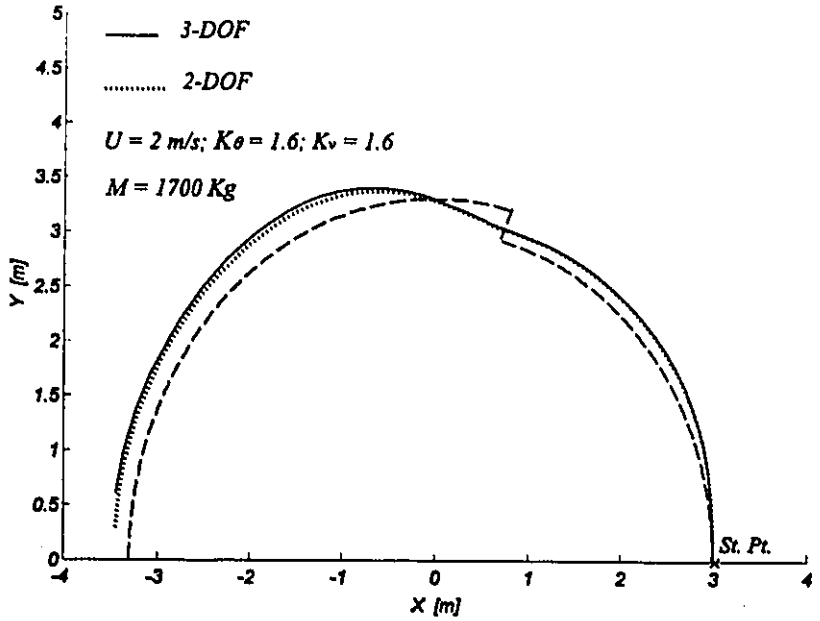

Figure 6.11 The effect of step disturbance, Step = 0.3 m.

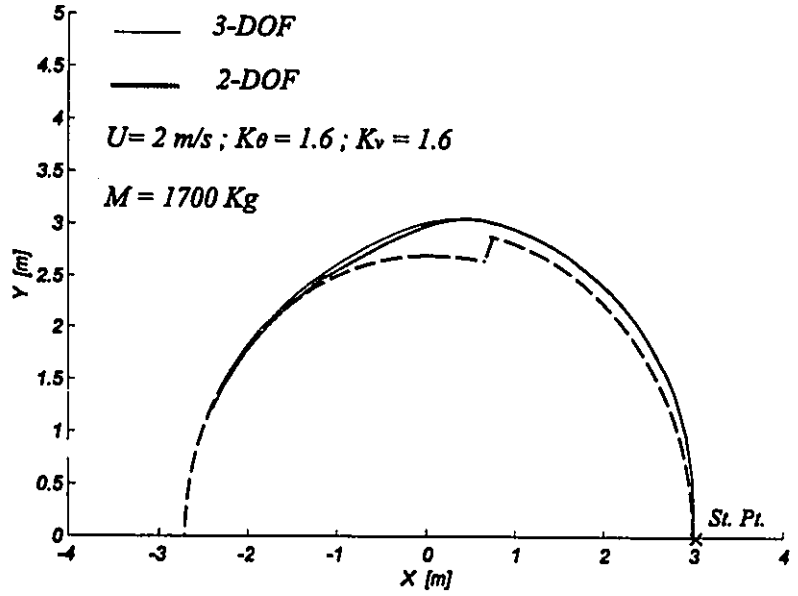

Figure 6.12 The effect of step disturbance, Step = -0.3 m.

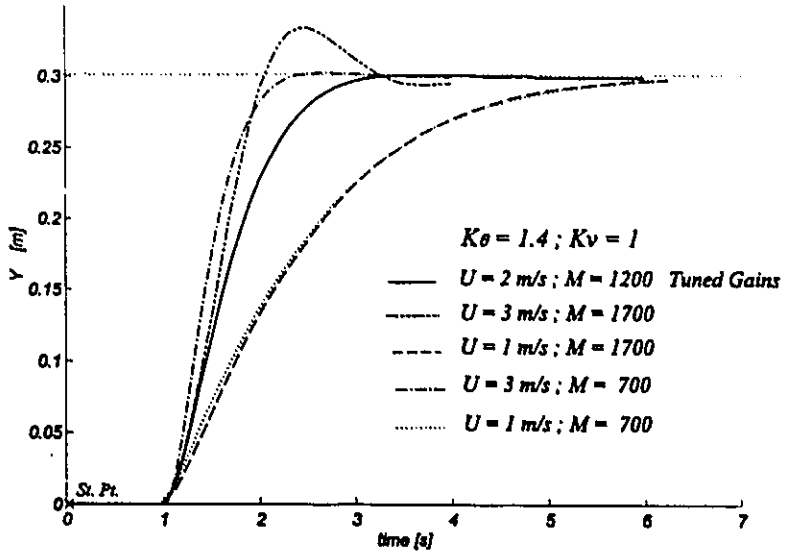

Figure 6.13 Step response of 3-DOF model using proportional controller for various loading and speed conditions.

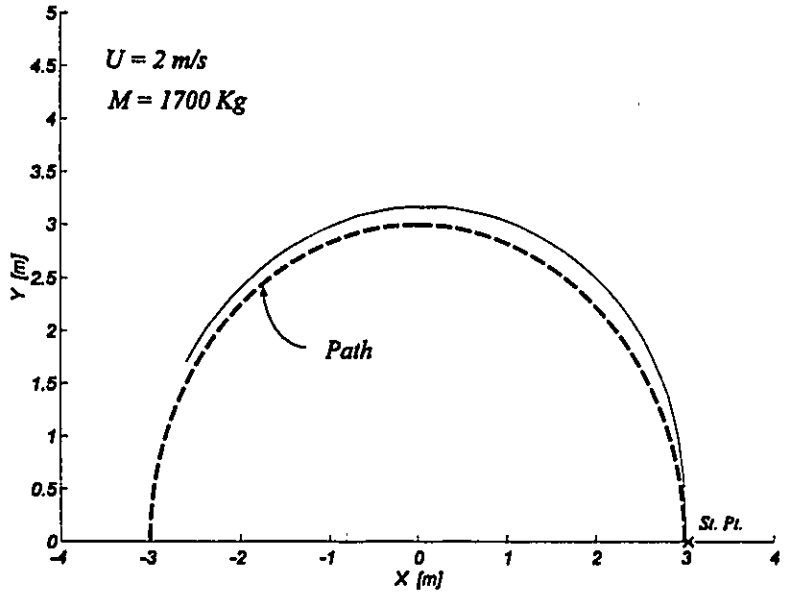

Figure 6.14 The 3-DOF AGV model tracking a circular path.

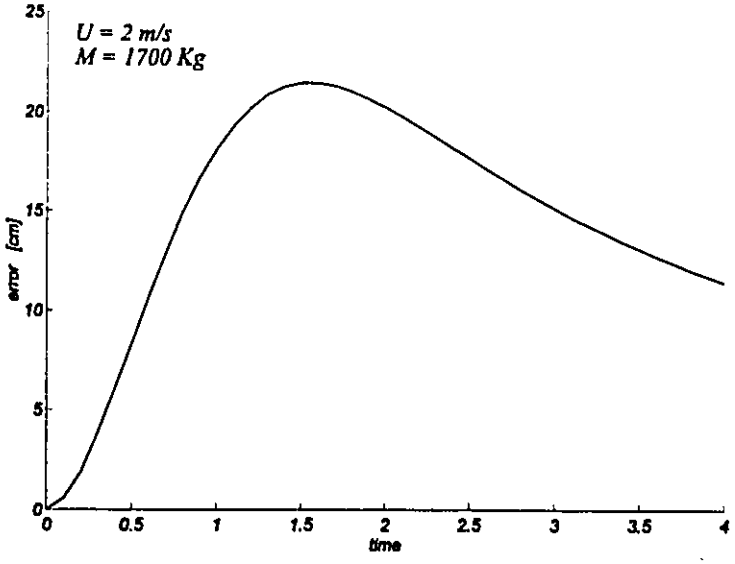

Figure 6.15 Distance error for tacking a circular path.

6.3. Performance Evaluation of the Control Schemes

In this section, the tracking capability of the AGV while utilizing the control schemes developed in Chapter 5 is studied. The vehicle parameters given in Appendix E will be used. The motors specifications are given in Appendix F. The emphasis here will be on controllers based on the Type I outputs. Some preliminary results of a controller design based on the Type VI outputs will also be presented.

6.3.1. PD Controller

When the PD controller developed in Section 5.5.1 is applied to a 2-DOF Side Slippage Free (SSF) model, it yields a critically damped response for the decoupled control position subsystem. This is accomplished by proper tuning of the controller gains in Equation5.37. Figure 6.16 depicts the 2-DOF SSF model responses for speeds of 2 and 3 m/s. The vehicle is simulated when tracking a straight path with initial lateral offset of 0.5

m and zero initial heading angle θ_i. In general, the initial velocity and initial heading angle are the most important factors that affect the trajectory of the 2-DOF SSF model. For this particular heading angle, identical response is observed for all the speeds and almost all the loading conditions. However, for the more complete 3-DOF model of the AGV, as shown in Figure 6.17, the vehicle response is highly dependent on the particular speed and load conditions. This is due to the inclusion of the tire model as well as other terms (like load transfer, roll...etc) that have been ignored in the 2-DOF SSF model.

6.3.2. SM controller

Simulation results of comparing the vehicle tracking capability using the PD and the SM controllers are presented in Figures 6.16-6.17. When applied to the 2-DOF SSF model, the SM controller is tuned to obtain a performance similar to that of the PD controller. To attain this the MIMO sliding mode controller terms λ_{i0}, and K_i are set to three and six, respectively. Referring to Figure 6.16, both controllers produce smooth exponential response for speeds of 2 and 3 m/s. However, for the 3-DOF model, considerably better tracking is realized when applying the SM controller, and the responses are almost identical with regard to variation in speed as shown in Figure 6.17. This is mainly due to the robust performance of the sliding mode controller which does not requires an accurate model of the system. For the remainder of this chapter, all the simulation will be based on the 3-DOF model.

The robustness in the presence of modelling imprecision and disturbance is obtained by applying discontinuous control law across the sliding surface. This results in chattering as the controller switches between the regimes across the sliding surface, and is shown in Figure 6.18 for output Y as an example. The resulting high frequency oscillations involve significant control activity and may excite unmodeled dynamic modes (Slotine and Li, 1991). Furthermore, for this study, chattering results in undesirable steering activity, as shown in Figure 6.19.

6.3.3. Boundary Layer Sliding Mode Controller

Introducing a thin boundary layer around the sliding surface as shown in Figure 6.20 results in reduced chattering with a considerably smoother steering, as shown in Figure 6.21. The chattering across the sliding surface is a function of the boundary layer thickness. As the thickness of the boundary layer decreases, the function *sat*(*S*) approaches the *sgn*(*S*). In the simulations the boundary layer thicknesses φ_1, and φ_2 are set to 0.1 m. The BLSM controller is studied in the remainder of this chapter, due to the chattering disadvantage of conventional SM controllers.

6.3.4. Comparison of PD and BLSM Controllers

The performance of PD and BLSM controllers are examined in this section under different operating conditions. The simulations presented here are carried out for an AGV having fixed parameters for the controllers. Since for all practical purposes the oscillatory response of the vehicle is not desirable, the PD controller gains of the linear decoupled control system are designed in such a way so as to obtain a non-oscillatory response even for the worst load-speed conditions. Consequently the response will be sluggish for other load-speed cases.

6.3.4.1. Effect of Speed

With Reference to Figure 6.22, the tracking performance of the PD controller is shown for the loaded vehicle at three different speeds of 1, 2, and 3 m/s. Under similar conditions results, for BLSM controller are shown in Figure 6.23. The Figures show that as the speed increases the effect of the terms not included in the design process of the controller becomes apparent.

6.3.4.2. Effect of Parameter Change and Model Uncertainty

Modelling uncertainties are the outcome of difficulty in measuring or estimating the kinematic or dynamic parameters, or in some cases lack of complete knowledge of the

system components. The modelling uncertainties in the payload and the tire cornering stiffness are simulated and the results are presented in this section. This is achieved by design of the controller for a given load and tire cornering stiffness, then carrying out simulations for different conditions.

Effect of Payload

One of the parameters that is being fed back to the plant in the feedback linearization scheme is the vehicle's mass m. In the following simulations this parameter is set to a fixed value of 1200 kg for the controller. The vehicle trajectories for PD and BLSM controllers when it is fully loaded (m=1700 kg) and unloaded (m=700 kg) are shown in Figure 6.24 and 6.25, respectively for a speed of 3 m/s. Both controllers show robust performances under given conditions. However, the vehicle response is faster and less sensitive to variation in payload when the BLSM controller is utilized.

Effect of Cornering Stiffness

The effect of tire characteristics on the vehicle's tracking performance is shown in Figure 6.26 and 6.27 for the PD and the BLSM controllers, respectively. The simulations for the present tire cornering stiffness C_α is compared with the cases of $2C_\alpha$ and $.6C_\alpha$. The vehicle speed is maintained constant at 2 m/s. The response of PD controller tends to oscillate as the tire cornering stiffness decreases, while a robust performance is observed for the BLSM controller. Also, the SM controller reacts more quickly to converge the vehicle to the desired path.

6.3.4.3. Effect of Disturbance

The disturbance is introduced here in the form of a sudden displacement from the intended path. Figure 6.28 shows the effect of such a step disturbance of 0.3 m when the vehicle is moving along a straight track. For AGV speeds of 2 and 3 m/s the transient response of BLSM controller is fast, accurate, and insensitive to step disturbance, while the PD controller performance is sluggish, speed dependent, and oscillatory at higher speeds.

The settling time for the SM controller is 4.2 seconds where as, the PD controller does not settle during the first 7 seconds of simulation.

6.3.4.4. Effect of Path Geometry

In practice the paths for routing automated guided vehicles within their workspace are generally composed of line and circular arc segments (Nelson, 1989). Also, it has been shown that for any given initial and final posture of the vehicle, a family of paths comprising only lines and circles segments can be found between the source and destination (Sarkar et al., 1994). Figure 6.29 depicts the tracking performance for the second basic path segment, i.e. circular arc segment. Both controllers are examined at speeds of 1.5 m/s and a fully loaded vehicle. The normal distance error is shown in Figure 6.30. The BLSM controller has a faster response with considerably smaller error when compared to the PD controller. Furthermore, the application of the PD controller results in a significant steady state error.

6.3.4.5. Effect of Initial Conditions

Among the factors which have a major effect on the convergence of the AGV to the required path of the vehicle is its initial heading. For tracking a straight path, the performance of the loaded vehicle for different initial headings is shown in Figure 6.31. Both controllers are tested for a speed of 2 m/s. Similar results for tracking a circular arc segment are shown in Figures 6.32-6.34. The vehicle speed is set to 1.5 m/s for circular path simulations. Examination of Figures 6.31 and 6.32 show that the BLSM controller reacts more quickly to bring the vehicle to the desired path. The steady state errors in Figure 6.33 and 6.34 shows the prominent results. The PD controller can not compensate for the steady state error because it does not have any integral compensator, where as the BLSM controller can compensate for the steady state error without any integral term.

6.3.5. Performance of Type VI Outputs

In this section the vehicle tracking capability with a PD controller implementation based on type VI outputs, PD-VI (i.e. vehicle speed and normal distance to the path) is compared with that based on type I outputs, PD-I. Figure 6.35, and 6.36 show the results for both controllers. The circular arc segment is used to simulate the performance of a loaded vehicle with a speed of 1.5 m/s. In both cases the trajectories converge toward the desired path. The PD- VI controller merges gradually with the intended path, while PD-I reacts more quickly and it has an overshoot. For most practical purposes a smoother response similar to that of the PD-VI is more desirable.

6.3.6. Modified BLSM Controller

Despite all the merits of the BLSM controller discussed so far, during the simulations this type of controller resulted in certain undesirable vehicle responses for particular cases. These cases are studied in detail in this section.

a) The robust performance of the BLSM controller was ensured through the high gain setting to the attractive surface. This however, causes the cornering force threshold to be reached for initial headings beyond $\pi/3$ rad, and would result in tire slippage. The resulting undesirable vehicle performance when tracking a circular path with initial heading of 1 rad at a speed of 1.5 m/s is shown as BLSM curve in Figures 6.37-6.38. The saturation of the cornering force was eliminated by reducing the gains K_η, this is shown as BLSM-1 curve in the figures. However, varying the gains K_η results in a non-smooth response for other critical operating conditions and contradicts the idea of unique adjustment of gains for the whole operating range of the AGV. This is observed when gain value of $K_\eta = 3$ and speed of 3 m/s for a loaded vehicle moving on a straight path as shown in Figure 6.39.

b) Referring to Figure 6.23, some distortion is observed in the BLSM controller response for the speed of 3 m/s and gains of $K_\eta = 5$. The distortion occurs after the first second of motion and is more pronounced for the case shown in Figure 6.39, when the gains are reduced to $K_\eta = 3$. To examine the BLSM controller behaviour further, the lateral deviation phase diagram for both gain settings is plotted in Figure 6.40. For both cases, the

system trajectory hits the sliding surface and proceeds to pass the boundary layer. Consequently the system is not in the sliding regime for a long period of time. Also, due to boundary layer thickness the system trajectory is not forced to sliding surface, and is oscillatory in spite of being within the boundary layer. This is magnified as the gains K_i decrease.

Two schemes may be used to deal with these shortcomings: 1) Increase the controller gains, K_1 and K_2 so as to strengthen the sliding surface attractiveness property. This approach, however, aggravates the problem described in part (a) above. 2) Reduce the boundary layer thickness. The comparison of vehicle response using the BLSM controllers with $\varphi_i = .1$ (BLSM curve) and $\varphi_i = 0.03$ (BLSM-1 curve) is shown in Figure 6.41. The corresponding system trajectories are also shown in Figures 6.40 and 6.42. Although this approach is helpful, it initiates the chattering as shown in Figure 6.42 (BSLM-2 curve).

In present work, the MBLSM controller developed in Chapter 5 is implemented to further enhance robustness and reduce the boundary layer thickness without elevating chattering. Application of VBL technique to reduce the chattering is shown in Figure 6.42 as VBL curve. Result of simultaneous application of MSS and VBL strategies to the vehicle are presented in Figure 6.43 and the corresponding phase diagram is shown in Figure 6.44. The vehicle speed is 3 m/s, the sliding surface slope varies from 1 to 3, the controller gains are reduced to $K_i = 3$, and boundary layer is defined as

$$\varphi_i = .03 + .1|e_i|$$

Noticeable improvements are observed. Compared to the BLSM, the MBLSM controller resulted in a smooth response with the same settling time as the BLSM controller. Results for tracking a circular path are also shown in Figures 6.45 and 6.46. The vehicle speed is 1.5 m/s. When compared to the PD and the BLSM controllers the MBLSM has a fast, and accurate response with no overshoot.

Although the MBLSM controller is designed for an AGV under the specified working condition given in Chapter 1, the controller's performance is robust when the speed exceeds beyond the design value of 3 m/s. Figures 6.47 shows the vehicle responses when the speed is increased up to 40 percent of the design value. Using the same controller gains as before, the vehicle response tends to oscillate as the speed is increased beyond 40 percent.

Robustness to overload has not been evaluated since an AGV overload would have other adverse effects and should be avoided.

6.4. Discussion of Results

The AGV's kinematic model that is most often used for simulation studies is compared to the dynamic model. It is shown that for high load and speed conditions the kinematic model is entirely incapable of representing the real vehicle behaviour. The characteristics of the pneumatic tires are modelled using a simple tire model. Significant differences in the vehicle response, due to tire parameters indicate the necessity for proper tire modelling. The performance of the 2-DOF and 3-DOF dynamic models are compared to investigate the effect of the roll degree of freedom and the load transfer. Notable differences are observed for the vehicle under study. Limitations in the proportional controller based on position and orientation errors show that a more sophisticated controller is required.

The performance of the proposed PD, and SM controllers are compared for different operating conditions. Due to presence of chattering in the steering angle the SM controller was not a suitable choice, therefore the boundary layer sliding mode controller was studied instead. Almost for all the cases the BLSM controller showed a superior robustness and faster response compared to the PD controller. The dominant factors affecting the AGV's tracking capabilities are identified as speed, load and cornering stiffness of tires. Some shortcomings were observed in the BLSM. These were compensated by implementing the MBLSM controller with simultaneous application of VBL and MSS strategies. The results for Type VI outputs were promising when compared to Type I outputs. The test results show that using velocity and normal distance error as the outputs to develop a decoupled control system results in a smoother tracking of circular path.

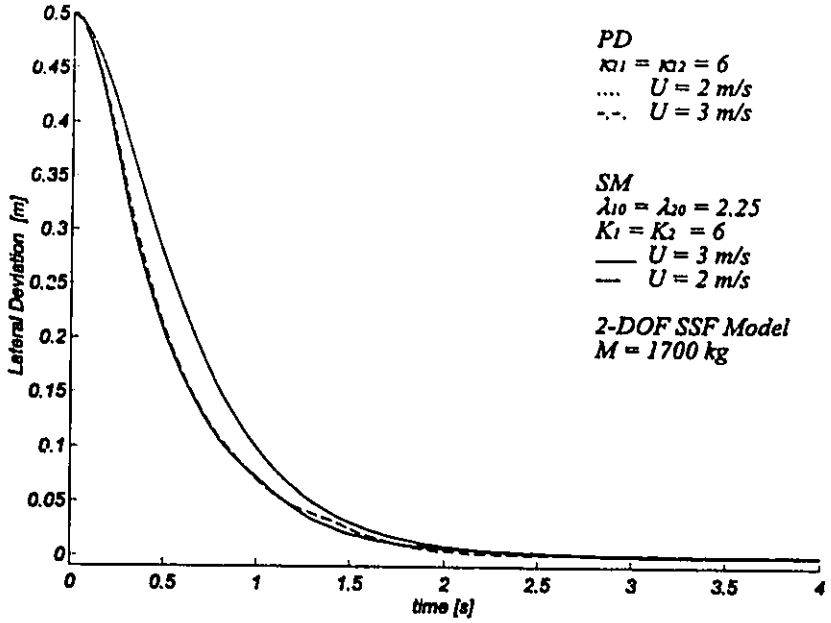

Figure 6.16 The performance of the PD and the SM controllers for tracking a straight path, utilizing the 2-DOF SSF vehicle model.

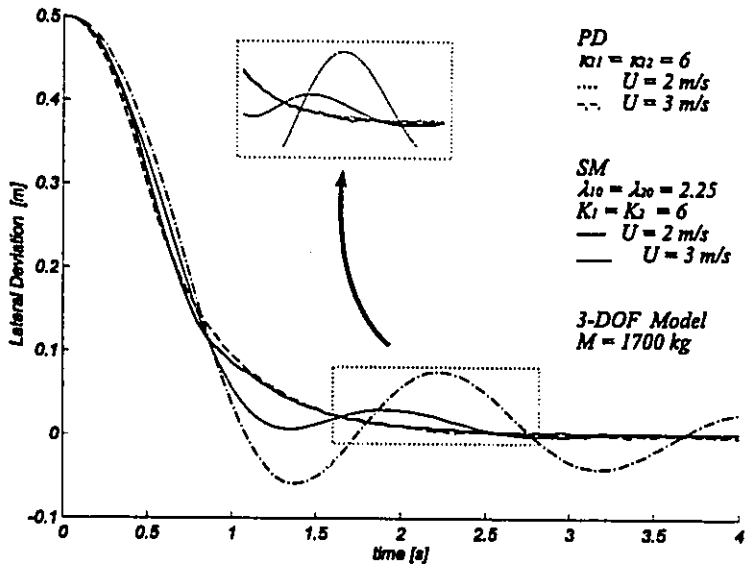

Figure 6.17 The performance of the PD and the SM controllers for tracking a straight path, utilizing the 3-DOF vehicle model.

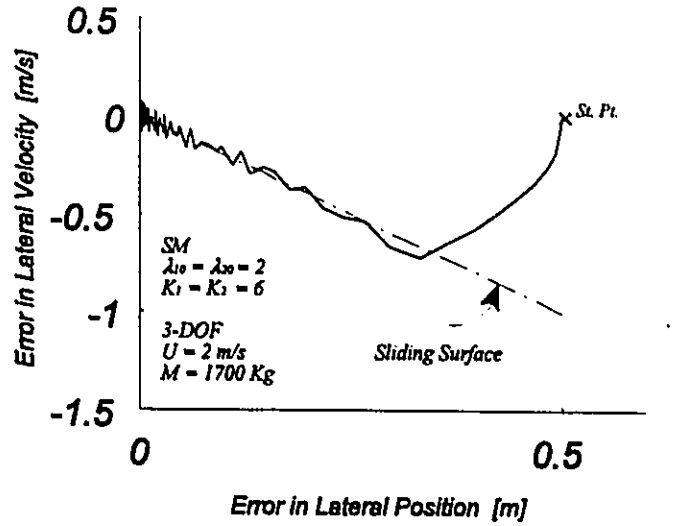

Figure 6.18 The phase portrait of vehicle's lateral position, utilizing the SM controller.

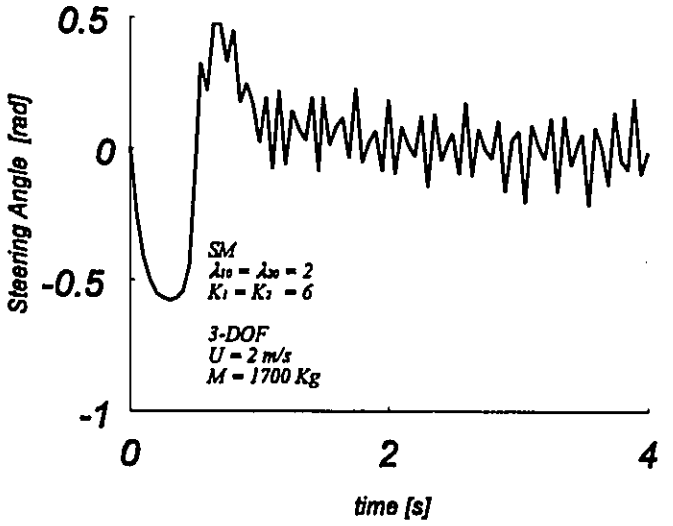

Figure 6.19 Chattering in the steering angle as a result of employing the SM controller.

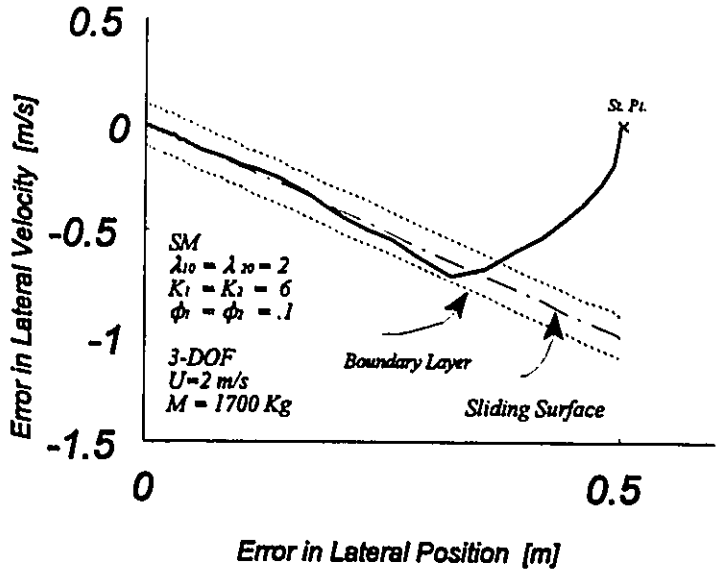

Figure 6.20 The phase portrait of vehicle's lateral position, utilizing the BLSM controller.

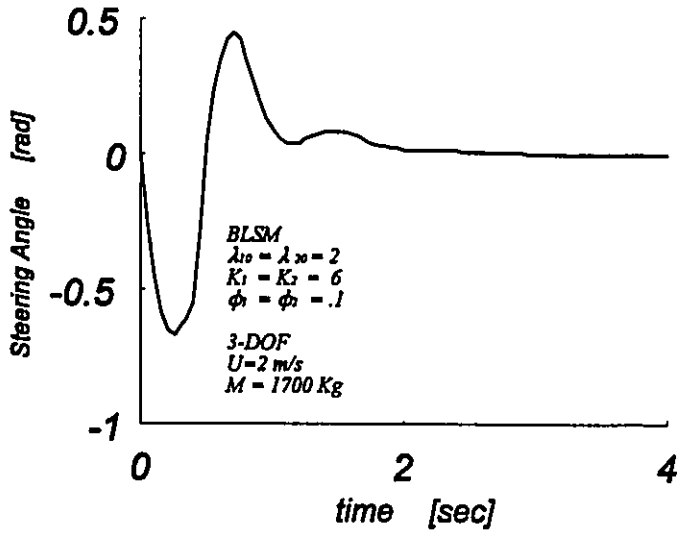

Figure 6.21 Improved steering activity due to introducing a thin boundary layer around the sliding surface.

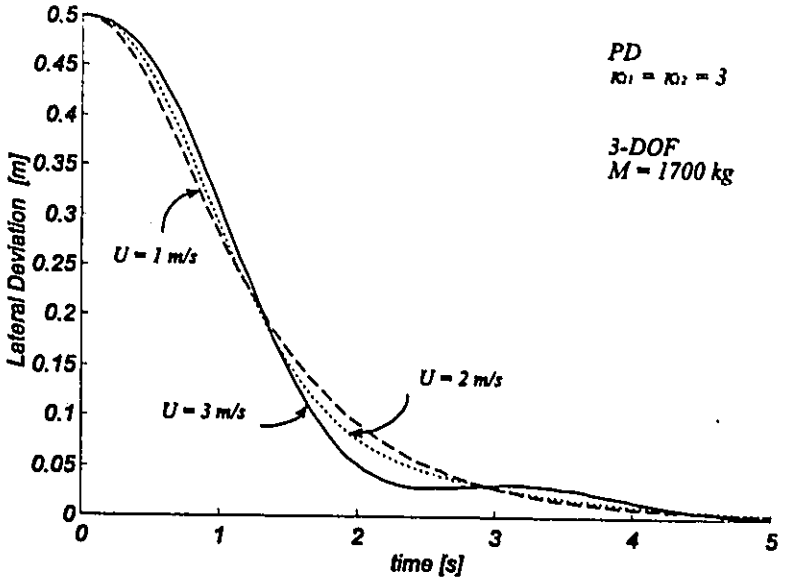

Figure 6.22 The effect of speed on the tracking performance of the PD controller.

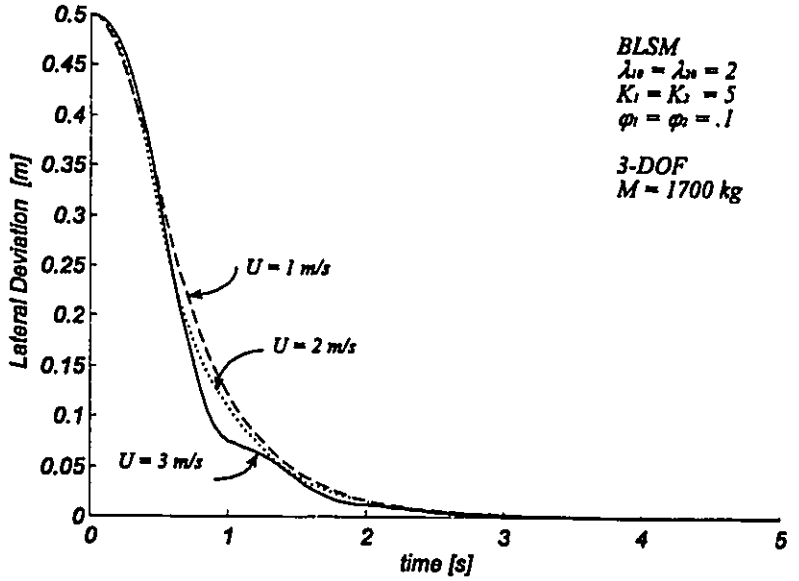

Figure 6.23 The effect of speed on the tracking performance of the BLSM controller.

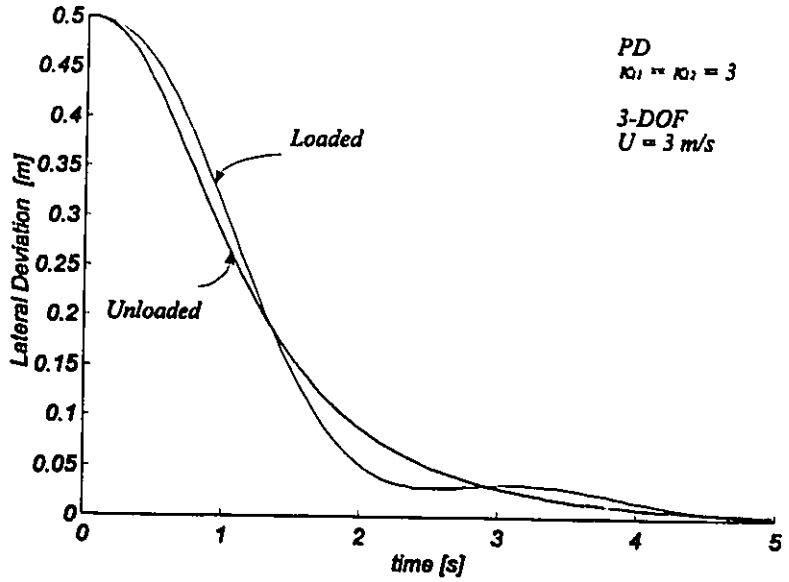

Figure 6.24 The effect of change in the payload on the PD controller performance.

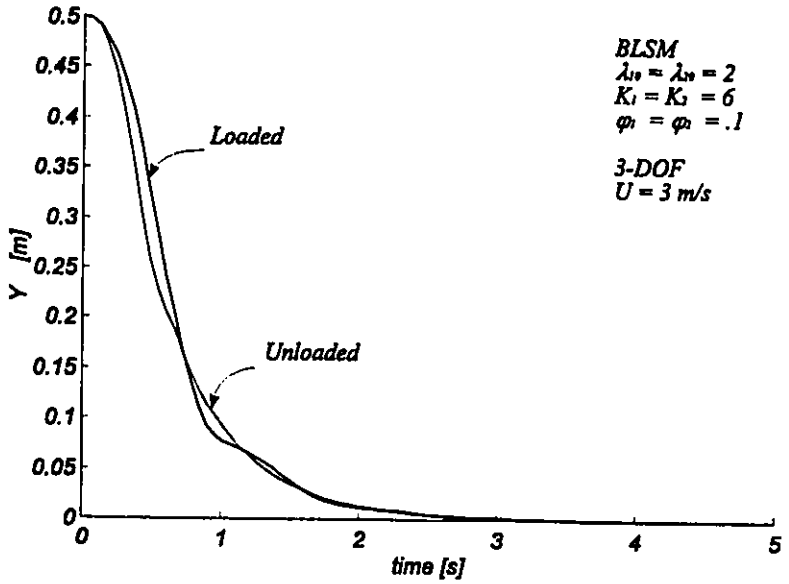

Figure 6.25 The effect of change in the payload on the BLSM controller performance.

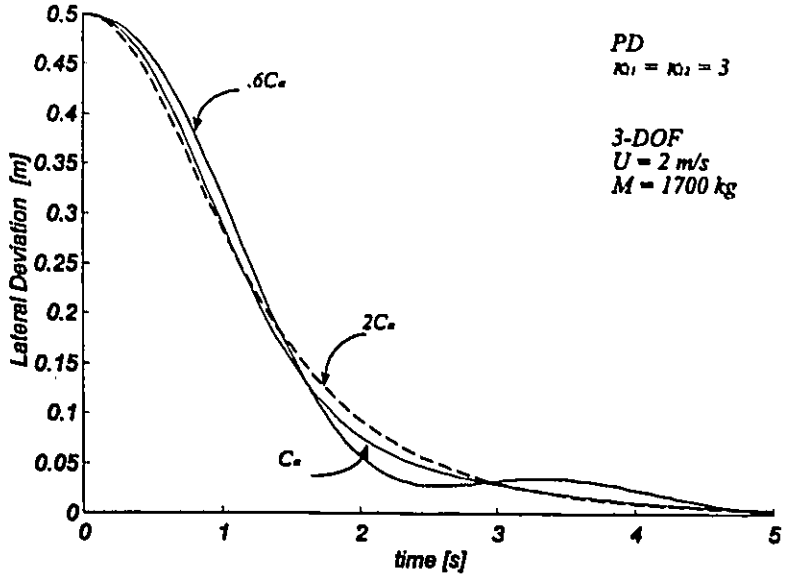

Figure 6.26 The effect of change in the tire cornering stiffness on the PD controller performance.

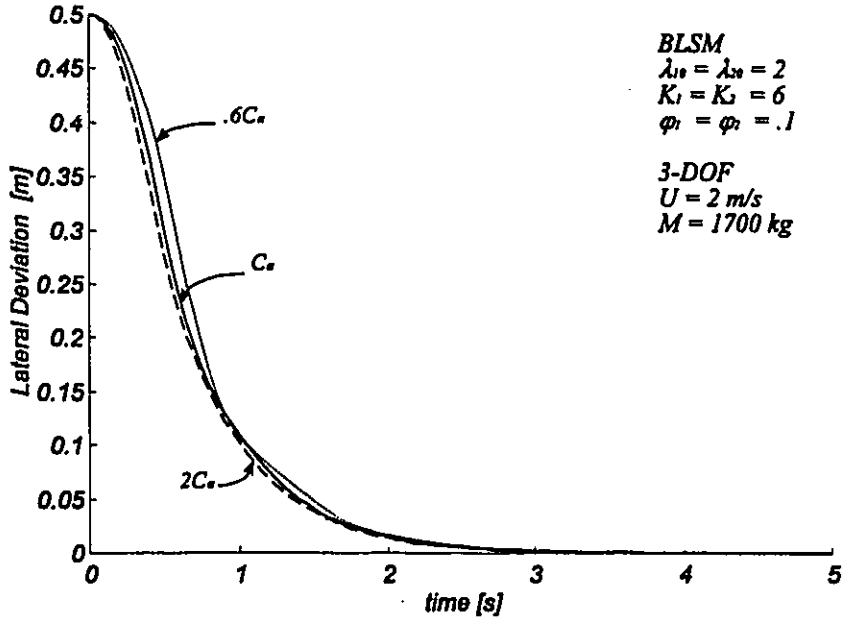

Figure 6.27 The effect of change in the tire cornering stiffness on the BLSM controller performance.

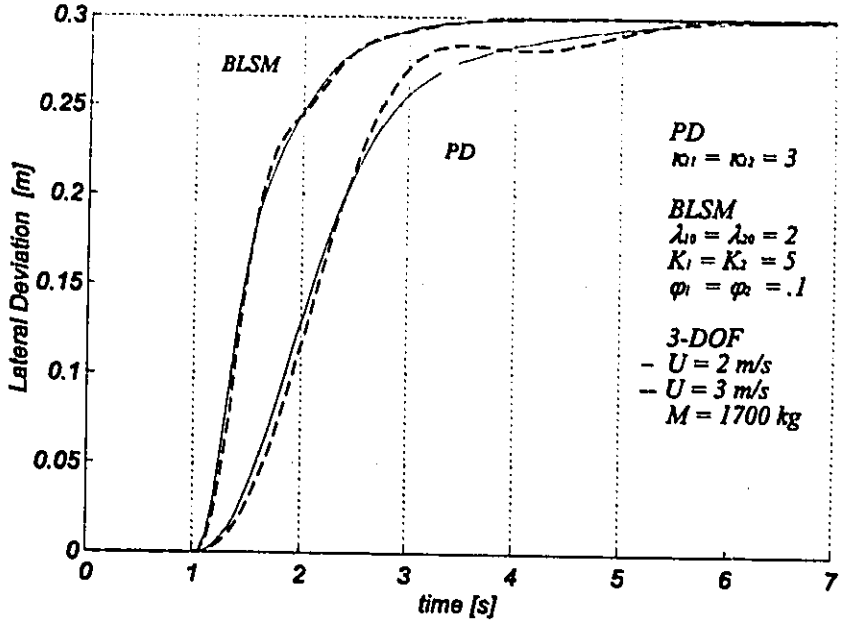

Figure 6.28 Performance in the presence of step disturbance in the path.

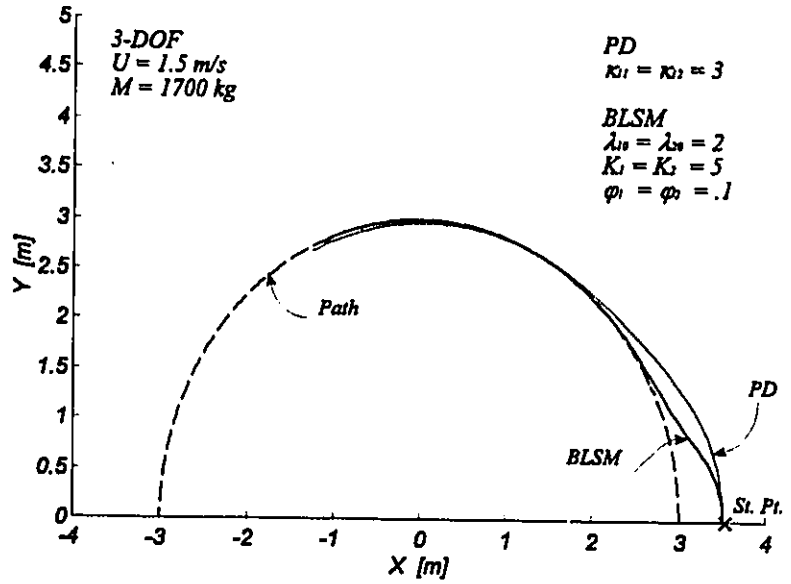

Figure 6.29 The performance of the PD and the BLSM controllers in tracking a circular path.

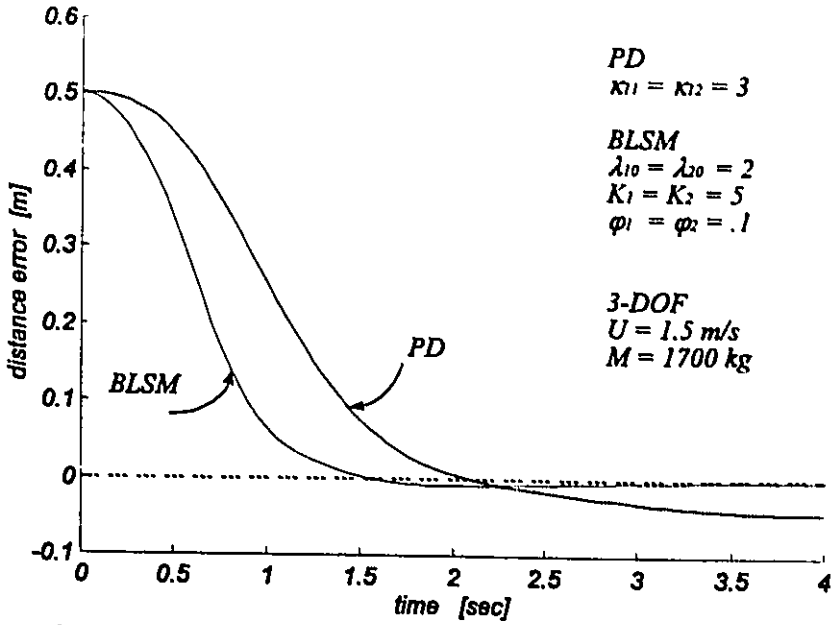

Figure 6.30 Comparison of distance error of the PD and the BLSM controllers in tracking a circular path.

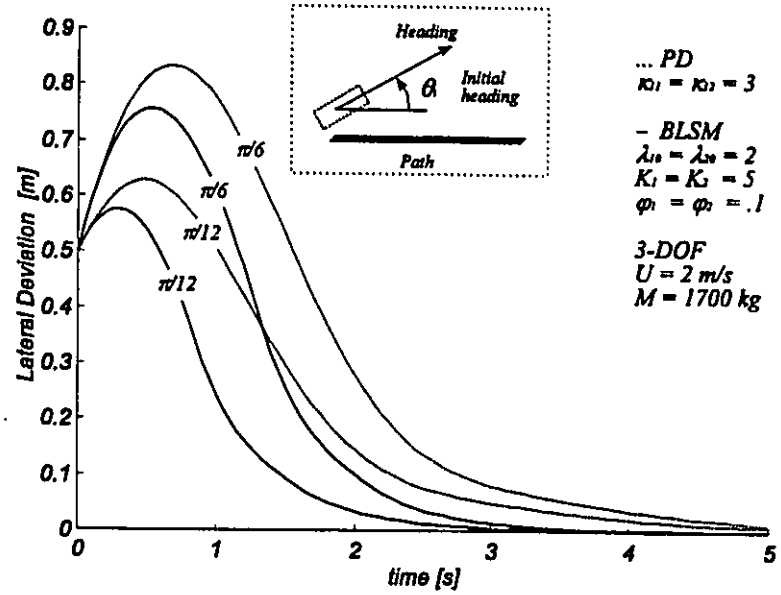

Figure 6.31 The effect of initial heading on the vehicle response utilizing the PD and the BLSM controllers.

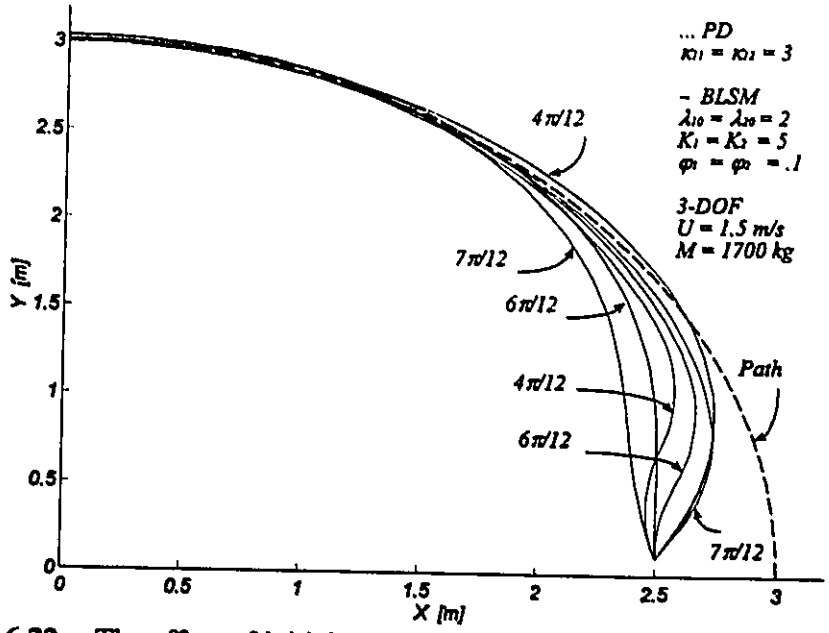

Figure 6.32 The effect of initial heading on the vehicle response for the PD and the BLSM controllers.

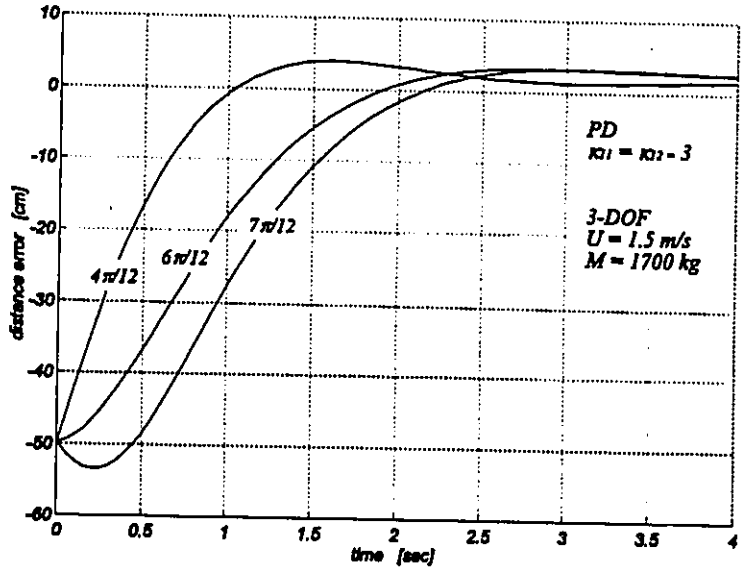

Figure 6.33 Comparison of distance error due to different initial headings for the PD controller.

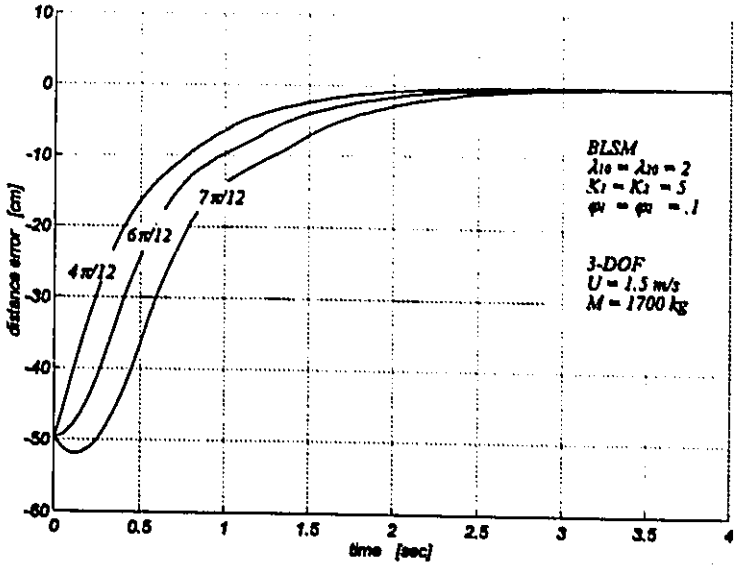

Figure 6.34 Comparison of distance error for the BLSM controller due to different initial conditions.

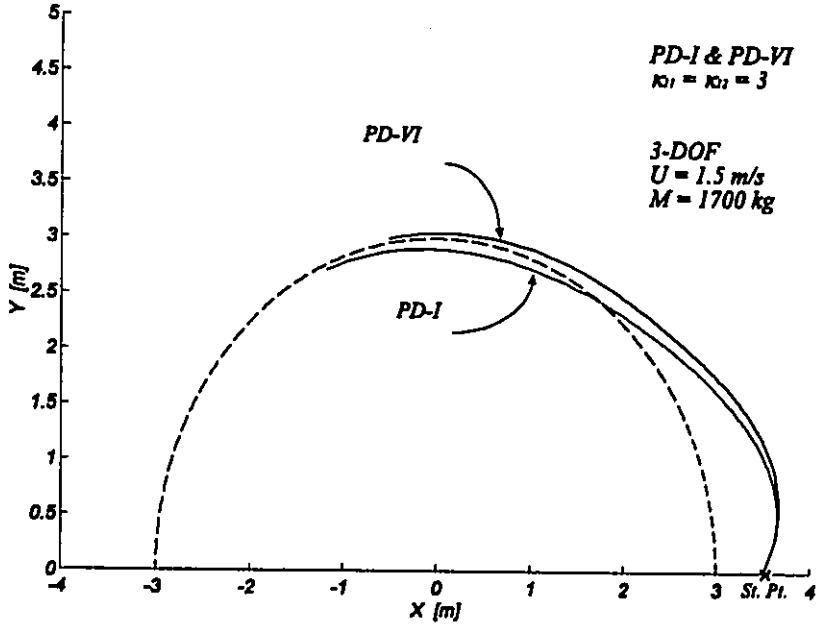

Figure 6.35 Comparison of vehicle's tracking capability implementing PD controllers based on type I and type VI outputs.

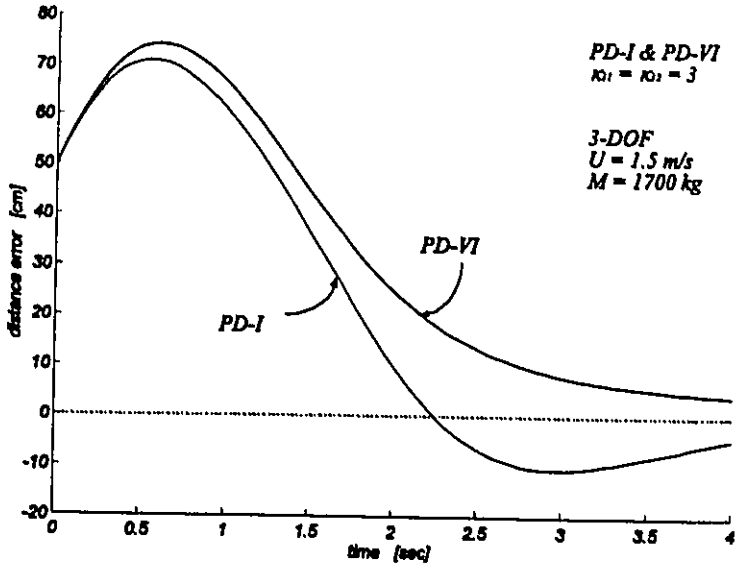

Figure 6.36 Distance error for PD controllers based on type I and type VI outputs.

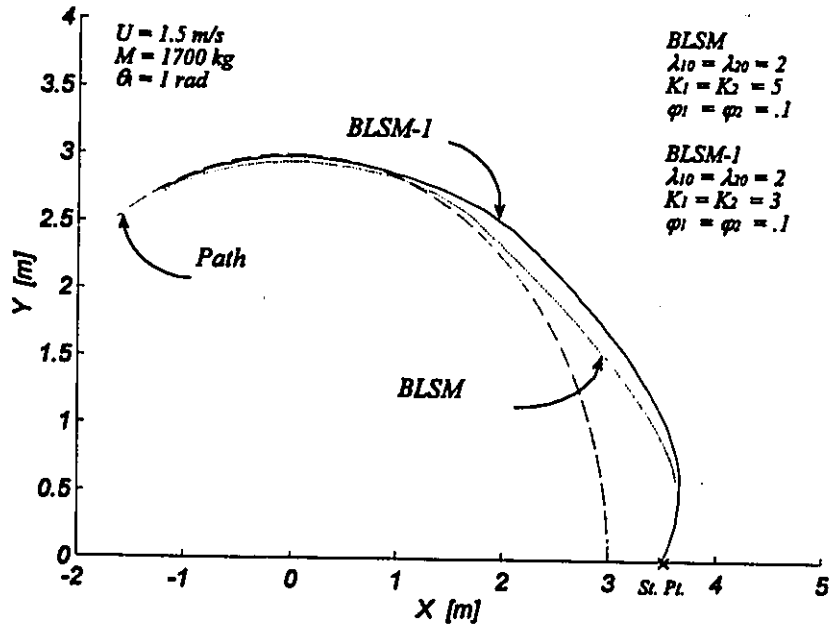

Figure 6.37 The effect of reducing K_1 and K_2 on the performance of the BLSM controller.

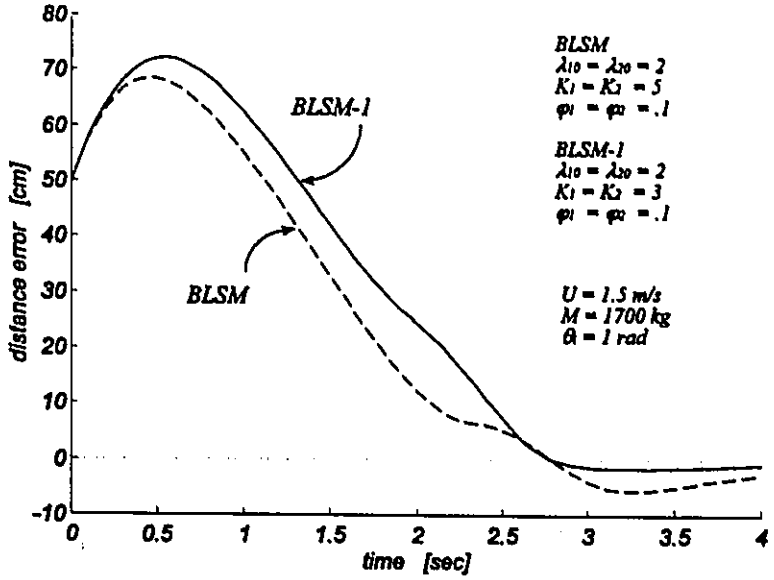

Figure 6.38 The effect of reducing K_1 and K_2 on the distance error for the BLSM controller.

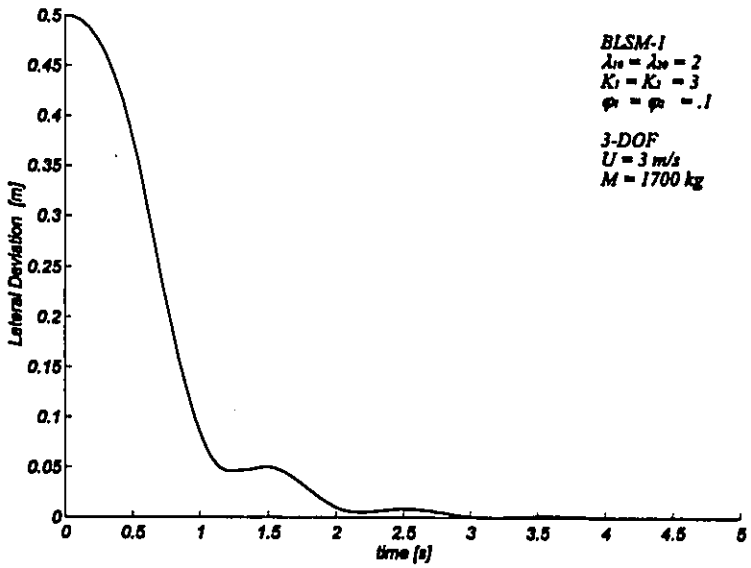

Figure 6.39 Non-smooth response of the BLSM controller for tracking a straight path at a speed of 3 m/s, due to reducing K_1 and K_2.

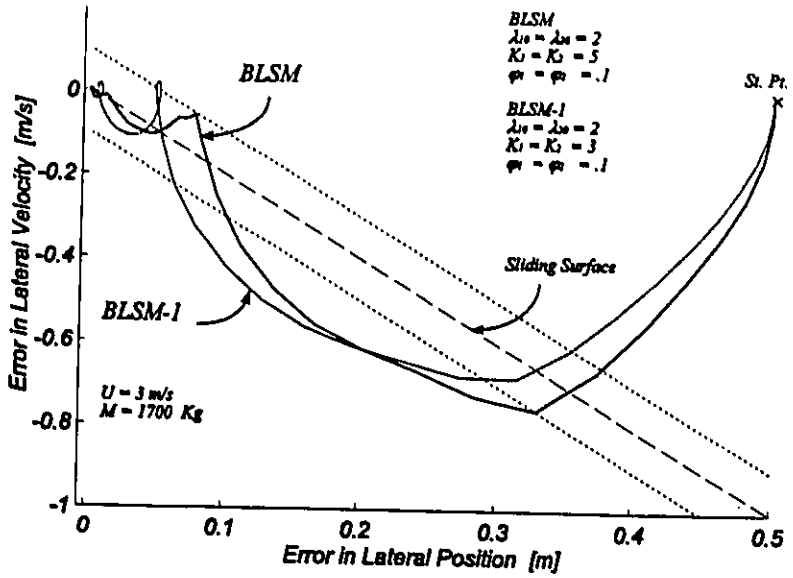

Figure 6.40 The effect of reducing K_1 and K_2 on the system's trajectory (output Y) for the BLSM controller.

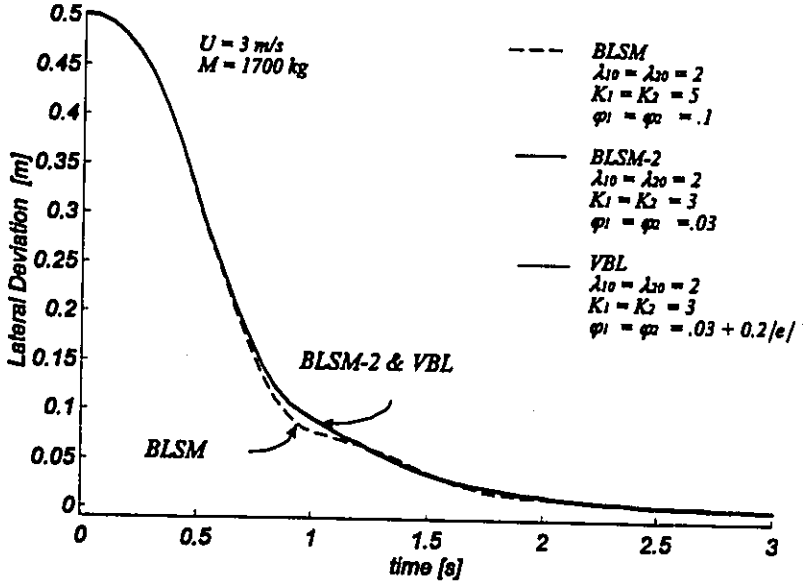

Figure 6.41 Performance of the BLSM controller using the VBL strategy.

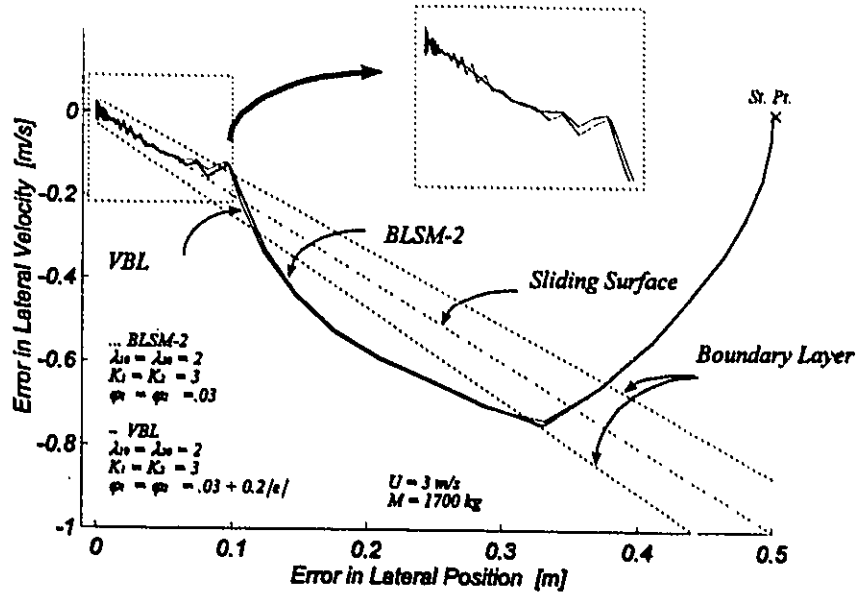

Figure 6.42 Phase portrait of the VBL controller and the BLSM controller with reduced boundary layer thickness.

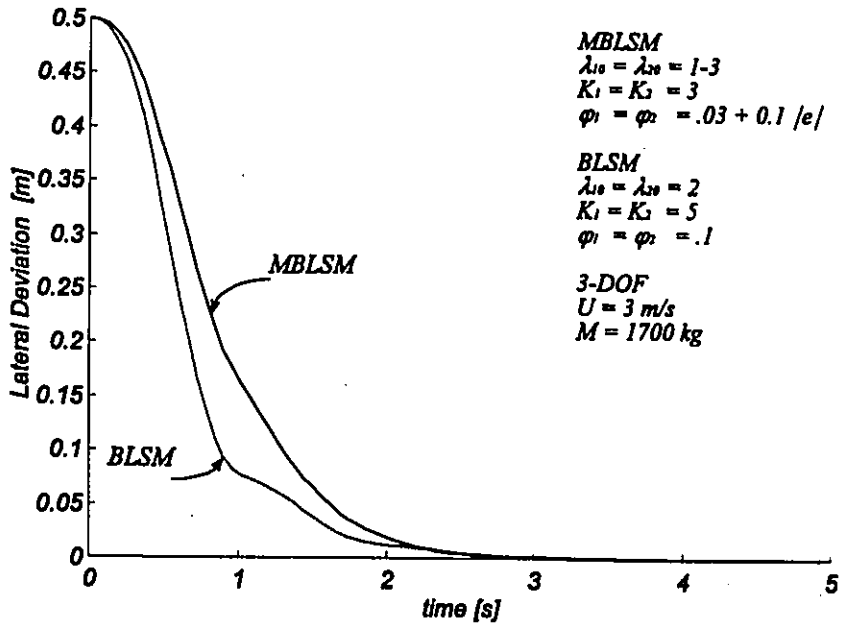

Figure 6.43 Performance of the BLSM and the MBLSM controllers for tracking a straight path.

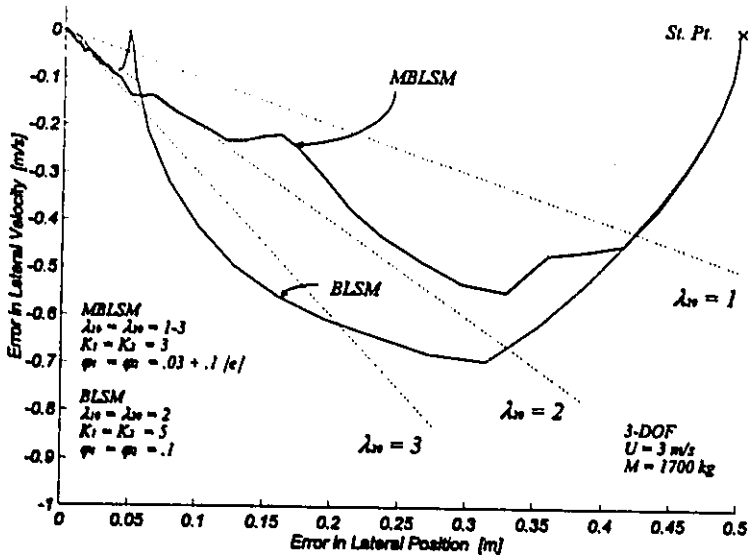

Figure 6.44 The phase portrait of output Y for the BLSM and the MBLSM controllers.

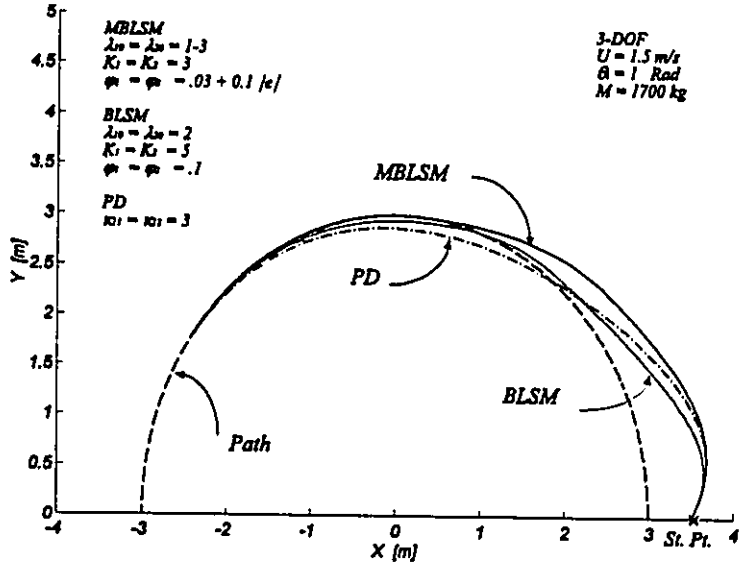

Figure 6.45 The performance of the PD, the BLSM and the MBLSM controllers for tracking a circular path.

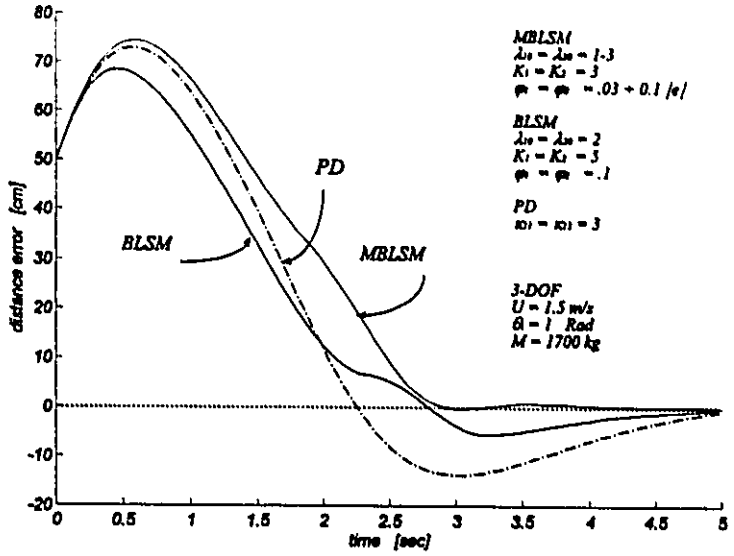

Figure 6.46 Comparison of distance error for the PD, the BLSM, and the MBLSM controllers.

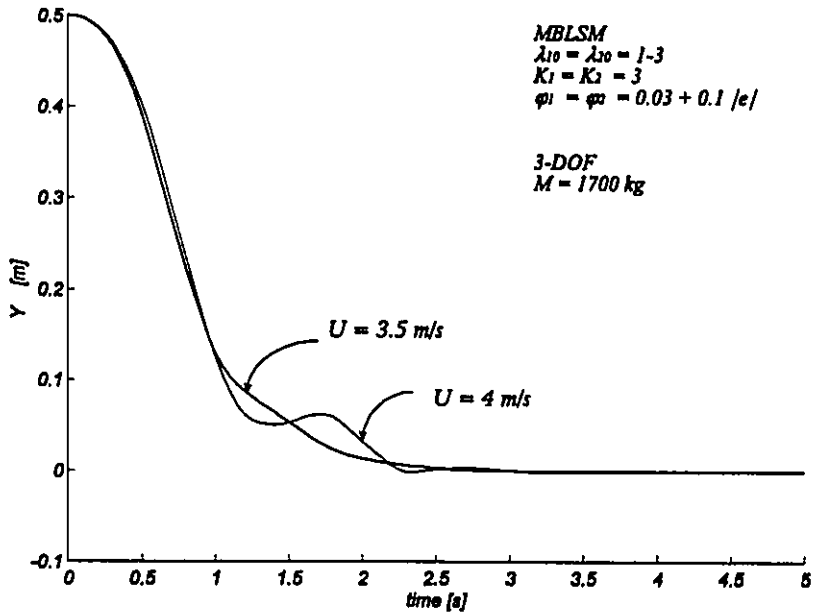

Figure 6.47 Response of the MBLSM controller for speed increase of up to 40 percent of the design value.

Chapter 7

Conclusion and Future Work

7.1. Summary

The ultimate goal of this research is to improve the path tracking and steering performance of a high load transport interfactory AGV with maximum travelling speed of 3 m/sec. Steering control of AGVs has been the subject of substantial research in the past. However, the focus has been to develop control strategies based on kinematic models, mainly due to the low speed and light weight of the vehicles analysed. These operating conditions do not resemble the actual requirements of automated transport systems in industry, where fast transport of heavy materials are essential to increase the overall efficiency. Some recent works exist on dynamic-based trajectory control of tricycle mobile robots applying Lagrangian formulation and input-output feedback linearization. Nevertheless, almost no reported work exists on dynamic-based control of AGVs taking into consideration the realistic loads, speeds, and the pneumatic tires used in practice. Other works that are available in the field of vehicle dynamics usually utilize linearized dynamic models for control purposes. This approach is generally valid for ATVs due to the small steering angles necessary for lane changes and curve negotiations of these vehicles. However, for the AGVs working in a flexible manufacturing plants, where curved routes of a few metres exist, this is not a satisfactory solution. As the AGV's load capacity and

travelling speed increases, the ensuing increase in lateral acceleration requires thorough dynamic modelling and more sophisticated controller design.

7.1.1. Dynamic Modelling

In this study, a nonlinear 3-DOF dynamic model, comprising yaw, lateral, and roll motions is developed. The suspension, lateral and longitudinal load transfer, nonlinear behaviour of tires, and steering dynamics are included in this model. The model also comprises the effect of actuators, differential gear box, steering and tractive gear boxes. To establish the sufficient level of model complexity necessary for this work, the 3-DOF model is compared with the commonly used kinematic model and a 2-DOF dynamic model. Also, the responses to step disturbance and various speeds and loading conditions are presented. Tracking performance of the 2-DOF and the 3-DOF models controlled by a conventional proportional controller are demonstrated as well. Based on simulation results for the particular AGV under study, the kinematic model is entirely incapable of representing the real vehicle. A proper tire modelling is required as load and speed increase. The 3-DOF model is adequate as a simulator for the design of the control system, however, a more sophisticated controller is required.

7.1.2. Control Design

The 2-DOF bicycle model was exploited to develop a dynamic based controller for the AGV. Assumption of a motion free of side slippage greatly simplified the kinematics and dynamics of the AGV model and led to a concise dynamic model. MIMO feedback linearization technique was employed to transform the given nonlinear system into two subsystems. A linear controllable subsystem of dimension r_t , which is the only one responsible for input-output behaviour, and a nonlinear subsystem of dimension n-r_t, whose stability should be inspected[1]. Among the six different output functions that were studied two were given more emphasise. These are designated as: a) type I outputs: based on vehicle

[1]Recalling that r_t, and n are total relative degree and order of system respectively.

position variables X, and Y, with the linearized decoupled subsystem of order four (r_t=4) and internal dynamics of order one (n-r_t=1) derived in the Cartesian coordinates. b) type VI outputs: based on the wheel angular speed ω_w (or vehicle forward speed U) and normal distance n. The order of the linearized decoupled subsystem in this case is three (r_t=3), and the internal dynamics is of order two (n-r_t=2) derived in path dependent coordinates. To analyse the internal dynamics and zero dynamics, both systems were transformed into normal form coordinates.

A number of controllers are designed for the decoupled linear subsystem and applied to the full 3-DOF system. Positive characteristics of variable structure system control were exploited to enhance robustness in the presence of disturbance, unmodeled dynamics and change in parameters. To achieve this a sliding mode controller was designed. Due to chattering the sliding mode controller was modified by introducing a thin boundary layer to the sliding surface. The boundary layer sliding mode controller was later modified for a better performance and enhance robustness using simultaneous variable boundary layer and multiple sliding surfaces strategies.

The proposed BLSM controller effectively suppressed disturbances and the control system is shown to be insensitive to the physical parameter variation such as payload and tire characteristics. The simulation results show good and robust performance against speed, path geometry and initial heading variations. The modified boundary layer sliding mode controller enhanced the robustness of the BLSM controller and improved its performance. The proposed control law is not complicated and is suitable for real time computer control.

7.2. Contributions

The major contributions of this research can be summarized as follows:

A complete dynamic model for a 4-wheel automated guided vehicle is developed. The 3-DOF nonlinear model comprises yaw, lateral, and roll motions. The suspension, lateral and longitudinal load transfer, nonlinear behaviour of tires, and steering dynamics are included in this model. The model also incorporates the effect of actuators, differential gear box, steering and tractive gear boxes.

A dynamic based approach to the control of AGVs for high load applications was introduced. Robustness of the controller was guaranteed by applying the sliding mode technique to the linearized model. Boundary Layers were introduced to reduce chattering. The BLSM controller was modified for enhanced robustness and better tracking performance. The formulation and implementation of a controller in this form for an AGV with complete 3-DOF dynamic model has not been addressed in the past.

Although input-output feedback linearization has been applied to mobile robots, and sliding mode technique is frequently used for robot manipulators control, the study of their simultaneous use for nonholonomic systems is a new subject.

Under side slippage free assumption a general approach to input output linearization of automated guided vehicle dynamics was studied. The choice of vehicle speed and normal distance as the system outputs, in the path dependent coordinate, resulted in a new controller for AGVs. Complete development of the theory and preliminary simulation results of vehicle control using this class of controllers are presented.

The boundary layer sliding mode controller was modified to enhance robustness in the presence of parameter change, modelling errors, and disturbance. In this regard both variable boundary layer and multiple sliding surfaces schemes were simultaneously implemented.

7.3. Future Work

The present work can serve as a basis for different areas of research in WMR's, AGV's and ATV's. This work can be extended in several directions. A few important directions of future research are:

1) Selection of type VI outputs based on vehicle speed and normal distance to the path, to develop a controller for the AGV in the path dependent coordinate system led to feasible results. Also, due to natural interpretation of outputs in task space this topic can be extrapolated for future work.

2) The sliding mode controller can be further enhanced using a methodology similar to the one proposed by Slotine(1984). In this regard, modelling uncertainties can be included

in the design of the sliding controller to obtain a time varying boundary layer for optimal tracking performance. However, this will be achieved at the cost of additional complexity of the controller.

3) The simulation results suggest that the performance of the proposed MBLSM controller is reasonably robust not only with respect to variation in vehicle parameters, but also with respect to assumption of side slippage free motion. This hints that this class of controllers can be recommended for control of AGV's at higher speeds or ATV's for low speed applications. A more detailed study of this subject is needed.

4) An experimental study of the proposed control system would be revealing and beneficial. This has to be done before the practical potentials of the proposed controller can be accurately assessed. Prospects for practical implementation are nevertheless promising.

References

Agullo, J., Cardona, S., and Vivancos, J., (1989), "Dynamics of Vehicles With Directionally Sliding Wheels," Mechanism & Machine Theory, Vol. 24, No. 1, pp. 53-60.

Alasty, A. and Naraghi, M., (1991), "Application of Variable Structure System in Position Control of A DC Motor," Internal Report, University of Ottawa.

Alexander J. C. and Maddocks J. H., (1989), "On Kinematics of Wheeled Mobile Robots," The International Journal of Robotics Research, Vol. 8, No. 5, October.

Allen, R. W., Rosenthal, T. J., and Szostak, H. T, (1987), "Steady State and Transient Analysis of Ground Vehicle Handling," SAE Technical Paper 870495.

Anderson, D. L., (1989), "Framework for Autonomous Navigation of a Continuous Mining Machine - Face Navigation," Information Circular - United States, Bureau of Mines No. 9214 1989 27p.

Aviles, W. A, Hughes, T. W, Everett, H. R., Umeda, A. Y., Martin, S.W., Koyamatsu, A. H., Solorzano, R. T., Laird, R. T., and McArthur, S. P., (1991), "Issues in mobile robotics: The Unmanned Ground Vehicle Program TeleOperated Vehicle (TOV)," Mobile Robots V, The SPIE - The International Society for Optical Engineering, 1991 pp 587-597.

Bakker, E., Nyborg, L., and Pacejka H., (1987), "Tyre Modelling for Use in Vehicle Dynamics Studies", SAE Technical Paper 870421.

Barraquand, J. and Latombe, J. C., (1990), "Controllability of Mobile Robots with Kinematic Constraints," Report No. STAN-CS-90-1317, Stanford University, Stanford, California.

Bloch, A. M. and McClamroch N. H., (1989), "Control of a Mechanical System with Classical Nonholonomic Constraints," Proceedings of the 28th Conference on Decision and Control Tampa, Florida, December, pp. 201-205.

Bloch, A. M., McClamroch N. H., and Reyhanoglu M., (1990), "Controllability and Stabilizability Properties of a Nonholonomic Control System," Proceedings of the 29th Conference on Decision and Control Honolulu, Hawaii, December, pp. 1312-1314.

Bloch, A. M., Reyhanoglu M., and McClamroch N. H., (1992), "Control and Stabilization of Nonholonomic Dynamic System," IEEE Transactions on Robotics and Automation, Vol. 37, No. 11, November, pp. 1746-1757.

Boegli, P., (1985), "A Comparative Evaluation of AGV Navigation Techniques," Proc. of the 3rd Int. Conf. on AGVS Stockholm, Sweden, Oct. 15-17, pp.169-180.

Borenstein, J. and Koren, Y., (1987), "Motion Control Analysis of a Mobile Robot," Journal of Dynamic Systems, Measurement and Control, Transactions ASME, Vol. 109 No. 2, June, pp. 73-79.

Bose, P. P., (1986), "Basics of AGV systems," American Machinist and Automated manufacturing, March, pp.106-122.

Boyden, F. D. and Velinsky S. A., (1994), "Dynamic Modelling of Wheeled Mobile Robots for High Load Applications," Proceedings - IEEE International Conference on Robotics and Automation, pp. 3071-3078.

Brach, R. M., (1991), "Vehicle Dynamics Model for Simulation on a Microcomputer," Journal of Vehicle Design, Vol. 12, Nov. 4.

Brockett, R. W., (1983), "Asymptotic Stability and Feedback Stabilization," R. W. Brockett, R. S. Millman, H. J. Sussmann (eds), 'Differential Geometric Control Theory', Birkhauser, pp. 181-191.

Campion, G., d'Andrea-Novel, B., and Bastin, G., (1990), "Controllability and State Feedback Stabilizability of Nonholonomic Mechanical Systems," Proc. Int. Workshop on Non-linear and Adaptive Control(Ed. C. Canudas de Wit), Springer-Verlag, pp. 106-124.

Canudas de Wit, C. and Roskam R., (1991), "Path Following of a 2-DOF Wheeled Mobile Robot Under Path and Input Torque Constraints," Proceedings - IEEE International Conference on Robotics and Automation Sacramento, California ,USA, April, pp. 1142-1147.

Canudas de Wit, C. and Sordalen, O. J., (1992), "Exponential Stabilization of Mobile Robots with Nonholonomic Constraints," IEEE Transactions on Robotics and Automation, Vol. 37, No. 11, November, pp. 1791-1797.

Canudas de Wit, C., H. , (1993), "Nonlinear Control Design for Mobile Robots," in the Recent Trends in Mobile Robots (Ed. Y. F. Zheng), IEEE Mobile Robot Technical Committee, World Scientific Publisher.

Cheng, R. M. H., Mehrabi, M. G. (1992), "Dynamic Modelling of Wheeled Mobile Robots and Automated Transit Vehicle Using Dimensionless Roll Number," First IEEE Conference on Control Applications, Dayton, Ohio, pp. 160-167.

Clark, S. K., (1971), "The Contact Between Tire and Roadway," in S. K. Clark, Ed., Mechanics of Pneumatic Tires, Monograph 112. Washington DC: National Bureau of Standards, 1971.

Cormier, W. H. and Fenton, R. E., (1980), "On the Steering of Automated Vehicles, a Velocity Adaptive controller," IEEE Transaction on Vehicle Technology, Vol. VT-29, No.4, November, pp. 375-385.

Cox, I. J, Wilfonge, G. T. (Eds), (1990), "Autonomous Robot Vehicles," Springer-Verlag.

Cyril, X, Cheng, R. M. H., and Sankar, T. S., (1989) "Dynamics Of Wheeled Mobile Robots (AGVs)," The Fourth International Conference on CAD, CAM, Robotics, Future Indian Institute of Technology, Vol 2.

Dahl, O. and Nielsen, L., (1989), "Torque Limited Path Following by On Line Trajectory Time Scaling," Proceedings - IEEE International Conference on Robotics and Automation, May, Scottsdale, Arizona, USA, pp. 1122-1128.

d'Andrea-Novel, B., Bastin, G., and Campion, G., (1991), "Modelling and Control of Nonholonomic Wheeled Mobile Robots," Proceedings - IEEE International Conference on Robotics and Automation Sacramento, California ,USA, April, pp. 1130-1135.

d'Andrea-Novel, B., Bastin, G., and Campion, G., (1992), "Dynamic Feedback Linearization of Nonholonomic Wheeled Mobile Robots," Proceedings - IEEE International Conference on Robotics and Automation Nice, France, May, pp. 2527-2532.

Deng, Z. and Brady M., (1993a), "Dynamics and Control of a Wheeled Mobile Robot," Proceedings of the American Control Conference, San Francisco, California, June, pp. 1830-1834.

Deng, Z. and Brady, M., (1993b), "Dynamic Tracking of a Wheeled Mobile Robot," Proceedings of the 1993 IEEE/RSJ International Conference on Intelligent Robots and Systems Yokohama, Japan, July 26-30, pp. 1295-1298.

DeSantis, R. M., (1993), "Path Tracking for a Carlike Mobile Robot ," Proceedings of the American Control Conference, San Francisco, California, June, pp. 64-68.

DeSantis, R. M., (1994), "Path Tracking For a Tractor-trailer-like Robot," The International Journal of Robotics Research, Vol. 13, No. 6, December, pp. 533-544.

DeSantis, R. M., (1995a), "Path-Tracking for Car-Like Robots with Single and Double Steering," IEEE Transactions on Vehicular Technology, Vol. 44, No.2, May, pp. 366-377.

DeSantis, R. M., (1995b), "Modelling and Path-Tracking Control of a Mobile Wheeled Robot with differential Drive," Robotica, Vol. 13, pp. 401-410.

Dugoff, H., Fancher, P. S., and Segel L., (1977), "A Analysis of Tire Traction Properties and Their Influence on Vehicle Dynamic Performance," SAE Trans., Paper 700377.

El-Gindy, M. and Ilosvai, L., (1983), "Computer Simulation Study on a Vehicle's Directional Response in some Severe Manoeuvres. Part 1: Rapid Lane-change Manoeuvres," International Journal of Vehicle Design, Vol. 4, No. 4, pp. 386-401.

El-Sharkawi, M. A. and Huang, C. H., (1989), "Variable Structure Tracking of DC Motor for High Performance Applications," IEEE Transactions on Energy Conversation, Vol. 4, No. 4, December, pp. 643-650.

Ellis, J. R., (1969), "Vehicle Dynamics," London Business Book Limited.

Ellis, J. R., (1994), "Vehicle Handling Dynamics," Mechanical Engineering Publications Limited, London.

Ervin, R. D., (1975), "Mobile Measurement of Truck Tire Traction," in Proc. Symposium on Commercial Vehicle Braking and Handling, Highway Safety Research Institute, University of Michigan Ann Arbor.

Evans, K., Pong, C., and Weiman, E., (1989), "HelpMate. A Robotic Materials Transport System," Robotics v 5 n 3 Nov 1989 p 251-256

Fenton, R. E., Melocik, G. C., and Olson, K. W., (1976), "On the Steering of Automated Vehicles: Theory and Experiment," IEEE Transactions on Automatic Control, Vol. AC-21, No.3, June, pp. 306-315.

Fenton, R. E. and Selim I., (1988), "On The Optimal Design of an Automotive Lateral Controller," IEEE Transaction on Vehicular Technology, Vol. 37, No. 2, May, pp. 108-113.

Fenton, R. E. and Mayhan J., (1991), "Automatic Highway Studies at the Ohio State University-an Overview," IEEE Transaction on Vehicular Technology, Vol. 40, No. 1, February, pp. 100-113.

Fernandez, B. and Hedrick, J. K., (1987), "Control of Multivariable Nonlinear Systems by the Sliding Mode Method," International Journal of Control, Vol. 46, No. 3, pp. 1019-1040.

Fraichard, T., (1993), "Dynamic Trajectory Planning with Dynamic Constraints: A 'State-time Space' Approach ," Proceedings of the 1993 IEEE/RSJ International Conference on Intelligent Robots and Systems, Yokohama, Japan, pp. 1393-1400.

Fujiwara, K. and Kawashima, Y., (1981), "Development of Guideless Robot Vehicle," Proceedings of the 11th International Symposium on Industrial Robots, Tokyo, pp. 195-202.

Gillespie, T. D., (1992), "Fundamentals of Vehicle Dynamics," Society of Automotive Engineers, Inc.

Gough, V. E., (1956), "Practical Tire Research," SAE Transactions, Vol. 64.

Graettinger T. J. and Krogh B. H., (1989), "Evaluation and Time-scaling of Trajectories for Wheeled Mobile Robots," Journal of Dynamic Systems, Measurement, and Control, Vol. 111, pp. 222-231.

Hamdy, A. and Badreddin E., (1992), "Dynamic Modelling of A Wheeled Mobile Robot for Identification, Navigation and Control," Robotics and Flexible Manufacturing Systems, Elsevier Science Publisher B. V. (North Holland), pp. 119-128.

Hammond, G. C., (1987), "International Trend in Manufacturing Technology, Automated Guided Vehicle Systems," (Ed. R. H. Hollier), IFS Publications Ltd, UK, pp. 3-9.

Hatwal, H. and Mikulcik, C., (1986), "Some Inverse Solutions to an Automobile Path Tracking Problem with Input Control of Steering and Brakes," Vehicle Dynamic System, 15, pp. 61-71.

Hedrick, J. K., (1993), "Analysis and Control of Nonlinear Systems," Journal of Dynamic Systems, Measurement, and Control, June, Vol. 511, pp. 351-361.

Hemami, A., Mehrabi, M. G., and Cheng, R. M. H., (1990), "A New Control Strategy for Tracking in Mobile Robots and AGV'S," IEEE Int Conf on Robotics and Automation, Cincinnati, OH, pp. 1122-1127.

Hemami, A., Mehrabi, M. G., and Cheng, R. M. H., (1992), "Synthesis of an Optimal Control Law for Path Tracking in Mobile Robots," Automatica, Vol. 28, No. 2, pp. 383-387.

Huang, M., (1991), "Dynamic Modelling of an AGV System (CONCIC-2)," Internal Report # CIC-0041, Concordia University, Montreal, Quebec, 1988.

Iida, S. and Yuta, S., (1991), "Control of Vehicle with Power Wheeled Steerings Using Feedforward Dynamics Compensation," IECON Proceedings (Industrial Electronics

Conference), Vol. 3. Publ. by IEEE, Computer Society, Los Alamitos, CA, USA (IEEE cat n 91CH2976-9), pp. 2264-2269.

Jagannathan, S, Zhu, S. Q., and Lewis, F. L. (1994), "Path Planning and Control of a Mobile Base with Nonholonomic Constraints," Robotica, Vol. 12. pp. 529-539.

Johnston, A., Assefi, T., and Lai, J. Y., (1979), "Automated Vehicle Guidance Using Discrete Reference Marker," IEEE Transaction on Vehicle Technology, Vol. VT-28, No.1, Feb.1979, pp. 95-106.

Jurie, F., Rives, P., Gallice, J., and Brame, J. L., (1994), "High Speed Vehicle Guidance Based on Vision," Control Engineering Practice, Vol. 2, No. 2, pp. 289-297.

Isidori, A., (1989), "Nonlinear Control Systems," 2nd Edition, Springer-Verlag Berlin Heidelberg New York.

Isidori, A., (1995), "Nonlinear Control Systems," 3rd Edition, Springer-Verlag Berlin Heidelberg New York.

Kanayama, Y., Nilipour, A., and Lelm, C. A., (1988), "A Locomotion Control Method for Autonomous Vehicle," Proceedings of the IEEE International Conference on Robotics and Automation, Philadelphia, Pennsylvania, pp. 1315-1317.

Kanayama, Y., Kimura, Y., Miyazaki, F., and Noguchi, T., (1990), "A Stable Tracking Control Method for an Autonomous Mobile Robot," Proceedings 1990- IEEE International Conference on Robotics and Automation Cincinnati, Ohio, USA, pp. 384-389.

Kaynak, M. O., Harashima, F., and Seiji, K., (1982), "Microprocessor Controlled Position Servo System With A Sliding Mode," ETG-Facberichte 11, Microelectronics in Power Electronics and Electrical Drives, VDE-Verlag, Berlin, pp. 273-279.

Khalil, H., K., (1992), "Nonlinear Systems," Macmillan Publishing Company.

Kim, O. H., (1987), "Optimal Steering Control of an Auto-guided-vehicle with Two Motored Wheels," Transactions of the Institute of Measurement and Control, Vol. 9, No.2, Apr-Jun pp. 58-63.

Klafter, R. D., (1988), "Mobile Robots, Research and Development," in the International Encyclopaedia of Robotics - Applications and Automation, (Ed. R. C. Dorf), Publ. by John Wiley and Sons Inc.

Koren, Y. and Borenstein, J., (1991), "Potential field Methods and Their Inherent Limitations for Mobile Robot Navigation," Proceedings - IEEE International Conference on Robotics and Automation Sacramento, California , USA, April, pp. 1398-1404.

Makino, T., (1993), "Study on Hunting Reduction of an Automated Guided Vehicle," JSME Series C, Vol. 36, No.3, pp 368-374.

Matsumoto, N., Tomizuka, M. (1992), "Vehicle Lateral Velocity and Yaw Rate Control with Two Independent Control Inputs," Journal of Dynamics, Measurement, and Control, Vol. 114, December, pp. 606-613.

McKerrow, P. J., (1991), "Introduction to Robotics," Addison-Wesley Publishers Ltd.

Mehrabi, M. G., Hemami, A., and Cheng, R. M. H., (1991), "Control of a Wheeled Mobile Robot with Double Steering," IEEE/RSJ International Workshop on Intelligent Robots and Systems IROS'91, Nov. 3-5, Osaka, Japan, pp. 806-810.

Mehrabi, M. G., Hemami, A., and Cheng, R. M. H., (1993), "Dynamic Modelling and Control of Wheeled Mobile Robots Theory and Experiment ," Second IEEE Conference on Control Applications, Vancouver, BC, Sept. 13-16, pp. 559-665.

Muir, P. F. and Neuman, C. P., (1986), "Kinematic Modelling of Wheeled Mobile Robots," Technical Report, No. CMU-RI-TR-86-12, The Robotics Institute, Carnegie Mellon University, Pittsburgh, PA, 15213, July, 1986.

Muir, P. F. and Neuman, C. P., (1987), "Kinematic Modelling of Wheeled Mobile Robots," Journal of Robotics Systems, Vol. 4, No. 2, pp. 281-340.

Muir, P. F. and Neuman, C. P., (1988), "Dynamic Modelling of Multibody Robotic Mechanisms: Incorporating Closed-chains, Friction, Higher-pair Joints, and Unactuated and Unsensed Joints," Proceedings of the 1988 IEEE International Conference on Robotics and Automation, pp. 1546-1551.

Muller, T., (1987), "International Trend in Manufacturing Technology, Automated Guided Vehicle Systems," (Ed. R. H. Hoiller), IFS Publications Ltd, UK, pp. 11-17.

Nalecz, A. G. and Bindemann, A. C., (1989), "Handling Properties of Four Wheel Steering Vehicles," SAE Technical Paper 890080.

Necsulescu, D. S., Eghtesad, M., and Kalaycioglu, S., (1994), "Dynamic Based Linearization and Control of an Autonomous Mobile Robot," Design: Analysis, and Applications American Society of Mechanical Engineers, Petroleum Division (Publication) PD, Vol. 64, No. 8-2, pp. 383-387.

Nelson, W. L. and Cox, I. J., (1988), "Local Path Control for an Autonomous Vehicle," Proceedings of the IEEE International Conference on Robotics and Automation, Philadelphia, PA, April 24-29, pp. 1504-1510.

Nelson, W., (1989), "Continuous-Curvature Paths for Autonomous Vehicles," Proceedings of IEEE International Conference on Robotics and Automation, May, Scottsdale, Arizona, USA, pp. 1260-1264.

Nisonger, R. and Wormley, D. N., (1979), "Dynamic Performance of Automated Guideway Transit Vehicle with Dual-axle Steering," IEEE Transaction on Vehicle Technology, Vol. VT-28, No.1, February, pp. 88-94.

Ogata, K., (1990), "Modern Control Engineering Control," Prentice-Hall Inc.

Pacejka, H. B. and Bakker, E, (1993), "The MAGIC Formula Tyre Model," Vehicle System Dynamics, Vol. 21, pp. 1-19.

Pears, N. E. and Bumby, J. R., (1991), "Steering Control of an Experimental Autonomous Vehicle," Transactions of the Institute of Measurement and Control, Vol. 13, No. 4, pp. 190-200.

Petrov, P. P., (1991), "Robust Trajectory Tracking Algorithms for a Wheeled Mobile Robot," IECON Proceedings (Industrial Electronics Conference), Vol. 2. Publ. by IEEE, Computer Society, Los Alamitos, CA, USA, (IEEE cat n 91CH2976-9), pp. 1071-1074.

Pomet, J. B., Thuilot, B., Bastin, G., and Campion, G., (1992), "A Hybrid Strategy for the Feedback Stabilization of Nonholonomic Mobile Robots," Proceedings - IEEE International Conference on Robotics and Automation, Vol. 1. Publ. by IEEE, IEEE Service Centre, Piscataway, NJ, USA, (IEEE cat n 92CH3140-1), pp. 129-134.

Premi, S. K. and Besant, C. B., (1983), "A Review of Various Vehicle Guidance Techniques that Can Be Used by Mobile Robots or AGVS," Proc. of the 2nd Int. Conf. on AGVS. Stuttgart, W. Germany, June 7-9, pp. 195-209.

Rajagopalan, R., Cheng, R. M. H., and Lequoc, S., (1992), "A Guidance Control Scheme for Accurate Track Following of AGVS," Proceedings of the IEEE International Conference on Robotics and Automation, Vol. 1. Publ. by IEEE, IEEE Service Centre, Piscataway, NJ, USA, (IEEE cat n 92CH3140-1), pp. 188-193.

Rajaram, N. S., (1988), "Automated Guided Vehicles," in the International Encyclopaedia of Robotics - Applications and Automation," (Ed. R. C. Dorf), Publ. by John Wiley and Sons Inc.

Richards, R. J., Ready, D. S., (1991), "The Real-Time Application of Variable Structure System (VSS) Controllers: An Experimental Comparative Study on Simple Robot Arm," Trans Inst MC Vol. 13, No. 4, pp. 201-210.

Rodseth, O. J. and Hallset, J. O., (1991), "ROV90--A Pragmatic Approach to Autonomous Underwater Vehicle Design," Ocean Technologies and Opportunities in the Pacific for the 90's, Proc Oceans 91 Oceans (New York) v 2. Publ. by IEEE, IEEE Service Centre, Piscataway, NJ, USA (IEEE cat n 91CH3063-5). p 1075-1081

Saha, S. K. and Angeles, J., (1989), "Kinematics and Dynamics of a Three Wheeled 2-DOF AGV," IEEE Int Conf Rob Auto., Vol. III (of 3). Publ. by IEEE, IEEE Service Centre, Piscataway, NJ, USA. Available from IEEE Service Cent (cat n 89CH2750-8), Piscataway, NJ, USA. pp. 1572-1577.

Samson, C., (1990a), "Mobile Robot Control Part 1: Feedback Control of a Nonholonomic Wheeled Cart in Cartesian Space," INRIA Report, No. 1288.

Samson, C., (1990b), "Velocity and Torque Feedback Control of a Nonholonomic Cart," Int. Workshop in Adaptive and Nonlinear Control: Issues in Robotics, Grenoble, France, Proc. in Advanced Robot Control, Spring Verlag, Vol. 162, pp. 125-151.

Samson, C. and Ait-Abderrahim, k., (1991a), "Feedback Control of a Nonholonomic Wheeled Cart in Cartesian Space," Proceedings - IEEE International Conference on Robotics and Automation Sacramento, California ,USA, April, pp. 1136-1141.

Samson, Claude, (1991b), "Time Varying Feedback Stabilization of Nonholonomic Car-like Mobile Robot," the 30th IEEE Conference on Decision and Control, 1991, pp. 1-24.

Samson, C. and Ait-Abderrahim, K., (1991c), "Feedback Stabilization of a Nonholonomic Wheeled Mobile Robot," IEEE/RSJ International Workshop on Intelligent robots and systems IROS'91, Nov. 3-5, Osaka, Japan, IEEE Cat. No. 91th0375-6.

Sarkar, N., Yun, X, and Kumar, V., (1994), "Control of Mechanical System with Rolling Constraints: Application to Dynamic Control of Mobile Robots," The International Journal of Robotics Research, Vol.13, No.1, February, pp. 55-59.

Schultz, R. J., Nakajima, R., Nomura, J., (1991), "Telepresence Mobile Robot for Security Applications," IECON Proceedings (Industrial Electronics Conference) v 2. Publ. by IEEE, Computer Society, Los Alamitos, CA, USA (IEEE cat n 91CH2976-9). p 1063-1066

Segel, L., (1956), "Theoretical Prediction and Experimental Substantiation of the Response of the Automobile to Steering Control," Proc. Of Institution of Mechanical Engineers, Automobile Division, pp. 310-330.

Sheth, P. N., Uicker, J. J., (1971), "A generalized Symbolic Notation for Mechanisms," Journal of Engineering for Industry, Series B, 93, 70-Mech-19, pp. 102-112.

Shiller, Z. and Gwo, Y., (1991), "Dynamic Motion Planning of Autonomous Vehicles," IEEE Transactions on Robotics and Automation, Vol. 7, No. 2, April, pp. 241-249.

Shin, D. H., Singh, S., and Lee, J., (1992), "Explicit Path Tracking by Autonomous Vehicles," Robotica, Vol. 10, Pt 6, Nov-Dec, pp. 539-554.

Shladover, S. E., Wormley, D. N., Richardson, H. H., and Fish, R., (1978), "Steering Controller Design for Automated Guideway Transit Vehicle," Journal of Dynamic Systems, Measurement and Control, Transactions ASME, Vol. 100, No. 3, March, pp. 1-8.

Shladover, S. E, Desoer C. A.., Hedrick, J. K., Tomizuka, M., Walrand, J., Zhang, W. B., McMahon, D. H., Peng, H., Sheikholeslam, S., and McKeown, N., (1991), "Automatic

Vehicle Control Developments in the PATH Program," IEEE Transaction on Vehicular Technology, Vol. 40, No. 1 February, pp. 114-130.

Singh, S., Feng, D., Keller, P., Shaffer, G., Shi, W. F., Shin, D. H., West, J., and Wu, B. X., (1991), "A System for Fast Navigation of Autonomous Vehicles," Technical Report, No. CMU-RI-TR-91-20, The Robotics Institute, Carnegie Mellon University, Pittsburgh, PA, 15213, September, 1991.

Slotine, J. J. E., (1984), "Sliding Controller Design for Non-Linear Systems," International Journal of Control, Vol. 40, No.2, pp. 421-434.

Slotine, J. J. E. and Li, W., (1991), "Applied Nonlinear Control," Prentice Hall Inc.

Smith, D. E. and Starkey J. M., (1991), "Overview of Vehicle Models, Dynamics, and Control Applied to Automated Vehicles," Advanced Automotive Technologies - American Society of Mechanical Engineers, Design Engineering Division (Publication) DE, Vol. 40. Publ.. by ASME, New York, NY, USA, pp. 69-87.

Smith, D. E. and Starkey J. M., (1994), "Effects of Model Complexity on the Performance of Automated Vehicle Steering Controllers: Controller Development and Evaluation," Vehicle System Dynamics, 23, pp. 627-645.

Sordalen, O. J. and Canudas de Wit, C., (1992), "Exponential Control Law for a Mobile Robots: Extension to Path Following," Proceedings - IEEE International Conference on Robotics and Automation, Nice, France, May, pp. 2158-2163.

Stone, H. W., Edmonds, G., (1992), "HAZBOT: A Hazardous Materials Emergency Response Mobile Robot," Proceedings - IEEE International Conference on Robotics and Automation v 1. Publ. by IEEE, IEEE Service Centre, Piscataway, NJ, USA (IEEE cat n 92CH3140-1), pp. 67-73.

Sung, E., Loon, N. K., and Yin Y. C., (1989), "Parallel Linkage Steering for an Automated Guided Vehicle," IEEE Control Systems Magazine, Vol. 9, No. 6, October, pp. 3-8.

Taborek, J. J., (1975), "Mechanics of Vehicles," Machine Design, May 30-Dec. 26.

Takahashi, T., (1988), "State of the Art of AGVS in Japan," Proceedings of the 6th International Conference on Automated Guided Vehicle Systems, October, pp. 55-60.

Treherne, I. M., (1990), "Autonomous Mobile Robots. An aid for the Handicapped," IEE Colloquium (Digest) n 054. Publ. by IEE, Michael Faraday House, Stevenage, Engl. 2p.

Tsumura, T., Fujiwara, N., Shirakawa, T., and Hashimoto, M., (1981), "An Experimental System for Automatic Guidance of Roboted Vehicle Following the Route Stored in Memory," Proc. of the 1st International Symposium on Industrial Robots, Tokyo, pp. 187-193.

Tsumura, T., (1986), "Survey of Automated Guided Vehicle in Japanese Factory," Proceedings of the IEEE International Conference on Robotics and Automation, pp. 1329-1334.

Vidyasagar, M., (1993), "Nonlinear System Analysis," 2nd Edition, Prentice Hall, Inc.

Wang, Y., Linnett, J. A., and Roberts, J. W., (1994), "Motion Feasibility of a Wheeled Vehicle with a Steering Angle Limit," Robotics, Vol. 12, pp. 217-226.

Wilcox, B. and Gennery, D. B., (1987), "A Mars Rover for 1990's," Journal of the British Interplanetary Society, Vol.40, No. 10, 1987, pp 484-488

Wong, J. Y., (1993), "Theory of Ground Vehicles", 2nd ed., Published by John Wiley & Sons, Inc.

Xia, X. and Law, E. H., (1992), "Nonlinear Analysis of Closed Loop Driver/ Automobile Performance with Four Wheel Steering Control," SAE Technical Paper 920055.

Yeung, K., Chen, Y. P., (1988), "A New Controller Design for Manipulators Using the Theory of Variable Structure Systems," IEEE Transaction on Automatic Control, Vol. 33, No. 2, February, pp. 200-206.

Yu, S. H., Moskwa, J. J, (1994), "A Global Approach to Vehicle Control: Coordination of Four Wheel Steering and Wheel Torques," Journal of Dynamics, Measurement, and Control, Vol. 116, December, pp. 659-667.

Yun, X. and Yamamoto, Y., (1993), "Internal Dynamics of a Wheeled Mobile Robot," Proc. IEEE/RSJ International Conference on Intelligent Robots and Systems Yokohama, Japan, July 26-30, pp. 1288-1294.

Zhao, Y. and BeMent, S. L., (1992), "Kinematics, Dynamics and Control of Wheeled Mobile Robots," Proceedings - IEEE International Conference on Robotics and Automation, Vol. 1. Publ. by IEEE, IEEE Service Centre, Piscataway, NJ, USA, (IEEE cat n 92CH3140-1), pp. 91-96.

Appendix A1

Tractive Motor Dynamics

The tractive force is the force, which the motor can provide to the vehicle and depends on the motor characteristics only. It is assumed that the whole effort of the motion is provided by the forces between driving wheels and working surface.

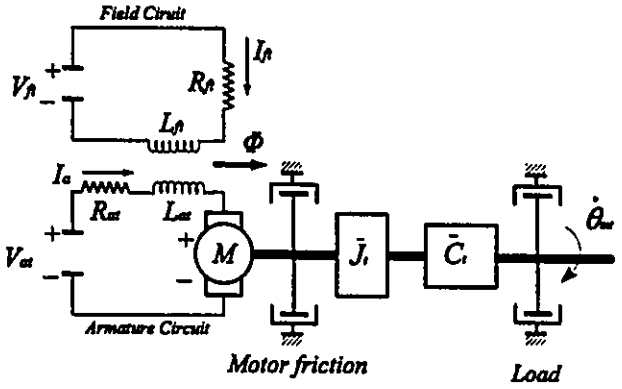

Figure A1.1 Model of motor and load system

Referring to Figure A1.1, the basic torque-voltage equation for the tractive dc motor is presented as (Ogata, 1990),

$$\tau_t = n_t\left[\frac{\bar{K}_t V_t}{R_{at}} - n_t\bar{J}_t\frac{d^2\theta_t}{dt^2} - \left(\frac{\bar{K}_t^2}{R_{at}} + n_t\bar{C}_t\right)\frac{d\theta_t}{dt}\right] \qquad \text{(A1.1)}$$

Where

$\bar{K}_t$ is the motor torque constant

τ_t is the torque referred to output shaft

V_t is the same as V_{at} and denotes terminal voltage

R_{at} is armature resistance

$\dot{\theta}_{mt}$ is the speed referred to motor shaft

$\dot{\theta}_t$ is the speed referred to output shaft (input to differential gear)

$\bar{J}_t$ is the motor moment of inertia

$\bar{C}_t$ is the motor viscous damping coefficient

n_t is the tractive motor gear ratio

In the Equation A1.1, subscript t denotes tractive motor specifications, and armature inductance is assumed to be small and negligible.

Differential Gear

A differential gear is being used to divide the input torque from the gearbox equally between the two rear wheels, despite their relative speeds of rotation, therefore the following holds

$$\begin{aligned} \dot{\theta}_{rl} + \dot{\theta}_{rr} &= 2\dot{\theta}_t \\ \tau_{rl} = \tau_{rr} &= \frac{\tau_t}{2} \end{aligned} \qquad \text{(A1.2)}$$

where

$\dot{\theta}_{rl}$ is the angular velocity of the left wheel

$\dot{\theta}_{rr}$ is the angular velocity of the right wheel

τ_{rl} is the torque on the rear-left wheel

τ_{rr} is the torque on the rear-right wheel

Differentiating first equation of the A1.2 results in

$$\ddot{\theta}_{rl} + \ddot{\theta}_{rr} = 2\ddot{\theta}_t \qquad \text{(A1.3)}$$

Let U_{xrl}, U_{xrr}, be the linear velocity of left and right wheels respectively, then angular velocities are

$$\begin{aligned}\dot{\theta}_{rl} &= \frac{U_{xrl}}{R_w} = \frac{1}{R_w}(U+tr)\\ \dot{\theta}_{rr} &= \frac{U_{xrr}}{R_w} = \frac{1}{R_w}(U-tr)\\ \dot{\theta}_t &= \frac{U}{R_w}\end{aligned} \tag{A1.4}$$

and the accelerations are

$$\begin{aligned}\ddot{\theta}_{rl} &= \frac{1}{R_w}\frac{dU_{xrl}}{dt} = \frac{1}{R_w}(\dot{U}+t\dot{r})\\ \ddot{\theta}_{rr} &= \frac{1}{R_w}\frac{dU_{xrr}}{dt} = \frac{1}{R_w}(\dot{U}-t\dot{r})\\ \ddot{\theta}_t &= \frac{\dot{U}}{R_w}\end{aligned} \tag{A1.5}$$

Substituting A1.4, and A1.5 into A1.1 and considering A1.2 the tractive forces for rear wheels are given by

$$(F_t)_{xrl} = (F_t)_{xrr} = \frac{n_t}{2R_w}\left[\frac{\bar{K}_t V_t}{R_{at}} - \frac{n_t \bar{J}_t}{R_w}\dot{U} - \frac{1}{R_w}\left(\frac{\bar{K}_t^2}{R_{at}} + n_t C_t\right)U\right] \tag{A1.6}$$

The total tractive force of rear wheels is gives by

$$F_t = 2(F_t)_{xrl} = 2(F_t)_{xrr} \tag{A1.7}$$

Appendix A2

Steering Motor Dynamics

Referring to Appendix A1, the basic torque-voltage equation for the steering dc motor is given by

$$\tau_s = n_s\left[\frac{\bar{K}_s V_s}{R_{as}} - n_s\bar{J}_s\frac{d^2\theta_s}{dt^2} - \left(\frac{\bar{K}_s^2}{R_{as}} + n_s\bar{C}_s\right)\frac{d\theta_s}{dt}\right] \qquad \textbf{(B2.1)}$$

Where

$\bar{K}_s$ is the motor torque constant

τ_s is the torque referred to output shaft

V_s is the same as V_{as} and denotes terminal voltage

R_{as} is armature resistance

$\dot{\theta}_{ms}$ is the speed referred to motor shaft

$\dot{\theta}_s$ is the speed referred to output shaft

$\bar{J}_s$ is the motor moment of inertia

$\bar{C}_s$ is the motor viscous damping coefficient

n_s is the steering gear ratio

In the Equation A2.1, subscript *s* denotes steering motor specifications, and armature inductance is assumed to be small and negligible. Also, the contribution of steering motor inertia to total steering torque is negligible, and can be ignored. The simplified equation is given by

$$\tau_s = n_s \left[\frac{\bar{K}_s V_s}{R_{as}} - \left(\frac{\bar{K}_s^2}{R_{as}} + n_s \bar{C}_s \right) \frac{d\theta_s}{dt} \right] \qquad \textbf{(B2.2)}$$

Alternatively the steering angle δ can be substituted for θ_s

Appendix B1

Input-Output Linearization: Outputs X, Y

For this case the outputs are defined as

$$\begin{aligned} y_1 &= h_1(\chi) = X \\ y_2 &= h_2(\chi) = Y \end{aligned} \tag{B1.1}$$

and the desired decoupling matrix determinant is given by

$$\det E(\chi) = \begin{vmatrix} L_{g_1} L_f h_1(\chi) & L_{g_2} L_f h_1(\chi) \\ L_{g_1} L_f h_2(\chi) & L_{g_2} L_f h_2(\chi) \end{vmatrix} \tag{B1.2}$$

The elements of B1.2 are obtained based on the following procedure

$$\begin{aligned} L_{g_1} h_1(\chi) &= \nabla h_1 g_1(\chi) \\ &= \begin{bmatrix} 0 & 0 & 0 & 1 & 0 \end{bmatrix} \begin{bmatrix} g_t & 0 & 0 & 0 & 0 \end{bmatrix}^T \\ &= 0 \\ L_{g_2} h_1(\chi) &= \nabla h_1 g_2(\chi) \\ &= \begin{bmatrix} 0 & 0 & 0 & 1 & 0 \end{bmatrix} \begin{bmatrix} g_s & \frac{1}{k_{1s}} & 0 & 0 & 0 \end{bmatrix}^T \\ &= 0 \end{aligned}$$

and similarly

$$\begin{aligned} L_{g_1} h_2(\chi) &= \nabla h_2 \, g_1(\chi) = 0 \\ L_{g_2} h_2(\chi) &= \nabla h_2 \, g_2(\chi) = 0 \end{aligned}$$

Thus

$$L_f\, h_1(\chi) = \nabla h_1\, f(\chi) = \frac{UD_1}{\cos\delta}$$

$$L_f\, h_2(\chi) = \nabla h_2\, f(\chi) = \frac{UD_2}{\cos\delta}$$

moreover

$$L_{g_1} L_f h_1(\chi) = \nabla(L_f h_1)\, g_1$$

$$= \begin{bmatrix} \frac{D_1}{\cos\delta} & -\frac{Ub\sin\theta}{\cos\delta^2} & -\frac{UD_2}{\cos\delta} & 0 & 0 \end{bmatrix} \begin{bmatrix} g_t & 0 & 0 & 0 & 0 \end{bmatrix}^T$$

$$= \frac{g_t D_1}{\cos\delta}$$

$$L_{g_2} L_f h_1(\chi) = \nabla(L_f h_1)\, g_2$$

$$= \frac{g_s D_1}{\cos\delta} - \frac{Ub\sin\theta}{Lk_{1s}\cos^2\delta}$$

Similarly the second row elements are obtained

$$L_{g_1} L_f h_2(\chi) = \nabla(L_f h_2)\, g_1$$

$$= \begin{bmatrix} \frac{D_2}{\cos\delta} & \frac{Ub\cos\theta}{\cos^2\delta} & \frac{UD_1}{\cos\delta} & 0 & 0 \end{bmatrix} \begin{bmatrix} g_t & 0 & 0 & 0 & 0 \end{bmatrix}^T$$

$$= \frac{g_t D_2}{\cos\delta}$$

$$L_{g_2} L_f h_2(\chi) = \nabla(L_f h_2)\, g_2$$

$$= \frac{g_s D_2}{\cos\delta} + \frac{Ub\cos\theta}{Lk_{1s}\cos^2\delta}$$

Thus the decoupling matrix for this case is given by

$$E(\chi) = \begin{bmatrix} \frac{g_t D_1}{\cos\delta} & \frac{g_s D_1}{\cos\delta} - \frac{Ub\sin\theta}{L k_{1s}\cos^2\delta} \\ \frac{g_t D_2}{\cos\delta} & \frac{g_s D_2}{\cos\delta} + \frac{Ub\cos\theta}{L k_{1s}\cos^2\delta} \end{bmatrix} \tag{B1.3}$$

and the determinant of E is obtained as

$$\det E = -\frac{g_t Ub}{k_{1s} L\cos^2\delta} \tag{B1.4}$$

Appendix B2

Input-Output Linearization: Outputs Y,θ

For this case the outputs are defined as

$$\begin{aligned} y_1 &= h_1(\chi) = Y \\ y_2 &= h_2(\chi) = \theta \end{aligned} \tag{B2.1}$$

and the desired decoupling matrix determinant is given by

$$\det E(\chi) = \begin{vmatrix} L_{g_1} L_f h_1(\chi) & L_{g_2} L_f h_1(\chi) \\ L_{g_1} L_f h_2(\chi) & L_{g_2} L_f h_2(\chi) \end{vmatrix} \tag{B2.2}$$

The elements of B2.2 are obtained based on the following procedure

$$L_{g_1} h_1(\chi) = \nabla h_1 \, g_1(\chi) = 0$$

$$L_{g_2} h_1(\chi) = \nabla h_1 \, g_2(\chi) = 0$$

and

$$L_{g_1} h_2(\chi) = \nabla h_2 \, g_1(\chi) = 0$$

$$L_{g_2} h_2(\chi) = \nabla h_2 \, g_2(\chi) = 0$$

thus

$$L_f h_1(\chi) = \nabla h_1 \, f(\chi) = \frac{UD_2}{\cos\delta}$$

$$L_f h_2(\chi) = \nabla h_2 \, f(\chi) = \frac{U\tan\delta}{L}$$

moreover

$$L_{g_1}L_f h_1(\chi) = \nabla(L_f h_1)\, g_1 = \frac{g_t D_2}{\cos\delta}$$

$$L_{g_2}L_f h_1(\chi) = \nabla(L_f h_1)\, g_2 = \frac{g_s D_2}{\cos\delta} + \frac{Ub\cos\theta}{Lk_{1s}\cos^2\delta}$$

Similarly the second row elements are obtained

$$L_{g_1}L_f h_2(\chi) = \nabla(L_f h_2)\, g_1 = \frac{g_t \tan\delta}{L}$$

$$L_{g_2}L_f h_2(\chi) = \nabla(L_f h_2)\, g_2 = \frac{g_s \tan\delta}{L} + \frac{U}{Lk_{1s}\cos^2\delta}$$

Thus the decoupling matrix for this case is given by

$$E(\chi) = \begin{bmatrix} \dfrac{g_t D_2}{\cos\delta} & \dfrac{g_s D_2}{\cos\delta} + \dfrac{Ub\cos\theta}{Lk_{1s}\cos^2\delta} \\ \dfrac{g_t \tan\delta}{L} & \dfrac{g_s \tan\delta}{L} + \dfrac{U}{Lk_{1s}\cos^2\delta} \end{bmatrix} \qquad \textbf{(B2.3)}$$

and the determinant of E is obtained as

$$\det E = \frac{g_t U \sin\theta}{k_{1s} L\cos^2\delta} \qquad \textbf{(B2.4)}$$

Appendix B3

Input-Output Linearization: Outputs U, δ

For this case the outputs are defined as

$$\begin{aligned} y_1 &= h_1(\chi) = U \\ y_2 &= h_2(\chi) = \delta \end{aligned} \tag{B3.1}$$

and the desired decoupling matrix determinant is given by

$$\det E(\chi) = \begin{vmatrix} L_{g_1} h_1(\chi) & L_{g_2} h_1(\chi) \\ L_{g_1} h_2(\chi) & L_{g_2} h_2(\chi) \end{vmatrix} \tag{B3.2}$$

The elements of B3.2 are obtained based on the following procedure

$$L_{g_1} h_1(\chi) = \nabla h_1 g_1(\chi) = g_t$$

$$L_{g_2} h_1(\chi) = \nabla h_1 g_2(\chi) = g_s$$

similarly the second row elements are obtained

$$L_{g_1} h_2(\chi) = \nabla h_2 g_1(\chi) = 0$$

$$L_{g_2} h_2(\chi) = \nabla h_2 g_2(\chi) = \frac{1}{k_{1s}}$$

and thus the decoupling matrix for this case is given by

$$E(\chi) = \begin{bmatrix} g_t & g_s \\ 0 & \frac{1}{k_{1s}} \end{bmatrix} \tag{B3.3}$$

and the determinant of E is obtained as

$$\det E = \frac{g_t}{k_{1s}} \tag{B3.4}$$

Appendix B4

Input-Output Linearization: Outputs U, Y

For this case the outputs are defined as

$$\begin{aligned} y_1 &= h_1(\chi) = U \\ y_2 &= h_2(\chi) = Y \end{aligned} \tag{B4.1}$$

and the desired decoupling matrix determinant is given by

$$\det E(\chi) = \begin{vmatrix} L_{g_1} h_1(\chi) & L_{g_2} h_1(\chi) \\ L_{g_1} L_f h_2(\chi) & L_{g_2} L_f h_2(\chi) \end{vmatrix} \tag{B4.2}$$

The elements of B4.2 are obtained based on the following procedure

$$L_{g_1} h_1(\chi) = \nabla h_1 g_1(\chi) = g_t$$

$$L_{g_2} h_1(\chi) = \nabla h_1 g_2(\chi) = g_s$$

and

$$L_{g_1} h_2(\chi) = \nabla h_2 g_1(\chi) = 0$$

$$L_{g_2} h_2(\chi) = \nabla h_2 g_2(\chi) = 0$$

The second row elements are obtained as

$$L_f h_2(\chi) = \nabla h_2 f(\chi) = \frac{UD_2}{\cos\delta}$$

moreover

$$L_{g_2}L_f h_1(\chi) = \nabla(L_f h_2)\, g_2 = \frac{g_s D_2}{\cos\delta} + \frac{Ub\cos\theta}{Lk_{1s}\cos^2\delta}$$

Thus the decoupling matrix for this case is given by

$$E(\chi) = \begin{bmatrix} g_t & g_s \\ \dfrac{g_t D_2}{\cos\delta} & \dfrac{g_s D_2}{\cos\delta} + \dfrac{Ub\cos\theta}{Lk_{1s}\cos^2\delta} \end{bmatrix} \qquad \text{(B4.3)}$$

and the determinant of E is obtained as

$$\det E = \frac{g_t Ub\cos\theta}{k_{1s} L\cos^2\delta} \qquad \text{(B4.4)}$$

Appendix C

Path Dependent I/O Linearization

Type I Outputs

For this case the outputs are defined as

$$\begin{aligned} y_1 &= h_1(\zeta) = s \\ y_2 &= h_2(\zeta) = \mathrm{n} \end{aligned} \tag{C.1}$$

and the desired decoupling matrix determinant is given by

$$\det E(\zeta) = \begin{vmatrix} L_{g_1} L_f h_1(\zeta) & L_{g_2} L_f h_1(\zeta) \\ L_{g_1} L_f h_2(\zeta) & L_{g_2} L_f h_2(\zeta) \end{vmatrix} \tag{C.2}$$

The elements of C.2 are obtained based on the following procedure

$$\begin{aligned} L_{g_1} h_1(\zeta) &= \nabla h_1 g_1(\zeta) \\ &= \begin{bmatrix} 0 & 0 & 0 & 1 & 0 \end{bmatrix} \begin{bmatrix} \frac{1}{R_w} g_t & 0 & 0 & 0 & 0 \end{bmatrix}^T \\ &= 0 \\ L_{g_2} h_1(\zeta) &= \nabla h_1 g_2(\zeta) \\ &= \begin{bmatrix} 0 & 0 & 0 & 1 & 0 \end{bmatrix} \begin{bmatrix} \frac{1}{R_w} g_s & \frac{1}{k_1 s} & 0 & 0 & 0 \end{bmatrix}^T \\ &= 0 \end{aligned}$$

and similarly

$$\begin{aligned} L_{g_1} h_2(\zeta) &= \nabla h_2 \, g_1(\zeta) = 0 \\ L_{g_2} h_2(\zeta) &= \nabla h_2 \, g_2(\zeta) = 0 \end{aligned}$$

Thus

$$L_f h_1(\zeta) = \nabla h_1 f(\zeta) = \frac{R_w \omega_w D_1}{\cos\delta}$$

$$L_f h_2(\zeta) = \nabla h_2 f(\zeta) = \frac{R_w \omega_w D_2}{\cos\delta}$$

moreover

$$L_{g_1} L_f h_1(\zeta) = \nabla(L_f h_1)\, g_1$$

$$= \begin{bmatrix} \frac{R_w D_1}{\cos\delta} & -\frac{R_w \omega_w b \sin\tilde{\theta}}{\cos^2\delta} & -\frac{R_w \omega_w D_2}{\cos\delta} & 0 & 0 \end{bmatrix} \begin{bmatrix} \frac{1}{R_w} g_t & 0 & 0 & 0 & 0 \end{bmatrix}^T$$

$$= \frac{g_t D_1}{\cos\delta}$$

$$L_{g_2} L_f h_1(\zeta) = \nabla(L_f h_1)\, g_2$$

$$= \frac{g_s D_1}{\cos\delta} - \frac{R_w \omega_w b \sin\tilde{\theta}}{L k_{1s} \cos^2\delta}$$

Similarly the second row elements are obtained

$$L_{g_1} L_f h_2(\zeta) = \nabla(L_f h_2)\, g_1$$

$$= \frac{g_t D_2}{\cos\delta}$$

$$L_{g_2} L_f h_2(\zeta) = \nabla(L_f h_2)\, g_2$$

$$= \frac{g_s D_2}{\cos\delta} + \frac{R_w \omega_w b \cos\tilde{\theta}}{L k_{1s} \cos^2\delta}$$

Thus, the determinant of E is obtained as

$$\det E = \frac{g_t R_w \omega_w b}{k_{1s} L \cos^2\delta} \qquad \text{(C.3)}$$

Type VI Outputs

The outputs are defined as

$$\begin{aligned} y_1 &= h_1(\zeta) = \omega_w \\ y_2 &= h_2(\zeta) = \mathrm{n} \end{aligned} \tag{C.4}$$

and the desired decoupling matrix determinant is given by

$$\det E(\chi) = \begin{vmatrix} L_{g_1} h_1(\chi) & L_{g_2} h_1(\chi) \\ L_{g_1} L_f h_2(\chi) & L_{g_2} L_f h_2(\chi) \end{vmatrix} \tag{C.5}$$

The elements of C.5 are obtained based on the following procedure

$$L_{g_1} h_1(\zeta) = \nabla h_1 g_1(\zeta) = \frac{1}{R_w} g_t$$

$$L_{g_2} h_1(\zeta) = \nabla h_1 g_2(\zeta) = \frac{1}{R_w} g_s$$

and

$$L_{g_1} h_2(\zeta) = \nabla h_2 g_1(\zeta) = 0$$

$$L_{g_2} h_2(\zeta) = \nabla h_2 g_2(\zeta) = 0$$

The second row elements are obtained as

$$L_f h_2(\zeta) = \nabla h_2 f(\zeta) = \frac{R_w \omega_w D_2}{\cos\delta}$$

moreover

$$L_{g_2} L_f h_1(\zeta) = \nabla(L_f h_2)\, g_2 = \frac{g_s D_2}{\cos\delta} + \frac{R_w \omega_w b \cos\tilde{\theta}}{L k_{1_s} \cos^2\delta}$$

Thus, the determinant of E is obtained as

$$\det E = \frac{g_t \omega_w b \cos\tilde{\theta}}{k_{1_s} L \cos^2\delta} \tag{C.6}$$

Appendix D

Diffeomorphic Transformation $\Phi(\chi)$

To verify that $\Phi(\chi)$ is indeed a diffeomorphism, it is easy to check if the Jacobian of Φ has full rank.

$$\nabla \Phi(\chi) = \begin{bmatrix} 0 & 0 & 0 & 1 & 0 \\ \frac{D_1}{\cos\delta} & -\frac{Ub\sin\theta}{\cos^2\delta} & -\frac{UD_2}{\cos\delta} & 0 & 0 \\ 0 & 0 & 0 & 0 & 1 \\ \frac{D_2}{\cos\delta} & \frac{Ub\cos\theta}{\cos^2\delta} & \frac{UD_1}{\cos\delta} & 0 & 0 \\ 0 & 0 & 1 & 0 & 0 \end{bmatrix} \tag{D.1}$$

Interchange the 3rd and 1st rows with the 5th and 4th rows respectively, will not change the determinant. The resulting matrix is given by

$$\nabla \Phi(\chi) = \begin{bmatrix} \frac{D_2}{\cos\delta} & \frac{Ub\cos\theta}{\cos^2\delta} & \frac{UD_1}{\cos\delta} & 0 & 0 \\ \frac{D_1}{\cos\delta} & -\frac{Ub\sin\theta}{\cos^2\delta} & -\frac{UD_2}{\cos\delta} & 0 & 0 \\ 0 & 0 & 1 & 0 & 0 \\ 0 & 0 & 0 & 1 & 0 \\ 0 & 0 & 0 & 0 & 1 \end{bmatrix} \tag{D.2}$$

Thus, the determinant of $\nabla \Phi(\chi)$ is obtained as (Ogata, 1990)

$$\det\left[\nabla\Phi(\chi)\right] = |A||D| \tag{D.3}$$

Where A and D are defined as follows

$$\nabla\Phi(\chi) = \begin{vmatrix} A_{(n\times n)} & B_{(n\times m)} \\ C_{(m\times n)} & D_{(m\times m)} \end{vmatrix}$$

An easy calculation of D.3 shows that

$$\begin{aligned} \det\left[\nabla\Phi(\chi)\right] &= (1)\left[\frac{D_2}{\cos\delta}\left(-\frac{Ub\cos\delta}{L\cos^2\delta}\right) - \frac{D_1}{\cos\delta}\left(\frac{Ub\cos\theta}{L\cos^2\delta}\right)\right] \\ &= \frac{Ub}{L\cos^2\delta} \end{aligned} \tag{D.4}$$

Thus, $\nabla\Phi(\chi)$ has the full rank if U, and b are non-zero which are the cases for this study.

Appendix E

AGV Specifications

Parameter		Value	
		Loaded	Unloaded
Total mass	Kg	1700	700
Sprung mass	Kg	1300	300
Front unsprung mass	Kg	200	200
Rear unsprung mass	Kg	200	200
Roll moment of inertia	$Kg\text{-}m^2$	1170	150
Yaw moment of inertia	$Kg\text{-}m^2$	500	200
Front roll axis stiffness	N-m/rad	45000	45000
Rear roll axis stiffness	N-m/rad	45000	45000
Front roll axis damping	N-m.s/rad	4500	4500
Rear roll axis damping	N-m.s/rad	4500	4500
Distance from front axle to C. G.	m	0.6	0.6
Distance from rear axle to C. G.	m	0.7	0.7
Vertical distance from sprung mass to C. G.	m	0.9	0.5
Longitudinal distance from sprung mass to C. G.	m	0	0
Height of sprung mass from C. G.	m	1.2	0.8
Front unsprung mass height	m	0.3	0.3

Parameter		Value	
		Loaded	**Unloaded**
Rear unsprung mass height	m	0.3	0.3
Front track width	m	0.85	0.85
Rear track width	m	0.85	0.85
Front tire cornering stiffness	N/rad	6000	6000
Rear tire cornering stiffness	N/rad	6000	6000

Appendix F

Motor Specifications

The specifications for tractive motor is given by

Parameter		Notation	Value
Torque constant	N-m	$\bar{K}_t$	.5085
Motor inertia	Kg-m^2	$\bar{J}_t$	3.5×10^{-3}
Motor armature resistance	Ohm	R_{at}	1.2
Motor damping coefficient	N-m/rad/s	$\bar{C}_t$	$.774\times10^{-3}$
Motor gear ratio		n_t	40

Also, for the steering motor the specifications are given as

Parameter		Notation	Value
Torque constant	N-m	$\bar{K}_s$	.339
Motor inertia	Kg-m^2	$\bar{J}_s$	2.33×10^{-3}
Motor armature resistance	Ohm	R_{as}	.8
Motor damping coefficient	N-m/rad/s	$\bar{C}_s$	$.516\times10^{-3}$
Motor gear ratio		n_s	5